

Evaluating and Comparing Longitudinal Control Strategies for Autonomous Vehicles

Louis Sungwoo Cho¹ and Alireza Talebpour²

¹Graduate Research Assistant, Department of Civil Engineering, University of Illinois at Urbana-Champaign, 205 N Mathews Ave, Urbana, IL, 61801. Email: louissc2@illinois.edu

²Assistant Professor, Department of Civil Engineering, University of Illinois at Urbana-Champaign,
205 N Mathews Ave, Urbana, IL, 61801. Email: ataleb@illinois.edu

Abstract

Maintaining appropriate inter-vehicle distances is crucial in enhancing safety and efficiency of traffic flow for autonomous vehicles. Various control spacing control policies affect traffic stability and vehicle dynamics, impacting road capacity and driving patterns. This comparative study analyzes Constant Spacing Policy (CSP), Constant Time Headway (CTH), Traffic Flow Stability (TFS), Constant Safety Factor (CSF), and the Intelligent Driver Model (IDM) by calibrating the genetic algorithm for optimizing the parameters of each spacing policy using highway datasets from I294, I90-94 and Waymo’s Phoenix data. Simulation results show that CSP and CSF models had the most robust performance, achieving the lowest RMSE and highest R^2 values. The CSP model achieved stability under low-density highway conditions by maintaining consistent vehicle spacing with minimal perturbations. The CSF policy was determined to be the most optimal policy for high-density traffic, effectively managing safety-critical scenarios involving abrupt acceleration and braking. The CTH model showed reliable performance in stable conditions but sensitive to speed fluctuations, resulting in higher errors during dynamic traffic scenarios. The TFS model consistently had higher errors, reflecting its limited adaptability to congested or complex traffic environments. The IDM model demonstrated strong adaptability and realistic driving behavior across diverse

24 conditions but required precise calibration to achieve optimal performance in high-density and
25 unpredictable scenarios.

26 **INTRODUCTION**

27 Controlling inter-vehicular spacing between vehicles is essential to maintain safety for au-
28 tonomous vehicles. Various research done by transportation engineers integrate concepts from
29 macroscopic and microscopic traffic properties to safely guide self-driving vehicles along the road
30 while mitigating the risk of major roadway accidents. However, real-world driving maneuvers
31 are overlooked by existing control policies in complex traffic conditions, limiting the ability to
32 adapt to scenarios such as sudden lane changes, varying vehicle interactions, or abrupt braking
33 events. Addressing these challenges requires robust calibration methods that can accurately replicate
34 observed vehicular behavior, ensuring both reliability and safety.

35
36 One significant challenge is the procedure of accurately calibrating the spacing policies to replicate
37 the vehicle trajectories. Existing models overlook the intricate interactions between kinematic
38 variables such as acceleration, spacing, and relative speed leading to discrepancies between predicted
39 maneuvers and the actual maneuver. The aforementioned challenges of the control spacing models
40 undermine the reliability in complex traffic scenarios.

41
42 This study addresses these challenges by leveraging vehicular trajectory data from Interstate high-
43 ways to calibrate the most optimal parameters for each control spacing policy by using the genetic
44 algorithm. This approach provides a robust framework for optimizing model parameters, and
45 replicating the observed behavior. The results from this sophisticated calibration process contribute
46 to the development of more reliable and adaptable control spacing policies, paving the way for safer
47 and more efficient autonomous systems.

48
49 The primary objective of this study is to evaluate the performance of various control spacing models
50 used for safely and efficiently maintaining spacings between autonomous vehicles. The goal is to

51 assess the ability of the control spacing models capturing critical driving dynamics such as vehicle
52 speed, spacing, acceleration, and relative speed which could be used for autonomous vehicles. The
53 genetic algorithm calibrates the most optimal parameter values needed for each control spacing
54 policy. By fine-tuning the parameters for control spacing policies, the results were calibrated to
55 closely align the simulated trajectories with the observed vehicle trajectories, ensuring improved
56 accuracy and consistency with real-world vehicular trajectory data.

57

58 To evaluate the performance of each model, the calibrated parameters were validated by comparing
59 the predicted trajectories generated by the model against the actual observations for a comprehensive
60 assessment of the model's accuracy and reliability. Additionally, the study examined how each
61 control spacing model performed under varying traffic conditions, from free-flowing scenarios to
62 congested scenarios. This in-depth analysis highlights the strengths and limitations of each control
63 spacing model under various traffic conditions.

64 BACKGROUND STUDY

65 Various research studies on control spacing models for car-following behavior in autonomous
66 vehicles have been conducted in recent years ([D. Swaroop and Ioannou 1994](#)). These models can be
67 broadly categorized into those that rely on Vehicle-to-Vehicle (V2V) communication, those that
68 function independently of communication systems, and hybrid approaches that integrate multiple
69 strategies ([Wu et al. 2020](#)). Communication-based models leverage real-time data exchange by
70 getting information through sensors to enhance vehicle coordination and string stability, while
71 non-communication-based approaches rely on predefined control spacing laws to safely maneuver
72 diverse traffic scenarios. Hybrid models aim to balance the advantages of both, improving adaptabil-
73 ity under varying traffic conditions.

74

75 The selection and fine-tuning of control parameters are critical in optimizing vehicle safety, im-
76 proving traffic flow efficiency, and maintaining stability across various driving conditions. It is
77 important to meticulously adjust the parameters that govern control spacing policies to enable

78 Adaptive Cruise Control (ACC) systems to adapt to diverse traffic environments. These refined
79 adjustments help mitigate stop-and-go oscillations, enhance traffic safety, and improve overall
80 traffic flow. Furthermore, precise tuning ensures a smoother transition between acceleration and
81 deceleration, reducing abrupt braking events and minimizing perturbations in vehicle platoons. This
82 process is critical in maintaining string stability, preventing abrupt changes in the vehicle's behav-
83 ior in small speed fluctuations that could propagate through traffic and lead to unnecessary congestion.

84

85 The most commonly studied spacing policies for vehicles are Constant Spacing Policy (CSP), Con-
86 stant Time Headway (CTH), and Traffic Flow Stability (TFS). The Intelligent Driver Model (IDM),
87 developed by Treiber, Hennecke, and Helbing ([Treiber et al. 2000](#)), is a widely used car-following
88 model for microscopic traffic flow simulations. The model provides a robust framework for modeling
89 vehicle interactions under various driving conditions, making it useful in research related to traffic
90 flow dynamics. In addition to these commonly used control spacing policies, Constant Safety
91 Factor (CSF) policy is essential for adjusting inter-vehicle spacing based on safety margins such
92 as adjusting safety factor to take into account of variations in speed, time headway, and braking.
93 These safety measures are critical to allow ACC systems to operate safely and mitigate collisions.
94 Thus, the Constant Factor Safety (CSF) policy was also used to compare the calibration among the
95 aforementioned commonly used control spacing policies.

96

97 Additionally, other approaches such as Variable Time Headway (VTH), Cooperative Adaptive Cruise
98 Control (CACC) with String Stability, Model Predictive Control (MPC), Lateral and Longitudinal
99 Control, and Closed-Loop Dynamics have been explored to optimize vehicle interactions and traffic
100 efficiency. The control spacing models for car-following behavior can further be classified based
101 on their reliance on communication systems: those that operate with Vehicle-to-Vehicle (V2V)
102 communication, those without communication, and hybrid approaches that integrate both strategies.

103 **Models with Communication**

104 Models that incorporate communication-based control strategies have various approaches to simulate
105 the car-following behavior of vehicles. Model Predictive Control (MPC) can help mitigate traffic
106 flow disturbances caused by lane-changing maneuvers while maintaining CTH (An and Talebpour
107 2019). The proposed approach optimizes both the lateral trajectory of a lane-changing Connected
108 Automated Vehicles (CAV) and the longitudinal control of a Connected and Automated Vehicles
109 (CAV) in the target lane for simulation. The study proposed a MPC framework for the target-lane
110 vehicle to effectively respond to lane changes, while a predefined set of lateral trajectories was
111 evaluated for the vehicle changing lanes. The optimal trajectory was selected based on its ability to
112 minimize the required deceleration of the impacted vehicle, reducing acceleration disturbances and
113 shockwave propagation. Analytical and simulation results show that the integrated control strategy
114 enhances traffic stability and abate perturbations in the vehicle platooning system.

115

116 Gap regulation and gap-closing controllers to enhance string stability in traffic flow (Milanés
117 et al. 2014) was analyzed in another study. These two main controllers take advantage of the
118 Vehicle-to-Vehicle (V2V) communication to enhance coordination between autonomous vehicles.
119 The Cooperative Adaptive Cruise Control (CACC) system that augments traditional Adaptive
120 Cruise Control (ACC) was used to model the vehicles by integrating wireless Vehicle-to-Vehicle
121 communication. One controller was in charge of managing in scenarios where a vehicle joins the
122 platoon. The other controller regulated the car-following behavior. The Infiniti M56s cars were used
123 for experimental validation to demonstrate the capability of the proposed CACC system being able
124 to significantly improve traffic stability and coordination.

125

126 Tuning control model parameters is a commonly used approach to enhance overall system stability
127 for car-following behavior. One study optimizes the ACC system parameters by leveraging the
128 Controller Area Network (CAN) communication framework to improve car-following behavior and
129 to preclude fatal traffic collisions (Moon et al. 2009). The proposed ACC system integrates collision

130 avoidance system by classifying driving scenarios into safe, warning, and dangerous modes using a
131 non-dimensional warning index and time to collision metrics. Various control strategies are utilized
132 based on the classifications. The parameters for the optimization process were fine-tuned through
133 a confusion-matrix method using manual-driving data in scenarios with no traffic accidents. The
134 study compares the vehicle-following characteristics of the system to real-world manual driving to
135 emphasize that integrating both ACC and collision avoidance systems can successfully replicate
136 human-driving behavior in both high-speed cruising and low-speed stop-and-go traffic scenarios.
137 Additionally, experimental validation in real-vehicle tests corroborates that the system effectively
138 prevents vehicles from following too close to each other enhancing both safety and driver comfort
139 across various driving conditions.

140

141 A study on Semi-Autonomous Adaptive Cruise Control (SAACC) systems explores the integration
142 of a radio-frequency communication framework to enhance highway safety and traffic flow capacity
143 ([Rajamani and Zhu 2002](#)). Unlike traditional Adaptive Cruise Control (ACC) or fully automated
144 highway systems (AHS) that rely on tightly coordinated vehicle platoons, SAACC operates without
145 having to form vehicle platoons or be too dependent on dynamic frequency allocation. The system
146 consistently maintains a user-defined cruising speed until a target vehicle is detected in the same
147 lane. Under this condition, the system adjusts the ego vehicle's following distance based on
148 real-time communication signals. The proposed SAACC approach enables vehicles to maintain
149 smaller time gaps safely while ensuring string stability and minimizing actuator input efforts
150 compared to standard autonomous ACC systems. Simulation results demonstrate that SAACC
151 are more accurate and smoother in tracking vehicles, mitigates control efforts, and increases ro-
152 bustness to variations in vehicle dynamics, making it a viable solution for mixed-traffic environments.

153

154 One study examines truck platooning with Cooperative Adaptive Cruise Control (CACC), emphasizing
155 the benefits and challenges of using the Constant Time Headway (CTH) model in uphill driving
156 conditions ([Chen et al. 2018](#)). The study highlights critical issues where truck platoons controlled

157 by the CACC model become asymptotically unstable on steep grades due to the limited acceleration
158 capabilities of heavy vehicles. This instability prevents trucks from tracking the vehicle platoon
159 after an uphill terrain, leading to spacing errors. In order to resolve this issue, the study proposes
160 new control strategies to complement existing controllers and enhance stability. These strategies
161 mitigate the adverse effects of low crawl speeds and ensure that truck platoons remain string stable
162 irrespective of uphill grades. The results underscore the need for refined control policies in uneven
163 road conditions where elevation changes impact the overall dynamics of the vehicle and traffic flow.

164

165 One study explores the Variable Time Headway (VTH) concept. This method dynamically adjusts
166 the inter-vehicle headway. The headway is increased during acceleration and decreased during
167 deceleration ([Yanakiev and Kanellakopoulos 1995](#)). This adaptive spacing policy enhances string
168 stability, ensuring that perturbations are not amplified during vehicle platooning. Unlike constant
169 spacing policies, which require inter-vehicle communication to maintain string stability, VTH allows
170 autonomous vehicles to achieve stability without explicit coordination by adjusting the time headway
171 based on velocity errors. This modification significantly abates transient spacing errors, improves
172 responsiveness to traffic fluctuations, and minimizes the risk of traffic shockwaves propagating in
173 the vehicle platoon and mitigates stop-and-go congestion. Additionally, VTH allows for smaller
174 inter-vehicle distances in autonomous platoon operation.

175

176 Constant spacing with communication is a widely used control model for enhancing vehicle coor-
177 dination in platooning. Several studies have investigated this approach, including the integration
178 of Adaptive Cruise Control (ACC), spacing policies, and Cooperative Adaptive Cruise Control
179 (CACC) to improve string stability ([Naus et al. 2010](#)). One study proposes a decentralized CACC
180 controller that relies on a wireless communication link with the nearest preceding vehicle, allowing
181 vehicles to maintain small inter-vehicle spacings. To take into consideration of vehicles with possibly
182 different characteristics, a frequency-domain condition for the string stability system was derived.
183 The study demonstrates that a velocity-dependent inter-vehicle spacing policy, supported by wireless

184 communication, enables stable platooning, whereas a constant spacing system that is independent of
185 velocity may lead to instability.

186

187 One study explores the use of linear kinetic properties in Adaptive Cruise Control (ACC) and Coop-
188 erative Adaptive Cruise Control (CACC) systems to optimize inter-vehicle spacing in platoons ([Luu et al. 2020](#)). The proposed spacing control algorithm leverages on-board sensors and communicates
189 only with the preceding vehicle to regulate following distances. The study evaluates string stability
190 by leveraging a frequency-domain analysis and Nyquist diagrams. The control algorithm ensures
191 that each vehicle maintains a stable spacing while mitigating perturbations that could propagate
192 through the platoon. Numerical simulations demonstrate the model's potential for improving platoon
193 coordination and roadway capacity.

195

196 Traffic flow stability analysis was conducted in this research by leveraging deterministic acceleration
197 models and Vehicle-to-Vehicle (V2V) communication ([Talebpour and Mahmassani 2016](#)). The
198 study proposed a simulation framework that differentiates between connectivity and automation,
199 modeling various vehicle types with distinct communication capabilities. A stability analysis of
200 mixed traffic streams demonstrates that CAVs significantly enhance string stability, with automation
201 proving more effective than connectivity alone in preventing shockwave formation and propagation,
202 underscoring the potential of V2V communication and automation in optimizing highway traffic
203 flow and mitigating congestion.

204

205 Model Predictive Control (MPC) is also a widely-known controller to address complex traffic
206 scenarios. These studies have experimented how MPC can be used in multi-stage lane-changing
207 movements of vehicles in dynamic traffic conditions ([Cesari et al. 2017](#)), predictive optimization
208 of lane-changing decisions through the integration of game theory and MPC ([Wang et al. 2015](#)),
209 and Distributed MPC for heterogeneous vehicle platoons, which tracks leader speed and maintains
210 desired gaps under unidirectional topologies ([Zheng et al. 2017](#)). MPC enhances Adaptive Cruise

211 Control (ACC) and Cooperative Adaptive Cruise Control (CACC) strategies, allowing vehicles
212 while maintaining traffic stability to adjust their speed and spacing dynamically. Some studies
213 have also integrated learning-based approaches with MPC to improve adaptability in uncertain
214 environments, where vehicles must anticipate and react to unpredictable traffic fluctuations. These
215 findings underscore the importance of optimizing vehicle control and coordination in scenarios
216 where lane-changing behavior happens frequently.

217

218 This study proposes a data-driven, stochastic optimization-based Model Predictive Control (MPC)
219 framework that enhances stability, robustness, and safety in longitudinal cooperative driving by
220 incorporating Vehicle-to-Vehicle (V2V) communication ([Zhao and Zhang 2020](#)). To address uncer-
221 tainties in traffic dynamics, the framework integrates an online learning-based driving dynamics
222 prediction model that anticipates the uncertain states of preceding vehicles. The predictions were
223 incorporated into a constrained finite horizon optimal control problem to optimize the acceleration
224 and deceleration commands for CAVs. The study calibrates the Distributionally Robust Stochastic
225 Optimization (DRSO) model with Distributionally Robust Chance Constraints (DRCC) to ensure
226 reliable control under uncertain conditions. Additionally, Semi-definite Programming (SDP) relax-
227 ation technique was applied to perform real-time computation. Experimental validation using Next
228 Generation Simulation (NGSIM) data demonstrates that the proposed approach maintains string
229 stability and robust cooperative driving performance under various traffic conditions by properly
230 tuning key parameters such as prediction horizon length and time headway parameters.

231

232 Hybrid models incorporating communication have been analyzed. One study integrates Adaptive
233 Cruise Control (ACC) and Model Predictive Control (MPC) to enable smooth platoon merging
234 through vehicle platooning control ([An and Talebpour 2022](#)). Another study examines the impact
235 of Vehicle-to-Vehicle (V2V) communication on traffic flow stability, analyzing how information
236 availability influences critical density and percolation within vehicular networks ([Talebpour et al.](#)
237 [2018](#)).

238
239 Cooperative Adaptive Cruise Control (CACC) has also been studied for its effects on traffic-flow
240 stability and throughput. By leveraging V2V communication, CACC systems provide reference
241 values that enhance traffic characteristics, such as string stability, particularly in mixed traffic
242 conditions (van Arem et al. 2006). Another study integrates lateral and longitudinal controllers
243 and develops a finite state system to improve autonomous vehicle platooning. The longitudinal
244 control system consists of upper and lower-level controllers, while the lateral controller ensures safe
245 lane-changing behavior (Rajamani et al. 2000).

246 **Models without Communication**

247 Constant Time Headway (CTH) can be used by models without having to rely on communication
248 between vehicles. One study analyzes the vehicle dynamics using a continuous-time deterministic
249 car-following model by leveraging Pipe's Model to simulate steady-state car-following behavior
250 (Sipahi et al. 2009). The study explores the effects of multiple driver reaction and actuation delays on
251 stability, providing a comprehensive characterization of stability regions within the delay parameter
252 space. By running the frequency-sweeping algorithms, the research simplifies the stability analysis
253 and analyzes how drivers' behavior, decision-making delays, and response times affect the overall
254 traffic flow stability.

255
256 A research on how string stability can be achieved without relying Vehicle-to-Vehicle (V2V)
257 communication was conducted by leveraging a kinematic linear model with multi-anticipation
258 (Donà et al. 2022). The study highlights that most commercially available ACC systems are unstable.
259 While increasing time headway intervals can stabilize traffic, it reduces roadway capacity. To
260 address this major issue, the study proposed an alternative solution that utilizes recent advancements
261 in RADAR sensing technology. By monitoring the behaviors of two vehicles downstream, the
262 proposed multi-anticipative ACC system ensures string stability across a wide range of traffic condi-
263 tions without requiring inter-vehicle communication. Analytical and simulation-based evaluations
264 demonstrate that this approach not only enhances traffic stability overall, but also increases road

capacity, even in the presence of external perturbations. Furthermore, Pareto optimization was performed to derive the optimal tuning conditions for the time headway policies. The results suggest that multi-anticipative ACC provides a viable solution for mitigating congestion and improving traffic flow without having to build connectivity-based infrastructure.

Additionally, the performance of commercially available Adaptive Cruise Control (ACC) systems has been analyzed, revealing significant limitations in achieving string stability (Ciuffo et al. 2021). A large-scale experiment involving ACC-equipped vehicles was conducted to study their car-following behavior under real-world driving conditions. The study evaluates how target time gaps were maintained based on observed distributions across different vehicle brands. Results indicate that current ACC implementations struggle to maintain consistent inter-vehicle spacing, leading to string instability and disruptions in traffic flow. This instability arises due to variations in control logic among different manufacturers and the inability of ACC systems to adapt dynamically to changes in vehicle ordering and settings. The findings underscore the critical role of Constant Time Headway (CTH) policies in mitigating these issues, highlighting the need for more robust control strategies to ensure stable car-following behavior and prevent unintended traffic disturbances as ACC adoption increases.

A study examining Constant Time Headway (CTH) policies proposed a novel framework for designing and evaluating spacing policies (Santhanakrishnan and Rajamani 2003). The research assesses spacing policies in terms of string stability, traffic flow stability, and roadway capacity. While the standard CTH policy guarantees string stability, findings indicate that this policy does not perform well in reduced traffic capacity and can cause instability in traffic flow. To address these limitations, the study introduces an "ideal" spacing policy, formulated as a nonlinear function of speed, which improves both string and traffic flow stability while enhancing overall capacity.

Several studies have used constant spacing approaches. One study explores intelligent cruise control

strategies within an Automated Vehicle Control System (AVCS) framework. A commonly used controllers for autonomous vehicles called PID controllers were used to adjust the inter-vehicle spacings effectively (Ioannou et al. 1993). Multiple control system tests were performed by using a validated nonlinear longitudinal vehicle model before implementation in real-world vehicles. The proposed control approach ensures smooth and reliable vehicle following by utilizing onboard sensors that measure relative distance and speed without relying on Vehicle-to-Vehicle (V2V) communication. The overall stability is maintained through a meticulously designed throttle and brake control systems in conjunction with the Constant Time Headway (CTH) policy. Simulation and experimental results emphasize that the integrated system provides stable and responsive vehicle spacing, even in scenarios where the lead vehicle exhibits erratic speed variations.

Another study utilizes partial differential equations (PDEs) to model traffic flow stability in intelligent cruise control systems operating under constant spacing policies (Darbha and Rajagopal 1999). The study distinguishes between two fundamental stability concepts in traffic flow analysis: string stability, which ensures predictable inter-vehicle spacing in a platoon, and traffic flow stability, which accounts for velocity and density variations due to vehicles entering or leaving the flow. The study also highlights that traffic flow stability depends not only on vehicle-following control laws but also on the spacing policy leveraged by the control system. By analyzing the coupled equations governing automatic vehicle following and traffic density, the study investigates the critical role of constant spacing policies in determining highway capacity and traffic stability.

Additionally, a comparative study evaluates various spacing policies, focusing on the impact on safety, traffic flow efficiency, and user acceptance (Wang and Rajamani 2004b). The study examines the stability of highway traffic under Adaptive Cruise Control (ACC) systems. This study shows that traffic flow stability under a CTH policy is highly dependent on boundary conditions at highway inlets and exits. Furthermore, the research proposes an unconditionally stable spacing policy, which guarantees stability under all boundary conditions. Simulation results highlight the practical

consequences of instability, showing that alternative spacing policies outperform the CTH policy in maintaining smooth and efficient traffic flow. One key finding from this study is that the ACC systems should not rely only on the CTH policy.

Other studies have utilized Model Predictive Control (MPC). One study investigates distributed MPC for managing headway and cruise control in vehicle platooning ([Maxim et al. 2017](#)). Another study focuses on adjusting ACC parameters to alleviate traffic congestion and improve flow efficiency ([Kesting et al. 2008](#)). Additionally, predictive optimization and non-linearity compensation were applied to enhance the longitudinal dynamics of vehicular systems ([Li et al. 2011](#)).

Furthermore, additional studies include a physics-based lumped mass model that incorporates braking and aerodynamic forces for control optimization ([Nilsson et al. 2016](#)), and a bidirectional control approach utilizing decentralized dynamics for improved stability ([Barooah et al. 2009](#)). Another study presents a microscopic traffic flow model that integrates both lateral and longitudinal dynamics to address two-dimensional traffic flow challenges. This model effectively handles collision avoidance, lane-changing, and lateral friction ([Delpiano et al. 2020](#)).

Alternative Models

Several studies analyze the performance of Adaptive Cruise Control (ACC) and Cooperative Adaptive Cruise Control (CACC) systems. One of the studies analyzes how the Constant Time Headway (CTH) approach can be integrated with ACC and CACC models under uncertainty conditions ([Zhou et al. 2017](#)). One research study leverages a rolling horizon stochastic optimal control strategy, taking into consideration for uncertainties in system dynamics and sensor measurements. Modeling uncertainties were perceived as normally distributed disturbances in both the state and measurement equations. A multi-objective function was defined by incorporating bounded acceleration limits and collision protection constraints. The resulting optimization problem was formulated as a linearly constrained Linear Quadratic Gaussian (LQG) problem, which is solved using the separation

346 principle.

347

348 One study analyzed how traffic flow stability can be induced by the Constant Time Headway (CTH)
349 policy using three different modeling paradigms: a microscopic model, a spatially discrete model,
350 and a spatially continuous model ([Li and Shrivastava 2002](#)). The analysis shows that traffic stability
351 properties can vary across these paradigms unless the control policy and traffic dynamics are
352 consistently formulated. To ensure consistency, a biasing strategy was introduced, determining
353 whether the feedback control being applied to the system is downstream, upstream, or collocated
354 with respect to the vehicle. According to the study results, it was determined that for ACC-equipped
355 vehicles utilizing forward-looking sensors, a downstream biasing strategy results in exponentially
356 stable traffic flow on circular highways. Furthermore, traffic stability can be maintained on open
357 highways if entry and exit conditions follow the downstream biasing strategy.

358

359 A research on integrating Adaptive Cruise Control (ACC) and Cooperative Adaptive Cruise Control
360 (CACC) traffic dynamics into a Gas-Kinetic (GKT) macroscopic traffic flow model was conducted
361 ([Delis et al. 2015](#)). In this approach, an acceleration/deceleration term to simulate the dynamics
362 of ACC and CACC vehicles on traffic flow was proposed. In addition to this, a novel relaxation-
363 based approach that tracks the time/space-gap principle was also introduced. This method assigns
364 relaxation time to multiple CACC leading vehicles and only the direct leader was assigned to
365 ACC leading vehicles. The partial differential equations for the nonlinear system were used for
366 numerical approximation using a high-resolution finite volume scheme with a weighted essentially
367 non-oscillatory (WENO) discretization method. The calibrated results calcify corroborates that
368 CACC enhances traffic flow stability, particularly in response to perturbations on a ring road and
369 merging flows at an on-ramp. Compared to ACC, the CACC model enhances dynamic equilibrium
370 capacity and mitigates congestion more effectively, particularly in bottleneck locations.

371

372 Human drivers tend to drive relying on the speed and position of the preceding and following

373 vehicles to adjust the state and control inputs of the vehicle. Longitudinal vehicle models can be
374 used to simulate real-world traffic maneuvers by incorporating engine, throttle, and brake dynamics
375 to replicate human-driving behaviors (Zhang et al. 1999). This study proposed an Autonomous
376 Intelligent Cruise Control (AICC) system, where the relative speed and inter-vehicle spacing
377 determines the actions the following vehicle can take to maintain a desired spacing between the
378 vehicles, ensuring platoon stability bi-directionally. This system has been effective in controlling
379 time headway between vehicles and maintaining constant inter-vehicle spacings.

380

381 One study (Kilic et al. 2015) leverages a hierarchical control approach to Adaptive Cruise Control
382 (ACC) as part of an Advanced Driver Assistance System (ADAS). The System-of-Systems (SOS)
383 framework to unify multiple ADAS functionalities was proposed. The ACC system was structured
384 into High-Level Control (HLC), Low-Level Control (LLC), and sensor units to enhance adaptability
385 and efficiency. Using a finite state machine, the HLC dynamically adjusts the vehicle's speed, either
386 by maintaining a minimum safe following distance or by tracking a desired velocity. The Model
387 Predictive Controller (MPC) tracks the movement of the target vehicle and generate optimal control
388 actions for the distance control state. The throttle and brake actions are maneuvered by the LLC. By
389 leveraging the hierarchical structure, the proposed ACC system enhances vehicle response, enhances
390 safety, and facilitates integration with other ADAS technologies such as collision avoidance and
391 blind spot detection.

392 DATA DESCRIPTION

393 The high-fidelity Third Generation Simulation (TGSIM) dataset (Federal Highway Admin-
394 istration (FHWA) 2024) was utilized for analyzing vehicle trajectories (Talebpour et al. 2024),
395 (Ammourah et al. 2024). The holistic dataset focuses on complex urban, multi-modal road networks
396 capable of traffic simulations of control algorithms (Ammourah et al. 2024) to be conducted. For
397 this research, datasets from the I90/94, and level 1 autonomy vehicles in I294 were utilized with
398 bi-directional lanes represented by positive and negative signs for each lane number.

399

400 Each control model in this study was calibrated using the dataset's high-resolution, 10 Hz data,
401 offering an intricate perspective on vehicular movements (Ammourah et al. 2024). The datasets
402 include important trajectory attributes such as time in seconds, longitudinal and lateral coordinates
403 in meters respectively, velocity in meters per second, and acceleration in meters per second squared,
404 enabling a comprehensive analysis of movement patterns and vehicle dynamics for control. In
405 addition to this, the datasets are utilized to track each vehicle's motion in highways.

406

407 In addition to the TGSIM datasets, the Phoenix dataset was also used for running simulations.
408 The Phoenix dataset has trajectory data including key attributes such as lateral and longitudinal
409 coordinates in meters, speed in meters per second, acceleration in meters per second squared
410 collected by the LiDAR sensors in the Waymo self-driving cars. By comparing simulations in the
411 Phoenix dataset with the TGSIM datasets, the simulated environments were analyzed to evaluate
412 the interactions between the ego vehicle and the surrounding vehicles in varying traffic conditions
413 (Zhang et al. 2025).

414 **MATHEMATICAL FORMULATION**

415 This study analyzes Constant Spacing Policy (CSP), Constant Time Headway (CTH), Traffic
416 Flow Stability (TFS), Constant Safety Factor (CSF), and the Intelligent Driver Model (IDM) The
417 aforementioned control spacing policies are widely used to safely maintain the distance between
418 vehicles which can be potentially used for safe autonomous driving.

419

420 The CSP model maintains fixed longitudinal gaps between the ego and the leader vehicles, commonly
421 used in vehicle platooning. The CTH model dynamically adjusts the following distance based on the
422 time interval between vehicles. The TFS policy aims to stabilize traffic flow and mitigate stop-and-go
423 traffic waves. The CSF policy prioritizes maintaining safety and to mitigate collision avoidance by
424 dynamically adjusting inter-vehicle spacings. Lastly, the IDM dynamically adjusts inter-vehicle
425 gaps based on the velocity difference to the leading vehicle, incorporating both acceleration and
426 deceleration dynamics to model realistic driving behavior.

427

428 This study conducts an in-depth analysis of optimizing the calibration performance of control
 429 spacing models, providing a comprehensive assessment of vehicle interactions on roadways. By
 430 examining dynamic behavior, the study evaluates how various control strategies influence traffic
 431 flow efficiency, safety, and stability.

432 Constant Spacing Policy

433 The Constant Spacing Policy (CSP) maintains a constant spacing between the vehicles from the
 434 preceding vehicle with a low computation load ([Wu et al. 2020](#)). The spacing error variable δ_i for
 435 the Constant Spacing Policy can be defined as:

$$436 \quad \delta_i = x_i - x_{i-1} + L \quad (1)$$

437 where x_i is the position of the ego vehicle and x_{i-1} is the position of the leading vehicle, and L being
 438 the desired spacing. The control law used in this policy is defined as ([Swaroop and Hedrick 1999](#)) :

$$439 \quad \ddot{x}_i = -k_v \dot{\delta}_i - k_p \delta_i \quad (2)$$

440 where k_v, k_p are constants and $\dot{\delta}_i$ is the relative speed between the ego and the leader vehicles.

441 Constant Time Headway Policy

442 To ensure that the desired spacing increases proportionally with the speed, the Constant Time
 443 Headway (CTH) dynamically adjusts inter-vehicle spacing in proportion to vehicle speed based on
 444 the time headway between the ego and the leader vehicles. ([Wu et al. 2020](#)). The spacing error
 445 variable δ_i for the Constant Time Headway policy can be defined as:

$$446 \quad \delta_i = x_i - x_{i-1} + h v_i + d_{min} \quad (3)$$

447 where d_{min} is the safety distance between the ego and the leader vehicles, h is the time headway
 448 between two vehicles, and v_i is the speed of the i-th vehicle,. The control law used in this policy is

449 defined as (Ioannou and Chien 1993):

450

$$\ddot{x}_i = -\frac{1}{h}(\dot{\epsilon}_i + \lambda\delta_i) \quad (4)$$

451 where $\dot{\epsilon}$ is the rate of change for the spacing error, and λ is an arbitrary constant.

452 **Traffic Flow Stability Spacing Policy**

453 However, the main challenge of the CTH spacing policy is that the stabilizing the traffic flow is
454 not guaranteed. To resolve this issue, the Traffic Flow Stability (TFS) spacing policy was devised.
455 The TFS spacing policy was designed based on the Greenshield's relation, providing better traffic
456 flow stabilization while ensuring safety (Wu et al. 2020). The spacing error variable δ_i used for the
457 Traffic Flow Stability spacing policy can be defined as:

458

$$\delta_i = x_i - x_{i-1} + \frac{1}{\rho_m(1 - \frac{v_h}{v_f})} \quad (5)$$

459 where ρ_m is the traffic density, v_f is the speed parameter, v_i is the speed of the i-th vehicle. The
460 control law used in this policy is defined as (Wang and Rajamani 2004a) :

461

$$\ddot{x}_i = -\rho_m(v_f - v_i)(1 - \frac{v_i}{v_f})(\dot{\epsilon}_i + \lambda\delta_i) \quad (6)$$

462 where $\dot{\epsilon}$ is the rate of change of spacing error, λ is the control gain and δ_i is the spacing error of the
463 i-th vehicle.

464 **Constant Safety Factor Policy**

465 Safety is an inevitable factor that must be taken account for autonomous driving. To mitigate the
466 possibility of road collisions and to improve driving safety, the Constant Safety Factor (CSF) spacing
467 policy was proposed. Specifically, the emergency braking process was meticulously analyzed for
468 the CSF policy (Wu et al. 2020). The spacing error variable δ_i used for the Constant Safety Factor
469 policy can be defined as:

470

$$\delta_i = x_i - x_{i-1} + d_{min} + t_d v + K D_{stop} \quad (7)$$

471 where t_d is the time delay, K is the safety factor and the stopping distance D_{Stop} defined as:

472

$$D_{stop} = -\frac{v_i^2}{2j_i} \quad (8)$$

473 where j_i is the max deceleration value of the i -th vehicle set as -7.32 m/s^2 . The control law used in
474 this policy is defined as (Zhao and El Kamel 2010) :

475

$$\ddot{x}_i = -\frac{\dot{\epsilon}_i + \lambda \delta_i}{t_d - \frac{\gamma}{j_i} \dot{x}_i} \quad (9)$$

476 where λ is a positive control gain, t_d is the time delay in the longitudinal control system, γ is the
477 safety coefficient, and j_i is the average deceleration value of the i -th vehicle during the maximum
478 brake action.

479

480 **Intelligent Driver Model**

481 The Intelligent Driver Model (IDM) is a widely-known model to emulate human driving behavior
482 using microscopic traffic properties. The spacing s between the ego vehicle and the leader vehicle
483 can be defined as (Treiber et al. 2000):

484

$$s = x_i - x_{i-1} \quad (10)$$

485 where x_i and x_{i-1} are the position of the ego vehicle and the leader vehicle respectively. The relative
486 velocity Δv is defined as:

487

$$\Delta v = v_i - v_{i-1} \quad (11)$$

488 where v_i is the speed of the ego vehicle and v_{i-1} is the speed of the leader vehicle. The acceleration
489 formula can be defined as:

490

$$\dot{v} = a \left(1 - \left(\frac{v}{v_0} \right)^4 - \left(\frac{s^*(v, \Delta v)}{s} \right)^2 \right) \quad (12)$$

491 where v is the velocity of the ego vehicle, v_0 is the desired velocity, T is the safe time headway, a is
 492 the maximum acceleration, s is the spacing between vehicles. The desired spacing $s^*(v, \Delta v)$ can be
 493 calculated by using the following formula below:

494

$$s^*(v, \Delta v) = s_0 + T v - \frac{v \Delta v}{2 \sqrt{ab}} \quad (13)$$

495 where s_0 is the minimum safe distance between vehicles, and b is the comfortable deceleration.

496

497 The analysis of the aforementioned spacing policies evaluate the ability to emulate real-world traffic
 498 dynamics effectively. This includes assessing the holistic impact on traffic flow stability, safety,
 499 efficiency, and adaptability to diverse traffic conditions. By analyzing the various spacing policies,
 500 the study provides a comprehensive analysis of each model's performance with the requirements
 501 of modern control systems, offering guidance for optimizing control strategies in both normal and
 502 complex driving scenarios to enhance the overall safety and efficiency of simulating trajectories for
 503 autonomous vehicles.

504

PARAMETER OPTIMIZATION

505 The genetic algorithm was leveraged in this study to determine the optimal parameters for each
 506 control spacing policy to model the car-following simulation. The algorithm iteratively evaluates
 507 possible solutions based on a fitness function that minimizes speed deviation between the simulated
 508 follower and the target follower. Through selection, crossover, and mutation, the population evolves
 509 over multiple generations to converge toward an optimal set of control parameters for each control
 510 spacing policy during calibration.

511

Fitness Function

512 The fitness function evaluates the effectiveness of the car-following model parameters by comparing
 513 simulated speed profiles with target speeds and minimizing the difference between the two variables.

514 Multiple error metrics, such as mean squared error (MSE) and root mean squared error (RMSE),
515 were integrated to quantify the deviation between the simulated follower generated by the control
516 parameters and the target follower. Lower deviation indicates better adherence to the desired
517 trajectory, leading to a higher fitness score. This approach ensures that the optimized parameters
518 conduce to optimal results.

$$\Delta v = v_{sim} - v_{target} \quad (14)$$

520 where v_{sim}, v_{target} are the speed of the simulated follower and the target follower respectively. In
 521 addition to this, the error metrics are calculated as follows:

- Mean Squared Error (MSE):

$$\text{MSE} = \frac{1}{N} \sum_{i=1}^N (\Delta v_i)^2 \quad (15)$$

- Root Mean Squared Error (RMSE):

$$\text{RMSE} = \sqrt{\text{MSE}} \quad (16)$$

- Mean Absolute Error (MAE):

$$\text{MAE} = \frac{1}{N} \sum_{i=1}^N |\Delta v_i| \quad (17)$$

- Mean Absolute Percentage Error (MAPE):

$$\text{MAPE} = \frac{100}{N} \sum_{i=1}^N \left| \frac{\Delta v_i}{v_{target}} \right| \quad (18)$$

- Normalized Root Mean Squared Error (NRMSE):

$$\text{NRMSE} = \frac{\text{RMSE}}{\max(v_{target}) - \min(v_{target})} \quad (19)$$

- 532 • Sum of Squared Errors (SSE):

533
$$\text{SSE} = \sum_{i=1}^N (\Delta v_i)^2 \quad (20)$$

- 534 • R-squared Value:

535
$$R^2 = 1 - \frac{\text{SSE}}{\sum_{i=1}^N (v_{target_i} - \bar{v}_{target})^2} \quad (21)$$

- 536 • Speed Deviation Penalty:

537
$$\sigma = \sum_{i=0}^N (v_{sim_i} - v_{target_i})^2 \quad (22)$$

- 538 • Total Difference:

539
$$\text{Total Difference} = \sum_{i=1}^N |\Delta v_i| \quad (23)$$

540 The fitness function $f(x)$ is defined as:

541
$$f(x) = \frac{1}{\sigma + 10^{-6}} \quad (24)$$

542 Genetic Algorithm

543 The genetic algorithm used in this study initializes a certain number of individuals with random
 544 values within the specified parameter ranges given an appropriate population size. For each iteration,
 545 the genetic algorithm runs for a set number of generations, computing fitness values and ranking
 546 individuals accordingly. The top $\frac{N}{2}$ individuals are selected, and the crossover operation is performed
 547 by swapping segments between two parents. The mutation step introduces a random adjustment
 548 of either -0.1 or 0.1 to the offspring to introduce noise. The new population was formed with
 549 these offspring, iteratively refining the parameters during the optimization process. This calibration
 550 effectively optimizes the parameters needed for the car-following model for each spacing policy
 551 ([Thede 2004](#)).

552 Car-following Behavior

553 The car-following behavior calculates the desired position depending on the control spacing policy
 554 being used initially, then the gap distance between the ego and the leader vehicle is calculated by

Algorithm 1 Genetic Algorithm for Car-Following Model Optimization

- 1: **Input:** Population size N , number of generations G
- 2: **Initialize:** Generate N individuals with random values in the parameter ranges:
- 3: **for** each generation $g = 1$ to G **do**
- 4: **Evaluate fitness:** Compute fitness for each individual
- 5: **Sort population:** Rank individuals based on fitness
- 6: **Select parents:** Choose top $N/2$ individuals
- 7: **Crossover:** Generate offspring by swapping parts of two parents
- 8: **for** each offspring **do**
- 9: Select crossover point randomly
- 10: Create child solutions:

 $\text{child}_1 = (\text{parent}_1[:, \text{crossover_point}], \text{parent}_2[\text{crossover_point} :])$
 $\text{child}_2 = (\text{parent}_2[:, \text{crossover_point}], \text{parent}_1[\text{crossover_point} :])$
- 11: **end for**
- 12: **Mutation:**
- 13: **for** each child i **do**
- 14: **if** random probability < mutation rate **then**
- 15: $\text{child}_i = \text{child}_i + \delta, \quad \delta \sim U(-0.1, 0.1)$
- 16: **end if**
- 17: **end for**
- 18: **Replace population:** Form the new population with parents and offspring
- 19: **end for**
- 20: **Return:** Best individual and associated error metrics

555 using the following formula:

556
$$\Delta_i = x_i - x_{i-1} \quad (25)$$

557 where x_i is the ego vehicle and x_{i-1} is the leader vehicle. The safety distance is then calculated
558 based on the control spacing model being used. The parameters are then fed into the function
559 which calculates the acceleration a of the vehicle for the specific control policy being leveraged.
560 The respective position and the speed are updated using the calibrated values. The speed of the
561 simulated vehicle is updated by the following equation:

562
$$v_{i+1} = v_i + at \quad (26)$$

563 where v_i is the previous speed of the vehicle at time t seconds and the acceleration a is calibrated
564 using the respective control spacing policy. The position of the vehicle is then updated by the
565 following equation:

566

$$x_{i+1} = x_i + v_i t + \frac{1}{2} a t^2 \quad (27)$$

567 where x_{i+1} is the updated position of the simulated vehicle, and x_i is the previous position of the
568 simulated vehicle during the simulation process. The car-following model is called through the
569 optimization process, where the genetic algorithm calibrates the most optimal parameters for the
570 five of the control spacing policies.

571

572 The calibration process iteratively refines the parameters by minimizing the error between simulated
573 trajectories and the ground truth trajectory by calling the fitness function, allowing the control
574 spacing models to adapt to various traffic conditions and maintain stability to mitigate sudden
575 fluctuations in position and speed.

576 **RESULTS AND DISCUSSION**

577 For each control spacing policy, the genetic algorithm was used to calibrate the car-following
578 model. The sophisticated calibration process fine-tunes the optimal parameters for each of the
579 control spacing policies by taking into account of the dynamic responses of surrounding vehicles
580 under various driving conditions. The I294, I90/94 and the Phoenix Waymo datasets were used for
581 calibrating the optimal parameters and simulating the trajectories generated by each control spacing
582 policy. The overall process is critical to enhance safety and maximize efficiency of traffic flow for
583 autonomous vehicles.

584 **Parameter Bound Selection and Limits**

585 To maintain consistency throughout the genetic algorithm calibration process, key parameters such
586 as population size, number of generations, and mutation rate were standardized across all control
587 spacing models analyzed in this study, as shown in Table 1. By fixing these parameters needed for

588 the genetic algorithm, this ensures that there are no inconsistencies in the optimization process.

589
590 In addition to predetermining the parameters for the genetic algorithm, the parameter bounds for
591 each control spacing model were meticulously selected. The bounds were adjusted to preclude
592 unrealistic acceleration values from being used for the calibration process which could result in the
593 simulated vehicle making impulsive behavior or instability.

594
595 Standardizing the parametric limits ensures that comparisons between different control spacing
596 models remain valid and to prevent fluke during the calibration process. Additionally, maintaining
597 fixed parameter boundaries prevent anomalies during the calibration process, reducing the likelihood
598 of convergence to unrealistic or non-generalizable solutions. This approach enhances the reliability
599 of the simulated results.

600

601 **CSP Parameter Ranges**

602 For the Constant Spacing Policy (CSP), the position tracking constant (k_p), speed correction coeffi-
603 cient (k_v), and desired spacing in meters ($S_{desired}$) parameters were optimized. The parameters
604 were assigned with appropriate ranges to facilitate the search for an optimal solution, as presented in
605 Table 2. The position tracking constant (k_p) adjusts the position relative to the target spacing. The
606 lower bound prevents slow reactions to ensure that the vehicle does not respond slowly to changes
607 in the leader vehicle's movement. The upper bound prevents excessive oscillations which could
608 lead to unstable behavior. The speed correction coefficient (k_v) adjusts the influence of the speed
609 differences between the ego and the leader vehicle. The minimum value ensures that the speed
610 correction is gradual while the upper value prevents the aggressive speed changes of the ego vehicle
611 which could lead to abrupt acceleration and deceleration cycles. The desired spacing ($S_{desired}$)
612 ensures the safe distance between the ego and the leader vehicle. The range allows the ego vehicle
613 not to follow too closely with the leader vehicle or unnecessarily slow down if the gap between the
614 ego and the leader vehicle is sufficient enough.

615

616 **CTH Parameter Ranges**

617 For the Constant Time Headway policy (CTH), the time headway in seconds (t_h), the minimum
 618 safety distance in meters (d_{min}), and damping factor (λ) parameters were optimized. The parameters
 619 were given an appropriate range respectively to ease finding an optimal solution shown in Table
 620 3. The time headway (t_h) represents the time interval between the ego and the leader vehicles
 621 to ensure safe following distance. The lower bound prevents the ego vehicle from dangerously
 622 following closely to the leader vehicle. The upper bound ensures that the ego vehicle does not
 623 unnecessarily slow down which could lead to big gaps causing inefficient traffic flow. The minimum
 624 safety distance (d_{min}) is the safety buffer between the ego and the leader vehicles. The lower bound
 625 is the minimum safe distance to ensure collisions and the upper bound prevents the ego vehicle from
 626 unnecessarily slowing down. The damping factor (λ) stabilizes the vehicle's response to speed
 627 fluctuations and time interval adjustments. The lower bound ensures that the damping factor is not
 628 too weak while the upper bound prevents the adjustments being too aggressive, allowing smooth
 629 transitions in vehicle dynamics.

630

631 **TFS Parameter Ranges**

632 For the Traffic Flow Stability policy (TFS), the traffic density in vehicles per meter (ρ_m), damping
 633 factor (λ), and free flow speed in meters per second (v_f) parameters were optimized. The parameters
 634 were given an appropriate range respectively to find an optimal solution shown in Table 4. The
 635 traffic density (ρ_m) ranges have been adjusted to ensure that the vehicle does not fall into unrealistic
 636 free-flow speed conditions. The range was chosen to replicate the typical traffic density along
 637 the freeways. The range for the damping factor (λ) balances the transient oscillations of the
 638 model and to stabilize traffic flow. The lower bound of the free flow speed (v_f) reflects the mod-
 639 erate traffic conditions and the upper bound represents the traffic conditions under optimal conditions.

640

641 **CSF Parameter Ranges**

642 For the Constant Safety Factor (CSF) policy, the safe distance in meters (d_{min}), damping factor
643 (λ), and braking dynamics coefficient (γ) were optimized to ensure safe and efficient car-following
644 behavior. The maximum deceleration for the i -th vehicle was set to -7.32 m/s^2 , while the time
645 delay was fixed at 0.05 seconds to account for realistic driver response times. Each parameter
646 was assigned an appropriate range to facilitate the search for an optimal solution, as presented
647 in Table 5. By calibrating these parameters using a genetic algorithm, the CSF policy enhances
648 stability and responsiveness, particularly in scenarios involving sudden braking or dense traffic
649 conditions. The range for the minimum safe distance (d_{min}) is slightly less than for other control
650 spacing policies because the safety factor (K) and braking dynamics coefficient (γ) were taken into
651 account for the CSF model. The damping factor smooths out the speed variations in response to the
652 changes in leader vehicle's movement. This range was chosen to enhance stability in both dense
653 traffic conditions and to prevent excessive stop-and-go oscillations. The lower bound of the safety
654 factor (K) ensures the vehicle reacts appropriately to speed changes while the upper bound prevents
655 aggressive responses to speed changes. The braking coefficient (γ) adjusts how aggressively the
656 braking is applied on the vehicle. The lower bound allows gradual braking adjustments while the
657 upper bound ensures braking in unprecedented situations.

658

659 **IDM Parameter Ranges**

660 Finally, for the Intelligent Driver Model (IDM), key parameters such as the minimum safe distance
661 (s_0) in meters, free-flow speed (v_0) in meters per second, time headway (T) in seconds, maximum
662 acceleration (a_{max}) in m/s^2 , and comfortable deceleration (b) in m/s^2 were optimized to ensure
663 safe and efficient car-following behavior. Each parameter was assigned a carefully chosen range
664 to balance realism and computational efficiency, facilitating the search for an optimal solution, as
665 presented in Table 6.

666

667 The chosen parameter ranges reflect realistic driving conditions and vehicle dynamics. The maxi-

668 mum acceleration range of 0.1 to 3.0 m/s^2 accounts for the diversity in vehicle performance, from
669 low-powered cars to high-performance vehicles. The desired velocity (v_0) is set between 10.0 and
670 30.0 m/s to cover typical urban and highway speed limits. The minimum spacing (s_0) is constrained
671 between 3.0 and 6.0 meters, ensuring that vehicles maintain a reasonable gap even at low speeds. A
672 time headway (T) range of 0.5 to 3.0 seconds accommodates variations in driver behavior, from
673 aggressive to conservative following. Finally, the comfortable deceleration (b) is limited between
674 0.5 and 3.0 m/s^2 to capture a balance between smooth and emergency braking scenarios. By
675 calibrating the chosen ranges for the parameters using a genetic algorithm, the IDM framework
676 enhances stability and responsiveness, particularly in challenging traffic conditions such as sudden
677 braking events or high-density congestion.

678
679 After determining the appropriate parameter ranges for optimization, the genetic algorithm calibrated
680 the car-following model for each control spacing policy. High-fidelity Interstate highway datasets
681 were utilized to model the simulated trajectories, ensuring realistic traffic conditions. Through
682 iterative evolution, the genetic algorithm performed multiple mutations and crossovers, refining the
683 intrinsic parameter values to achieve optimal performance. The final set of optimized parameters
684 was selected based on their ability to enhance vehicle stability, responsiveness, and overall traffic
685 efficiency.

686
687 **Simulated Trajectories**
688 The position-versus-time and speed-versus-time graphs were plotted to visualize the behavior of
689 the simulated follower vehicle in relation to both the leader vehicle and the target vehicle under
690 the various control spacing policies implemented. The following plots illustrate how the follower
691 vehicle adjusts its position and velocity over time in response to changes in the leader's motion,
692 allowing for a comparative analysis of the effectiveness of each spacing policy. Each graph assesses
693 the ability of each policy to maintain safe following distances, minimizing speed fluctuations, and
694 ensuring smooth acceleration and deceleration transitions.

695

696 **CSP I294 Simulated Results**

697 For the Constant Spacing Policy (CSP), the simulated results for I294 are illustrated in Figures 1a, 1b,
 698 2a, 2b, 3a, 3b, 4a, 4b, 5a, 5b, 6a, 6b, 7a, 7b, 8a, 8b, 9a, 9b, 10a, 10b, 11a, 11b, 12a, 12b, 13a and
 699 13b. Overall, the CSP policy effectively aligns the simulated trajectories with the target trajectories,
 700 demonstrating strong consistency in position tracking. However, speed deviations were observed
 701 during simulation, where the model occasionally followed the leader vehicle's speed pattern or
 702 slightly deviated from the target vehicle's speed profile. These variations indicate potential minor
 703 adjustments in the CSP model's responsiveness, particularly in adapting to dynamic traffic conditions.

704

705 The optimized parameter ranges for the CSP policy in the I294 dataset are shown in Figure 14.
 706 The desired spacing ($S_{desired}$) had the largest range, strongly indicating variability among the
 707 optimized values and suggesting that vehicle spacing preferences fluctuate across different driving
 708 conditions. Conversely, the control gains (k_v) and (k_p) were tightly clustered at lower values,
 709 ensuring consistent stability in vehicle acceleration and deceleration behavior.

710

711 Figure 15 shows that the distributions of (k_v) and (k_p) are skewed to the right, indicating that most op-
 712 timized values are concentrated near the lower end of the range but with occasional higher values. The
 713 ($S_{desired}$) is skewed to the left, showing that while some vehicles can maneuver traffic with relatively
 714 smaller gaps, in some situations, the vehicles may need larger spacing. The wide spread in ($S_{desired}$)
 715 suggests that variations in traffic density and driving behavior strongly influence optimal spacing.
 716 These observations indicate that CSP maintains consistent vehicle control while allowing adap-
 717 tive spacing flexibility, making it suitable for highway driving scenarios with varying traffic densities.

718

719 **CSP I90/94 Simulated Results**

720 The simulated results for I90/94 are presented in Figures 16a 16b, and 17 using the Constant Spacing
 721 Policy. From Figure 16a, the simulated follower tracks the target follower with minimum deviation.

722 This shows that the CSP model performs well on the I90-94 highway dataset. Although there is a
723 slight position deviation for vehicle 195 shown in Figure 16b, the simulated follower closely tracks
724 the simulated speed overall. Despite the speed deviation between the simulated follower and the
725 target follower for vehicle 286 shown in Figure 17, the simulated follower's position is well aligned
726 with the target follower's position.

727

728 The optimized parameter ranges for the I90/94 dataset using the CSP policy, illustrated in Figure
729 18, presents a significant variation across parameters. The desired spacing ($S_{desired}$) shows the
730 largest range, suggesting variability in vehicle gap preferences, which could be influenced by traffic
731 density and individual driving behaviors. In contrast, the control gains (k_v) and (k_p) remain
732 tightly clustered, indicating consistent vehicle response and stability in acceleration and deceleration
733 adjustments.

734

735 Figure 19 further reveals that the parameters follow discrete distributions, highlighting the presence
736 of distinct optimized values rather than a continuous spread. The narrow range of (k_v) and (k_p)
737 ensures the uniformity in control behavior, ensuring reliable adjustments in response to speed
738 changes. Meanwhile, the broader distribution of ($S_{desired}$) suggests that while most vehicles maintain
739 a consistent following distance, some scenarios demand significantly larger gaps to ensure safe and
740 stable car-following behavior. These findings indicate that CSP effectively maintains consistent
741 vehicle dynamics while allowing adaptability in spacing preferences, ensuring reliability for highway
742 driving conditions.

743

744 **CSP Phoenix Simulated Results**

745 The simulated results for the Phoenix dataset are presented in Figures 20a, 20b, 21a, and 21b.
746 The simulated follower closely aligns with the calibrated position and speed of the target fol-
747 lower, as shown in Figures 20a and 21b for vehicles 13 and 2 in run 9NS. However, noticeable
748 speed deviations are observed for vehicles 31 and 2 in run 9ES, as illustrated in Figures 20b and

749 21a. These deviations suggest that certain factors, such as acceleration responsiveness or vary-
750 ing traffic conditions, may have influenced the model's performance in maintaining a consistent speed.

751
752 The optimized parameter ranges for the CSP policy in the Phoenix dataset, as shown in Figure
753 22, highlight contrasts in parameter ranges. The desired spacing ($S_{desired}$) exhibits wider range
754 compared to the tightly clustered values of the control gains (k_v) and (k_p). This suggests that
755 vehicles demonstrate more variability in maintaining inter-vehicle distances, potentially due to
756 differences in traffic flow conditions and driver behaviors unique to the Phoenix dataset.

757
758 Figure 23 shows that the optimized parameters follow discrete distributions, with values concentrated
759 at specific points rather than being continuously spread. The clustering of (k_v) and (k_p) indicates
760 that acceleration and speed control adjustments remain relatively stable across different scenarios,
761 ensuring uniform response characteristics. Conversely, the broader distribution of ($S_{desired}$) implies
762 that spacing preferences are more dynamic, possibly adapting to varying traffic densities and driving
763 patterns. These findings suggest that while CSP effectively maneuvers the vehicle control dynamics,
764 allowing flexibility in spacing between vehicles under the Phoenix dataset.

765
766 **CTH I294 Simulated Results**
767 For Constant Time Headway policy (CTH), the simulated results for I294 are presented in Figures
768 24a,24b, 25a, 25b, 26a,26b, 27a,27b, 28a,28b, 29a, 29b, 30a, 30b, 31a,31b, 31b, 32a, 32b, 33a,
769 33b, 34a, 34b, 35a, 35b, 36a and 36b. By dynamically adjusting the time intervals, the simulated
770 trajectories generated by the CTH policy was able to closely track the target trajectories. Despite
771 some speed variations between the simulated follower and target follower, the position was closely
772 aligned.

773
774 The optimized parameter ranges for the CTH model in the I294 dataset, as shown in Figure 37,
775 strongly indicate variation among key parameters used for optimization. The parameters (t_h) and

776 d_{min} exhibit broad ranges, suggesting significant tuning variability in time headway and minimum
777 distance settings. In contrast, (λ) is tightly clustered around low values, indicating a high degree of
778 stability and minimal fluctuation during optimization.

779

780 Figure 38 illustrates the skewed distributions of (t_h) and (d_{min}) , where certain values appear more
781 frequently than others, implying potential biases toward specific parameter configurations. The
782 distribution of (λ) is notably sparse. This suggests that while (t_h) and d_{min} require more flexible
783 adjustments to accommodate diverse traffic conditions, (λ) remains relatively fixed to ensure
784 consistency in the CTH model's control strategy, indicating that the CTH model effectively adapts
785 to different traffic dynamics.

786

787 **CTH I90/94 Simulated Results**

788 The simulated results for I90/94 are presented in Figures 39a 39b, and 40 using the CTH policy. For
789 vehicle 5366 and 195, it can be determined that the controller can track the position with minimum
790 speed pattern deviations shown in Figures 39a and 39b. There is a deviation with speed patterns for
791 vehicle 286 shown in Figure 40 although the simulated position closely aligns with the target position.

792

793 The optimized parameter ranges for the CTH model in the I90/94 dataset illustrates variations across
794 different parameters. Figure 41 shows that (t_h) and (d_{min}) have relatively wider ranges, indicating
795 greater flexibility in their tuning to adapt to different traffic conditions. In contrast, (λ) remains
796 tightly clustered around low values, suggesting that this parameter is more constrained to ensure
797 stability in the model's response.

798

799 Furthermore, Figure 42 shows that all optimized parameters follow discrete distributions, implying
800 that the parameter tuning converges to specific values rather than a continuous range. This suggests
801 that certain parameter settings are more favorable for achieving stable and reliable control behavior
802 under varying highway conditions. The narrow clustering of (λ) shows that consistent system

803 dynamics were maintained, while the broader range of (t_h) and (d_{min}) indicates that time headway
804 and minimum distance must be more adaptable to handling fluctuations in traffic flow.

805

806 CTH Phoenix Simulated Results

807 The simulated results for the CTH model in the Phoenix dataset are presented in Figures 43a, 43b,
808 44a, and 44b. The simulated follower closely aligns with the calibrated position and speed of
809 the target follower, as shown in Figures 43a and 44b for vehicles 13 and 2 in run 9NS. However,
810 noticeable speed deviations are observed for vehicles 31 and 2 in run 9ES, as illustrated in Figures 43b
811 and 44a. These deviations suggest that certain factors, such as acceleration responsiveness or vary-
812 ing traffic conditions, may have influenced the model's performance in maintaining a consistent speed.

813

814 The optimized parameter ranges for the CTH model in the Phoenix dataset illustrate variations
815 across parameters. As shown in Figure 45, (d_{min}) shows a relatively wider range compared to (t_h),
816 indicating flexible tuning parameters. In contrast, the (λ) values remain tightly clustered, suggesting
817 minimal variations in controlling fluctuating behavior and ensuring system stability.

818

819 Figure 46 clearly shows a bimodal distribution for both (t_h) and (d_{min}), implying that certain values
820 are consistently favored during calibration. This strongly indicates the presence of distinct driving
821 conditions or vehicle behaviors leading to the model selecting preferred parameter values over
822 others. The narrow spread of (λ) maintains smooth acceleration adjustments and prevents excessive
823 fluctuations in speed. These findings highlight the importance of adaptive tuning for (t_h) and (d_{min}),
824 while (λ) remains a relatively stable control parameter across different scenarios.

825

826 TFS I294 Simulated Results

827 For Traffic Flow Stability policy (TFS), the simulated results for I294 are presented in Figures 47a,
828 47b, 48a, 48b, 49a, 49b, 50a, 50b, 51a, 51b, 52a, 52b, 53a, 53b, 54a, 54b, 54b, 55a, 55b, 56a, 56b,
829 57a, 57b, 58a, 58b, 59a and 59b. The TFS model emphasizes stabilizing the traffic flow of vehicles

830 and the generated simulated follower has performed well aligning the simulated position and speed
831 with the target follower with some deviations.

832
833 The optimized parameter ranges for the TFS model in the I294 dataset shows variability across
834 different parameters, as shown in Figure 60. The (v_f) had the largest range, indicating significant
835 variations in free-flow speed due to changing traffic conditions and driving behaviors. In contrast,
836 (ρ_m) and (λ) remain tightly clustered, suggesting that these parameters have maintained consistency
837 during the calibration process.

838
839 Figure 61 illustrates the skewness of the parameter distributions. Specifically, (ρ_m) and (λ) are
840 left-skewed, implying that lower values were more frequently selected during optimization, while
841 (v_f) is skewed to the right, indicating that higher values were more frequently selected, reflecting
842 varying traffic flow speeds and free-flow conditions in the dataset.

843
844 **TFS I90/94 Simulated Results**

845 The simulated results for TFS model in the I90/94 dataset are presented in Figures 62a 62b, and 63
846 using the TFS model. For vehicle 5366 and 195, it can be determined that the controller can track
847 the position with minimum speed pattern deviations shown in Figures 62a and 62b. However, there
848 is a minor deviation with speed patterns for vehicle 286 shown in Figure 63 although the simulated
849 position closely aligns with the target position.

850
851 The optimized parameter ranges for the TFS model in the I90/94 dataset, as shown in Figure
852 64, indicate small variations across parameters. While (v_f) has the highest range, the numeric
853 values remain tightly clustered, suggesting a consistent free-flow speed across different calibration
854 instances. Similarly, (ρ_m) and (λ) maintain low ranges with minimal variation, indicating that
855 traffic flow sensitivity and stability adjustments are relatively uniform across different traffic scenarios.

856

857 Figure 65 illustrates that the optimized parameters follow discrete distributions, with values concen-
858 trated at specific numeric points rather than being continuously spread out. This pattern suggests that
859 the model favors specific parameter values during optimization, potentially due to traffic dynamics
860 constraints in the dataset. The consistent clustering of (ρ_m) and (λ) stabilizes flow fluctuations,
861 while the narrow distribution of (v_f) suggests the vehicle maintaining appropriate free-flow speed.

862

863 **TFS Phoenix Simulated Results**

864 The simulated results for the TFS model in the Phoenix dataset are presented in Figures 66a, 66b,
865 67a, and 67b. The simulated follower closely aligns with the calibrated position and speed of
866 the target follower, as shown in Figures 66a and 67b for vehicles 13 and 2 in run 9NS. However,
867 noticeable speed deviations are observed for vehicles 31 and 2 in run 9ES, as illustrated in Figures
868 66b and 67a.

869

870 The optimized parameter ranges for the TFS model in the Phoenix dataset, as shown in Figure 68,
871 indicate minimal variability across parameters. The free-flow speed (v_f) remains highly consistent,
872 with values tightly clustered around a high range, suggesting a uniform traffic flow behavior in the
873 dataset. Similarly, (ρ_m) and (λ) has minimal variation, indicating that traffic density sensitivity and
874 stability adjustments remain relatively consistent across different calibration runs.

875

876 Figure 69 shows that the optimized parameters follow discrete distributions, with values concentrated
877 at specific numeric points rather than being continuously spread. This pattern suggests that the
878 TFS model consistently selects specific parameter values during calibration. The narrow clustering
879 of (ρ_m) and (λ) suggests that their roles in regulating flow stability remain uniform, maintaining
880 consistent traffic dynamics.

881

882 **CSF I294 Simulated Results**

883 For Constant Safety Factor policy (CSF), the simulated results for I294 are presented in Figures
884 70a, 70b, 71a, 71b, 72a, 72b, 73a, 73b, 74a, 74b, 75a, 75b, 76a, 76b, 77a, 77b, 77b, 78a, 78b,
885 79a, 79b, 80a, 80b, 81a, 81b, 82a, and 82b. The CSF model adjusts the trajectories by taking into
886 safety parameters such as the safety factor (K), braking coefficient (γ), and safety distance (d_{min})
887 to closely align the simulated position and speed with the target position and speed. Overall, the
888 simulated position strongly aligns with the target position despite some speed variations.

889 The optimized parameter ranges for the CSF model in the I294 dataset, as illustrated in Figure
890 83, shows significant variability across parameters. The parameter (d_{min}) has the highest degree
891 of variability, with a broad range, indicating that the minimum desired spacing fluctuates based
892 on different traffic conditions. Conversely, (K), (λ), and (γ) has relatively narrower distributions.
893 However, multiple outliers have been shown, suggesting that in certain calibration cases, the
894 optimization process deviated from the primary values chosen.

895
896 Figure 84 shows that the distribution of (λ) is skewed to the right, with lower values appearing more
897 frequently, indicating that most optimized solutions favor smaller stability coefficients. Similarly,
898 the majority of (γ) values are concentrated near zero, implying that braking adjustments were
899 not applied aggressively in the optimization process. Additionally, the multi-modal distributions
900 observed for (d_{min}) and (K) suggest that multiple distinct parameter groupings exist, due to safety
901 adjustments in response to varied traffic conditions.

902
903 The outliers in (K), (λ), and (γ) suggests occasional extreme parameter values, which may be the
904 result of unusual traffic flow dynamics or specific cases where it was necessary for the TFS model
905 to apply more aggressive control actions to maintain stability and safety. It is indicative that the
906 outlier numeric values had to be used in response of the vehicle trying to adjust the unusual traffic
907 condition to ensure safety in driving.

908

909 **CSF I90/94 Simulated Results**

910 The simulated results for I90/94 are presented in Figures 85a 85b, and 86 using the CSF Policy. For
911 vehicle 5366 and 195, it can be determined that the controller can track the position with minimum
912 speed pattern deviations shown in Figures 85a and 85b. However, there is a minor deviation with
913 speed patterns for vehicle 286 shown in Figure 86 although the simulated position closely aligns
914 with the target position.

915
916 The optimized parameter ranges for the CSF model in the I90/94 dataset, as depicted in Figure
917 87, show limited variation across most parameters. The parameter (d_{min}) shows the widest range,
918 evidently showing the CSF policy's emphasis on maintaining safe following distances under varying
919 traffic conditions. Conversely, the parameters (K), (λ), and (γ) remain tightly clustered, suggesting
920 that the control gains and braking adjustments are more consistent across different scenarios.

921
922 Figure 88 shows that the optimized parameters follow discrete distributions, with values concentrated
923 at specific numerical points rather than being continuously spread out. The tight clustering of (K) and
924 (λ) indicates that the model consistently stabilizes around particular parameter values, minimizing
925 fluctuations in vehicle behavior. Similarly, (γ) is clustered near the value zero, suggesting that
926 braking was not applied too aggressively. Thus, smoother deceleration patterns were shown rather
927 than abrupt braking maneuvers.

928
929 There were no outlier values during calibration which suggests that the optimization process consis-
930 tently converged to a well-defined solution space, ensuring the model's reliability in maintaining
931 stable vehicle behavior. However, the broader spread in (d_{min}) indicates greater adaptability in
932 determining safe spacing based on external traffic conditions.

933

934 **CSF Phoenix Simulated Results**

935 The simulated results for the for the CSF model in the Phoenix dataset are presented in Figures 89a,
936 89b, 90a, and 90b. The simulated follower closely aligns with the calibrated position and speed of
937 the target follower, as shown in Figures 89a and 90b for vehicles 13 and 2 in run 9NS. However,
938 noticeable speed deviations are observed for vehicles 31 and 2 in run 9ES, as illustrated in Figures
939 89b and 90a.

940

941 The optimized parameter ranges for the CSF policy in the Phoenix dataset are presented in Figure
942 91, showing variations across different parameters. The parameter (K) exhibits the widest range,
943 suggesting greater adaptability in control response under varying traffic conditions. The parameter
944 (d_{min}) also shows a relatively wide range, indicating that safe following distances are more flexible
945 just like the parameter (K).

946

947 In contrast, the parameters (λ) and (γ) remain tightly clustered, suggesting consistent values across
948 different calibration scenarios. An outlier value is observed in (d_{min}), indicating a result where
949 the optimized parameter deviates from the general range calibrated. Figure 92 illustrates that the
950 parameters follow discrete distributions, with values concentrated at specific points rather than being
951 continuously spread out. This suggests that the optimization process consistently favors certain
952 parameter values.

953

954 **IDM I294 Simulated Results**

955 For Intelligent Driver Model (IDM), the simulated results for I294 are presented in Figures 93a, 93b,
956 94a, 94b, 95a, 95b, 96a, 96b, 97a, 97b, 98a, 98b, 99a, 99b, 100a, 100b, 100b, 101a, 101b, 102a,
957 102b, 103a, 103b, 104a, 104b, 105a, and 105b. The IDM calibrates the trajectories by finding the
958 most optimal parameter such as the max acceleration (a), desired speed (v_0), safe distance (s_0),
959 time headway (T), and comfort deceleration value (b) for braking. Overall, the simulated position
960 strongly aligns with the target position despite some speed variations.

961
962 The optimized parameter ranges for the IDM model in the I294 dataset are presented in Figure 106,
963 illustrating variability among different parameters. The desired speed (v_0) exhibits the widest range,
964 indicating that vehicles frequently operate at a relatively higher free-flow speed while maintaining
965 safe following distances while driving in the highway.

966
967 Conversely, the parameters maximum acceleration (a_{max}), time headway (T), and comfortable
968 deceleration (b) remain tightly clustered at the calibrated ranges, implying that the system requires
969 minimal abrupt adjustments to ensure stability in traffic flow. The safe distance between vehicles
970 (s_0) also shows moderate variability, indicating some adaptation in stopping distances based on
971 different driving behaviors.

972
973 Furthermore, as illustrated in Figure 107, the optimized parameters follow multi-modal distributions,
974 reflecting the diversity in driving behavior across different traffic conditions. This suggests that the
975 calibration process effectively captures varying driving tendencies, from conservative to more aggres-
976 sive driving styles, ensuring robust adaptation of the IDM model in real-world highway environments.

977
978 **CSF I90/94 Simulated Results**

979 The simulated results for I90/94 are presented in Figures 108a 108b, and 109 using IDM. For vehicle
980 5366 and 195, it can be determined that the controller can track the position with minimum speed
981 pattern deviations shown in Figures 108a and 108b. However, there is a minor deviation with speed
982 patterns for vehicle 286 shown in Figure 109 although the simulated position closely aligns with the
983 target position.

984
985 The optimized parameter ranges for IDM in the I90/94 dataset are illustrated in Figure 110, showing
986 variations across different parameters. The desired speed (v_0) has the widest range, suggesting
987 that vehicles frequently travel at free-flow speed while maintaining a safe following distance. This

988 indicates flexibility in speed adaptations.

989

990 In contrast, parameters such as the maximum acceleration (a_{max}), time headway (T), and comfort-
991 able deceleration (b) remain within a tighter range, implying consistent acceleration and braking
992 behaviors with minimal sudden adjustments required for maintaining traffic stability. The safe
993 distance between vehicles (s_0) also shows some variation, indicating variations in stopping distance.

994

995 Furthermore, as shown in Figure 111, the optimized parameters follow multi-modal distributions,
996 suggesting varying driving behaviors across different traffic conditions. This variability of opti-
997 mized parameters calibrated shows both conservative and aggressive driving behaviors replicating
998 real-world driving patterns.

999

1000 **IDM Phoenix Simulated Results**

1001 The simulated results for the for IDM in the Phoenix dataset are presented in Figures 112a, 112b, 113a,
1002 and 113b. The simulated follower closely aligns with the calibrated position and speed of the target
1003 follower, as shown in Figures 112a and 113b for vehicles 13 and 2 in run 9NS. However, noticeable
1004 speed deviations are observed for vehicles 31 and 2 in run 9ES, as illustrated in Figures 112b and 113a.

1005

1006 The optimized parameter ranges for the Intelligent Driver Model (IDM) in the Phoenix dataset are
1007 presented in Figure 114, revealing notable variability across different parameters. The desired speed
1008 (v_0) exhibits the largest variation, indicating that vehicles operate under diverse speed conditions,
1009 due to differences in driver behavior or fluctuating traffic conditions.

1010

1011 In contrast, the maximum acceleration (a_{max}), time headway (T), and comfortable deceleration (b)
1012 remain within a more confined range. These results indicate that vehicles experience fewer abrupt
1013 acceleration and braking maneuvers, leading to more stable and safe car-following behavior. The
1014 safe distance between vehicles (s_0) is relatively small, strongly suggesting that vehicles maintain

1015 close following distances, due to high-density traffic scenarios in the dataset.

1016
1017 Additionally, some outliers are observed across multiple parameters during calibration, particularly
1018 in (s_0) and (b), suggesting that some vehicles had more aggressive or conservative driving behaviors.
1019 These outliers indicate that the vehicles had to adjust its control inputs in response to exceptional
1020 cases of unusually short headways or higher deceleration rates, deviating from the general traffic trend.

1021
1022 Figure 115 presents the distributions of the calibrated IDM parameters following multi-modal
1023 distributions. The distribution of (v_0) suggests distinct driving groups with varying speed values,
1024 while the acceleration and deceleration distributions indicate that most of the times, the vehicles
1025 adhere to a common driving pattern with minimal deviations. Multiple peaks of the calibrated
1026 parameters in the histograms shows the adaptability of IDM in replicating changing driving behaviors,
1027 ensuring a realistic representation of vehicle interactions within the Phoenix dataset.

1028
1029 **Model Comparison**

1030 The control spacing policies were evaluated across the major highway datasets from I294, I90/94
1031 and Phoenix. While the genetic algorithm calibrates the optimal parameters for each control spacing
1032 policy, the fitness function calculates the critical error metrics including the Mean Squared Error
1033 (MSE), Root Mean Squared Error (RMSE), Mean Absolute Error (MAE), Mean Absolute Percentage
1034 Error (MAPE), Normalized Root Mean Squared Error (NMSE), Sum of Squared Errors (SSE),
1035 and R^2 values to evaluate how well the model can align the simulated trajectories with the target
1036 trajectories. Results for each model in different highway datasets are shown in Table 7. The overall
1037 performance of the models across all the highway datasets are presented in Table 8. These results
1038 implies that some control spacing policies may be suitable for varying traffic environments where
1039 other control spacing policies may be more appropriate for less fluctuating traffic environments.
1040 The CSP model has demonstrated stable performance across all the highway datasets used for this
1041 study, showing relatively low error values across all metrics calculated by the fitness function.

1042 The CSP model had the lowest RMSE value of 0.243 and the highest R^2 value of 0.964 in the
1043 I90/94 dataset, indicating a strong alignment between the simulated and target trajectories during
1044 calibration. However, the MAPE value of 8.949% in the Phoenix dataset suggests that the CSP
1045 model struggles to encounter the external factors that affect the inter-vehicular spacing. Stability has
1046 been maintained most of the time and the simulated trajectories generated by the CSP model closely
1047 aligns then target trajectories.

1048

1049 The CTH model had slightly higher MSE and RMSE values compared to the CSP model, suggesting
1050 a marginally weaker performance in tracking the trajectories. The high MAPE value of 13.556% in
1051 the I90/94 dataset implies that the model is more sensitive to speed variations between the leading
1052 and the surrounding vehicles. However, the R^2 values consistently remained above 0.940, suggesting
1053 that the simulated trajectories were mostly well-aligned with the target trajectories. Overall, the
1054 CTH model performs comparably to CSP, although it appears more prone to speed variations in
1055 dynamic traffic conditions.

1056

1057 The TFS policy had the highest error metrics across all the highway datasets, evidently showing
1058 higher deviations between the simulated and target trajectories. The MAPE value of 15.661% in
1059 the I90/94 dataset is significantly higher than the MAPE values of other models, suggesting that
1060 the TFS policy struggles to maintain stability in congested traffic conditions. While the R^2 values
1061 remain above 0.91, the high error values indicate that the TFS policy is less robust compared to the
1062 other models considered in this study. This suggests that TFS may not effectively handle variations
1063 in acceleration and deceleration, leading to suboptimal trajectory predictions. Additionally, the
1064 relatively higher RMSE and SSE values indicate that errors accumulate over time, further impacting
1065 the ability to align itself with the target trajectory in dynamic highway conditions.

1066

1067 The CSF policy has demonstrated overall stable performance by effectively balancing vehicle
1068 dynamics and trajectory alignment while prioritizing safety. The CSF model achieved the lowest

1069 RMSE value of 0.566 in the I294 dataset, indicating strong predictive accuracy. However, the
1070 relatively high MAPE value of 14.533% suggests some difficulties in adapting to varying traffic
1071 conditions, particularly in scenarios with abrupt speed changes. Despite this, with R^2 values
1072 consistently above 0.94, the CSF model exhibits strong target trajectory tracking capabilities, making
1073 it a reliable choice for maintaining smooth and stable traffic flow.

1074
1075 The IDM model has exhibited mixed performance across the highway datasets. The model achieved
1076 the lowest RMSE value of 0.204 in the I90/94 dataset, indicating strong trajectory alignment under
1077 relatively stable highway conditions. However, the model struggled in the Phoenix dataset, where it
1078 had the highest MAPE value of 22.665%, suggesting significant difficulty in adapting to varying
1079 traffic conditions and external disturbances. The overall R^2 values remained high, exceeding 0.92,
1080 showing that IDM can reasonably align itself with the target trajectories. However, the MAPE in
1081 Phoenix indicates that IDM may be more sensitive to traffic flow variations and abrupt decelerations
1082 compared to CSP and CSF.

1083
1084 Based on the overall dataset performance, it can be determined that the CSP and CSF policies are
1085 the most reliable control spacing models, having the lowest RMSE values and consistently high
1086 R^2 scores. The CTH model, while effective, appears less suitable for scenarios involving frequent
1087 speed variations. In contrast, the TFS policy displayed the highest errors, indicating challenges
1088 in maintaining stable traffic flow. The IDM model, while effective in stable conditions, exhibited
1089 higher errors in complex environments, suggesting a need for refined parameter tuning. Given the
1090 calibration results, CSP and CSF are the most appropriate models for simulating car-following
1091 behavior, while the TFS policy and IDM may require additional modifications to improve robustness
1092 in fluctuating traffic conditions.

1093
1094 **CONCLUSION**

1095 Maintaining appropriate and safe following gap between vehicles is critical for autonomous

1096 vehicles. The five most commonly used policies which are Constant Spacing Policy (CSP), Constant
1097 Time Headway (CTH), Traffic Flow Stability (TFS), Constant Safety Factor (CSF), and the Intelligent
1098 Driver Model (IDM) were calibrated using the genetic algorithm to find the optimized parameters
1099 for each policy respectively using the highway datasets from I294, I90/94, and Phoenix Waymo
1100 vehicle trajectories for simulating the control spacing models.

1101
1102 The simulated plots comparing trajectories generated by control spacing policies and observed
1103 trajectories illustrate how well the generated trajectories align with the observed trajectories. The
1104 trajectories simulated by CSP and CSF models closely aligned with the observed vehicle trajectories,
1105 demonstrating minimal perturbations in both position and speed of the vehicles across stable traffic
1106 conditions. These models effectively and safely maintained the inter-vehicular spacing, achieving
1107 smoother trajectory profiles with fewer oscillations. Conversely, the IDM model showed greater
1108 variability in certain conditions but the model was able to replicate realistic acceleration and deceler-
1109 ation patterns, making it suitable for dynamic traffic environments. The CTH model was effective in
1110 controlled conditions, despite the occasional perturbations under conditions where the surrounding
1111 vehicles rapidly change their speeds. The TFS model consistently demonstrated higher trajectory er-
1112 rors, particularly in congested scenarios, indicating its limited reliability in complex traffic conditions.

1113
1114 The performance of the control spacing policies were contingent on the traffic conditions. The
1115 CSP and CSF policies were relatively more reliable by consistently achieving the lowest Root
1116 Mean Squared Error (RMSE) and highest R^2 values. The CSP model showed stable performance
1117 under low-density highway conditions by maintaining uniform spacing effectively with minimal
1118 perturbations. The CSF policy was determined to be performing optimally in high-density scenarios,
1119 effectively managing critical safety concerns, including abrupt acceleration and braking events, due
1120 to the dynamic safety-margin adjustments.

1121
1122 While the CTH policy showed robust performance similar to CSP in stable conditions, it exhibited

1123 increased sensitivity and higher errors under scenarios with significant speed variations. This high-
1124 lights the model's limitations in adapting swiftly to fluctuating speeds. The TFS policy consistently
1125 produced higher errors across datasets, reflecting challenges in handling congested, dynamically
1126 complex traffic scenarios, and thus was the least reliable for accurate trajectory prediction.

1127

1128 The Intelligent Driver Model (IDM) demonstrated strong performance in accurately simulating
1129 realistic driver behavior across diverse traffic conditions. The IDM model was also able to replicate
1130 smooth acceleration and deceleration patterns. However, achieving optimal performance required
1131 precise calibration, especially in high-density scenarios where dynamic adjustments to speed and
1132 spacing are frequent.

1133

1134 In conclusion, the CSP model is recommended for scenarios prioritizing stability and uniform
1135 traffic flow, typically in lower-density highway conditions. The CSF policy is effective when safety
1136 considerations need to be prioritized, such as dense traffic conditions requiring frequent adjustments
1137 to spacing between the surrounding vehicles. The IDM is suitable for accurately modeling realistic
1138 vehicle behavior but demands meticulous calibration. Future research should explore hybrid spacing
1139 policies integrating multiple strategies to integrate individual models for more adaptive and resilient
1140 implementations for self-driving technology.

1141 **ACKNOWLEDGMENTS**

1142 Special thanks to Assistant Professor Alireza Talebpour at the Department of Civil and Environmental
1143 Engineering at the University of Illinois at Urbana-Champaign, and to Post Doc Gihyeob An for the
1144 suggested control spacing models that were analyzed for this research.

1145

1146 **References**

1147 Ammourah, R., Beigi, P., Fan, B., Hamdar, S. H., Hourdos, J., Hsiao, C.-C., James, R., Khajeh-
1148 Hosseini, M., Mahmassani, H. S., Monzer, D., Radvand, T., Talebpour, A., Yousefi, M., and

- 1149 Zhang, Y. (2024). “Introduction to the third generation simulation dataset: Data collection and
1150 trajectory extraction.” *Transportation Research Record*, 1–17.
- 1151 An, G. and Talebpour, A. (2019). “Lane-changing trajectory optimization to minimize traffic flow
1152 disturbance in a connected automated driving environment.” *2019 IEEE Intelligent Transportation
1153 Systems Conference (ITSC)*, 1794–1799.
- 1154 An, G. and Talebpour, A. (2022). “Vehicle platooning control for merge coordination: A hybrid
1155 acc-dmpc approach.” *2022 IEEE 25th International Conference on Intelligent Transportation
1156 Systems (ITSC)*, 1611–1616.
- 1157 Barooah, P., Mehta, P. G., and Hespanha, J. P. (2009). “Mistuning-based control design to improve
1158 closed-loop stability margin of vehicular platoons.” *IEEE Transactions on Automatic Control*,
1159 54(9), 2100–2113.
- 1160 Cesari, G., Schildbach, G., Carvalho, A., and Borrelli, F. (2017). “Scenario model predictive control
1161 for lane change assistance and autonomous driving on highways.” *IEEE Intelligent Transportation
1162 Systems Magazine*, 9(3), 23–35.
- 1163 Chen, D., Ahn, S., Chitturi, M., and Noyce, D. (2018). “Truck platooning on uphill grades
1164 under cooperative adaptive cruise control (cacc).” *Transportation Research Part C: Emerging
1165 Technologies*, 94, 50–66 ISTTT22.
- 1166 Ciuffo, B., Mattas, K., Makridis, M., Albano, G., Anesiadou, A., He, Y., Josvai, S., Komnos, D.,
1167 Pataki, M., Vass, S., and Szalay, Z. (2021). “Requiem on the positive effects of commercial
1168 adaptive cruise control on motorway traffic and recommendations for future automated driving
1169 systems.” *Transportation Research Part C: Emerging Technologies*, 130, 103305.
- 1170 D. Swaroop, J.K. Hedrick, C. C. C. and Ioannou, P. (1994). “A comparision of spacing and headway
1171 control laws for automatically controlled vehicles.” *Vehicle System Dynamics*, 23(1), 597–625.
- 1172 Darbha, S. and Rajagopal, K. (1999). “Intelligent cruise control systems and traffic flow stability.”
1173 *Transportation Research Part C: Emerging Technologies*, 7(6), 329–352.
- 1174 Delis, A., Nikolos, I., and Papageorgiou, M. (2015). “Macroscopic traffic flow modeling with
1175 adaptive cruise control: Development and numerical solution.” *Computers and Mathematics with*

- 1176 *Applications*, 70(8), 1921–1947.
- 1177 Delpiano, R., Herrera, J. C., Laval, J., and Coeymans, J. E. (2020). “A two-dimensional car-following
1178 model for two-dimensional traffic flow problems.” *Transportation Research Part C: Emerging
1179 Technologies*, 114, 504–516.
- 1180 Donà, R., Mattas, K., He, Y., Albano, G., and Ciuffo, B. (2022). “Multianticipation for string
1181 stable adaptive cruise control and increased motorway capacity without vehicle-to-vehicle
1182 communication.” *Transportation Research Part C: Emerging Technologies*, 140, 103687.
- 1183 Federal Highway Administration (FHWA) (2024). “Third Generation Simulation (TGSIM) Data.
1184 Available: https://catalog.data.gov/dataset/?q=Third+Generation+Simulation+Data&sort=views_recent+desc&publisher=Federal+Highway+Administration&organization=dot-gov&ext_location=&ext_bbox=&ext_prev_extent=. Accessed: Nov.
1185 25, 2024.
- 1186 Ioannou, P. and Chien, C. (1993). “Autonomous intelligent cruise control.” *IEEE Transactions on
1187 Vehicular Technology*, 42(4), 657–672.
- 1188 Ioannou, P., Xu, Z., Eckert, S., Clemons, D., and Sieja, T. (1993). “Intelligent cruise control: theory
1189 and experiment.” *Proceedings of 32nd IEEE Conference on Decision and Control*, 1885–1890
1190 vol.2.
- 1191 Kesting, A., Treiber, M., Schönhof, M., and Helbing, D. (2008). “Adaptive cruise control design for
1192 active congestion avoidance.” *Transportation Research Part C: Emerging Technologies*, 16(6),
1193 668–683.
- 1194 Kilic, I., Yazici, A., Yildiz, O., Özçelikors, M., and Ondoan, A. (2015). “Intelligent adaptive cruise
1195 control system design and implementation.” *2015 10th System of Systems Engineering Conference,
1196 SoSE 2015*, 232–237.
- 1197 Li, P. Y. and Shrivastava, A. (2002). “Traffic flow stability induced by constant time headway policy
1198 for adaptive cruise control vehicles.” *Transportation Research Part C: Emerging Technologies*,
1199 10(4), 275–301.
- 1200 Li, S., Li, K., Rajamani, R., and Wang, J. (2011). “Model predictive multi-objective vehicular

- adaptive cruise control.” *IEEE Transactions on Control Systems Technology*, 19(3), 556–566.
- Luu, D. L., Lupu, C., Ismail, L. S., and Alshareefi, H. (2020). “Spacing control of cooperative adaptive cruise control vehicle platoon.” *2020 IEEE International Conference on Automation, Quality and Testing, Robotics (AQTR)*, 1–6.
- Maxim, A., Caruntu, C. F., and Lazar, C. (2017). “Cruise and headway control for vehicle platooning using a distributed model predictive control algorithm.” *2017 21st International Conference on System Theory, Control and Computing (ICSTCC)*, 146–151.
- Milanés, V., Shladover, S. E., Spring, J., Nowakowski, C., Kawazoe, H., and Nakamura, M. (2014). “Cooperative adaptive cruise control in real traffic situations.” *IEEE Transactions on Intelligent Transportation Systems*, 15(1), 296–305.
- Moon, S., Moon, I., and Yi, K. (2009). “Design, tuning, and evaluation of a full-range adaptive cruise control system with collision avoidance.” *Control Engineering Practice*, 17(4), 442–455.
- Naus, G. J. L., Vugts, R. P. A., Ploeg, J., van de Molengraft, M. J. G., and Steinbuch, M. (2010). “String-stable cacc design and experimental validation: A frequency-domain approach.” *IEEE Transactions on Vehicular Technology*, 59(9), 4268–4279.
- Nilsson, P., Hussien, O., Balkan, A., Chen, Y., Ames, A. D., Grizzle, J. W., Ozay, N., Peng, H., and Tabuada, P. (2016). “Correct-by-construction adaptive cruise control: Two approaches.” *IEEE Transactions on Control Systems Technology*, 24(4), 1294–1307.
- Rajamani, R., Tan, H.-S., Law, B. K., and Zhang, W.-B. (2000). “Demonstration of integrated longitudinal and lateral control for the operation of automated vehicles in platoons.” *IEEE Transactions on Control Systems Technology*, 8(4), 695–708.
- Rajamani, R. and Zhu, C. (2002). “Semi-autonomous adaptive cruise control systems.” *Vehicular Technology, IEEE Transactions on*, 51, 1186 – 1192.
- Santhanakrishnan, K. and Rajamani, R. (2003). “On spacing policies for highway vehicle automation.” *IEEE Transactions on Intelligent Transportation Systems*, 4(4), 198–204.
- Sipahi, R., Niculescu, S.-I., and Delice, I. I. (2009). “Asymptotic stability of constant time headway driving strategy with multiple driver reaction delays.” *2009 American Control Conference*,

- 1230 4898–4903.
- 1231 Swaroop, D. and Hedrick, J. K. (1999). “Constant spacing strategies for platooning in automated
1232 highway systems.” *Journal of Dynamic Systems, Measurement, and Control*, 121(3), 462–470.
- 1233 Talebpour, A. and Mahmassani, H. S. (2016). “Influence of connected and autonomous vehicles on
1234 traffic flow stability and throughput.” *Transportation Research Part C: Emerging Technologies*,
1235 71, 143–163.
- 1236 Talebpour, A., Mahmassani, H. S., and Hamdar, S. H. (2018). “Effect of information availability
1237 on stability of traffic flow: Percolation theory approach.” *Transportation Research Part B:
1238 Methodological*, 117, 624–638 TRB:ISTTT-22.
- 1239 Talebpour, A., Mahmassani, H. S., and Hamdar, S. H. (2024). “Third generation simulation data
1240 (tgSim): A closer look at the impacts of automated driving systems on human behavior.” *Report
1241 No. FHWA-JPO-24-133*, Federal Highway Administration, University of Illinois at Urbana-
1242 Champaign, Urbana, Illinois 61801 (5). The project CORs were Rachel James and John Hourdos.
1243 The JPO Program Manager was Hyungjun Park.
- 1244 Thede, S. (2004). “An introduction to genetic algorithms.” *Journal of Computing Sciences in
1245 Colleges*, 20.
- 1246 Treiber, M., Hennecke, A., and Helbing, D. (2000). “Congested traffic states in empirical observations
1247 and microscopic simulations.” *Physical Review E*, 62(2), 1805–1824.
- 1248 van Arem, B., van Driel, C. J. G., and Visser, R. (2006). “The impact of cooperative adaptive cruise
1249 control on traffic-flow characteristics.” *IEEE Transactions on Intelligent Transportation Systems*,
1250 7(4), 429–436.
- 1251 Wang, J. and Rajamani, R. (2004a). “The impact of adaptive cruise control systems on highway
1252 safety and traffic flow.” *Proceedings of the Institution of Mechanical Engineers, Part D: Journal
1253 of Automobile Engineering*, 218(2), 111–130.
- 1254 Wang, J. and Rajamani, R. (2004b). “Should adaptive cruise-control systems be designed to maintain
1255 a constant time gap between vehicles?” *IEEE Transactions on Vehicular Technology*, 53(5),
1256 1480–1490.

- 1257 Wang, M., Hoogendoorn, S. P., Daamen, W., van Arem, B., and Happee, R. (2015). “Game theoretic
1258 approach for predictive lane-changing and car-following control.” *Transportation Research Part*
1259 *C: Emerging Technologies*, 58, 73–92.
- 1260 Wu, C., Xu, Z., Liu, Y., Fu, C., Li, K., and Hu, M. (2020). “Spacing policies for adaptive cruise
1261 control: A survey.” *IEEE Access*, 8, 50149–50162.
- 1262 Yanakiev, D. and Kanellakopoulos, I. (1995). “Variable time headway for string stability of automated
1263 heavy-duty vehicles.” *Proceedings of 1995 34th IEEE Conference on Decision and Control*,
1264 Vol. 4, 4077–4081 vol.4.
- 1265 Zhang, Y., Kosmatopoulos, B., Ioannou, P., and Chien, C. (1999). “Using front and back information
1266 for tight vehicle following maneuvers.” *IEEE Transactions on Vehicular Technology*, 48(1),
1267 319–328.
- 1268 Zhang, Y., Monzer, D., Li, N., Okoth, V., Chen, Z., Hsiao, C.-C., Radvand, T., Mahmassani, H. S.,
1269 Hamdar, S. H., and Talebpour, A. (2025). “Coexistence in motion: Unveiling the behavioral
1270 dynamics of humans and highly automated vehicles in naturalistic mixed traffic.” *Presented at the*
1271 *TRB 103rd Annual Meeting* Paper No. TRBAM-25-05831, Washington, D.C.
- 1272 Zhao, J. and El Kamel, A. (2010). “Coordinated throttle and brake fuzzy controller design for vehicle
1273 following.” *13th International IEEE Conference on Intelligent Transportation Systems*, 659–664.
- 1274 Zhao, S. and Zhang, K. (2020). “A distributionally robust stochastic optimization-based model
1275 predictive control with distributionally robust chance constraints for cooperative adaptive cruise
1276 control under uncertain traffic conditions.” *Transportation Research Part B: Methodological*, 138,
1277 144–178.
- 1278 Zheng, Y., Li, S. E., Li, K., Borrelli, F., and Hedrick, J. K. (2017). “Distributed model predictive
1279 control for heterogeneous vehicle platoons under unidirectional topologies.” *IEEE Transactions*
1280 *on Control Systems Technology*, 25(3), 899–910.
- 1281 Zhou, Y., Ahn, S., Chitturi, M., and Noyce, D. A. (2017). “Rolling horizon stochastic optimal
1282 control strategy for acc and cacc under uncertainty.” *Transportation Research Part C: Emerging*
1283 *Technologies*, 83, 61–76.

1284	List of Tables		
1285	1	Constant parameters for simulating the genetic algorithm.	52
1286	2	Parameter ranges for Constant Spacing Policy.	53
1287	3	Parameter ranges for Constant Time Headway policy.	54
1288	4	Parameter ranges for Traffic Flow Stability policy.	55
1289	5	Parameter ranges for Constant Safety Factor policy.	56
1290	6	Parameter ranges for Intelligent Driver Model.	57
1291	7	Performance comparison of different models on various datasets.	58
1292	8	Overall performance of models across the highway datasets.	59

Parameter	Range
Population Size	100
Number of Generations	100
Mutation Rate	0.1

Table 1. Constant parameters for simulating the genetic algorithm.

Parameter	Range
k_p	(0.01, 1.5)
k_v	(0.01, 0.9)
S_{desired}	(2.5, 10.0)

Table 2. Parameter ranges for Constant Spacing Policy.

Parameter	Range
t_h	(1.5, 2.0)
d_{min}	(2.5, 3.5)
λ	$(1.0 \times 10^{-5}, 1.0 \times 10^{-4})$

Table 3. Parameter ranges for Constant Time Headway policy.

Parameter	Range
ρ_m	(0.10, 0.15)
λ	(0.10, 0.40)
v_f	(25.00, 35.00)

Table 4. Parameter ranges for Traffic Flow Stability policy.

Parameter	Range
d_{min}	(2.50, 3.00)
λ	(0.01, 0.40)
K	(0.50, 3.00)
γ	(0.10, 0.50)

Table 5. Parameter ranges for Constant Safety Factor policy.

Parameter	Range
a_{max}	(0.1, 3.0)
v_0	(10.0, 30.0)
s_0	(3.0, 6.0)
T	(0.5, 3.0)
b	(0.5, 3.0)

Table 6. Parameter ranges for Intelligent Driver Model.

Model	Dataset	Error	MSE	RMSE	MAE	MAPE	NRMSE	SSE	R²
CSP	I294L1	494.344	0.473	0.604	0.435	3.359	0.066	49.174	0.902
CSP	I90/94	125.986	0.063	0.243	0.188	11.443	0.052	44.904	0.964
CSP	Phoenix	177.835	0.252	0.443	0.337	8.949	0.047	136.000	0.968
CTH	I294L1	514.590	0.527	0.639	0.457	3.805	0.069	48.538	0.894
CTH	I90/94	129.926	0.067	0.245	0.198	13.556	0.054	45.883	0.956
CTH	Phoenix	166.755	0.227	0.421	0.311	8.501	0.044	125.144	0.971
TFS	I294L1	526.597	0.493	0.619	0.428	3.845	0.063	55.824	0.911
TFS	I90/94	162.373	0.094	0.305	0.246	15.661	0.068	63.905	0.939
TFS	Phoenix	175.720	0.290	0.458	0.336	11.781	0.048	153.492	0.966
CSF	I294L1	495.446	0.417	0.566	0.400	3.897	0.058	42.474	0.929
CSF	I90/94	137.392	0.074	0.266	0.208	15.025	0.059	50.214	0.952
CSF	Phoenix	182.762	0.270	0.473	0.363	14.353	0.051	143.946	0.964
IDM	I294L1	414.087	0.368	0.538	0.384	2.993	0.064	389.799	0.893
IDM	I90/94	106.421	0.046	0.204	0.161	8.302	0.045	31.795	0.971
IDM	Phoenix	176.835	0.370	0.577	0.448	22.665	0.072	152.224	0.916

Table 7. Performance comparison of different models on various datasets.

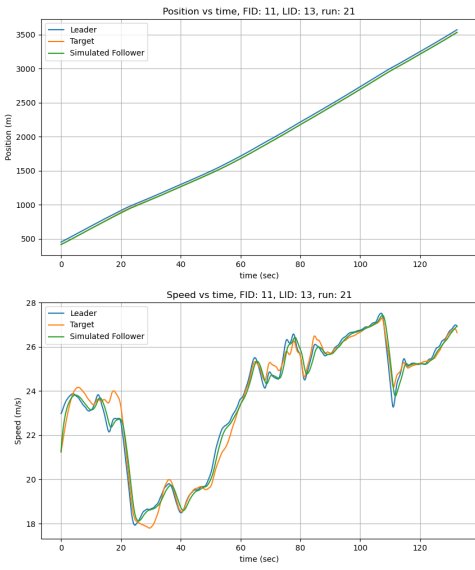
Model	Error	MSE	RMSE	MAE	MAPE	NRMSE	SSE	R²
CSP	266.055	0.263	0.430	0.320	7.917	0.055	232.296	0.945
CTH	270.424	0.274	0.435	0.322	8.621	0.056	241.246	0.940
TFS	288.230	0.293	0.461	0.337	10.429	0.060	265.179	0.939
CSF	271.867	0.254	0.435	0.324	11.092	0.056	229.596	0.948
IDM	232.448	0.261	0.440	0.331	11.320	0.060	191.273	0.927

Table 8. Overall performance of models across the highway datasets.

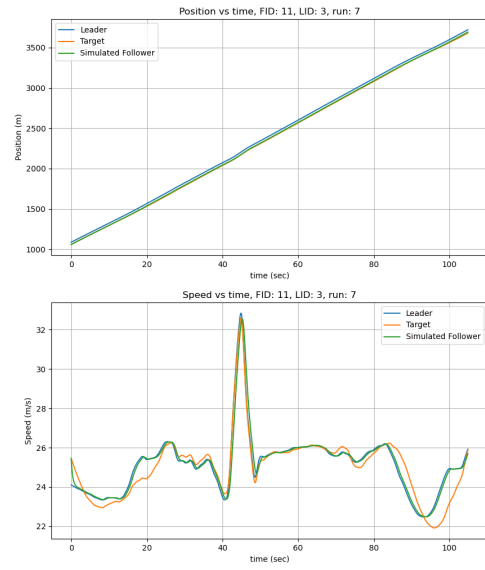
1293 **List of Figures**

1294	14	Parameter ranges for CSP in I294L1 dataset.	75
1295	15	Parameter histogram for CSP in I294L1 dataset.	76
1296	17	Position and speed for CSP for vehicle 286 in I90/94 dataset.	78
1297	18	Parameter ranges for CSP in I90/94.	79
1298	19	Parameter histogram for CSP in I90/94.	80
1299	22	Parameter ranges for CSP in Phoenix.	83
1300	23	Parameter histogram for CSP in Phoenix.	84
1301	37	Parameter ranges for CTH in I294L1 dataset.	98
1302	38	Parameter histogram for CTH in I294L1 dataset.	99
1303	40	Position and speed for CTH for vehicle 286 in I90/94 dataset.	101
1304	41	Parameter ranges for CTH in I90/94.	102
1305	42	Parameter histogram for CTH in I90/94.	103
1306	45	Parameter ranges for CTH in Phoenix.	106
1307	46	Parameter histogram for CTH in Phoenix.	107
1308	60	Parameter ranges for TFS in I294L1 dataset.	121
1309	61	Parameter histogram for TFS in I294L1 dataset.	122
1310	63	Position and speed for TFS for vehicle 286 in I90/94 dataset.	124
1311	64	Parameter ranges for TFS in I90/94.	125
1312	65	Parameter histogram for TFS in I90/94.	126
1313	68	Parameter ranges for TFS in Phoenix.	129
1314	69	Parameter histogram for TFS in Phoenix.	130
1315	83	Parameter ranges for CSF in I294L1 dataset.	144
1316	84	Parameter histogram for CSF in I294L1 dataset.	145
1317	86	Position and speed for CSF for vehicle 286 in I90/94 dataset.	147
1318	87	Parameter ranges for CSF in I90/94.	148
1319	88	Parameter histogram for CSF in I90/94.	149

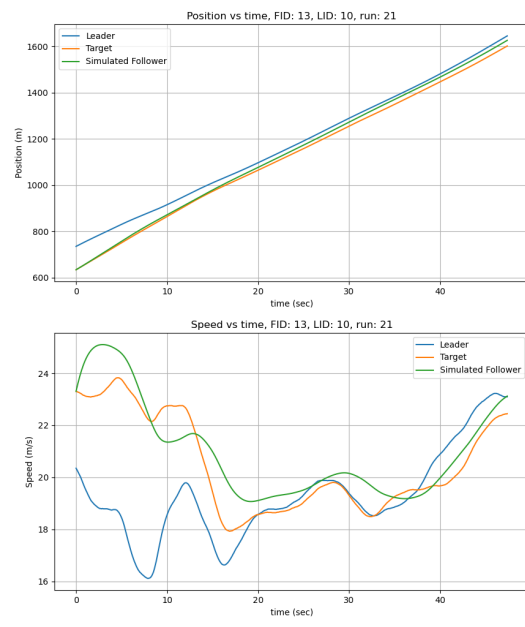
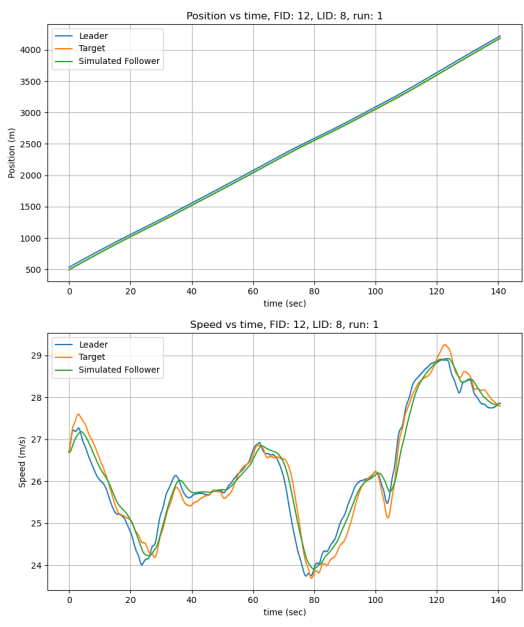
1320	91	Parameter ranges for CSF in Phoenix.	152
1321	92	Parameter histogram for CSF in Phoenix.	153
1322	106	Parameter ranges for 04IDM in I294L1 dataset.	167
1323	107	Parameter histogram for 04IDM in I294L1 dataset.	168
1324	109	Position and speed for IDM for vehicle 286 in I90/94 dataset.	170
1325	110	Parameter ranges for IDM in I90/94.	171
1326	111	Parameter histogram for IDM in I90/94.	172
1327	114	Parameter ranges for IDM in Phoenix.	175
1328	115	Parameter histogram for IDM in Phoenix.	176

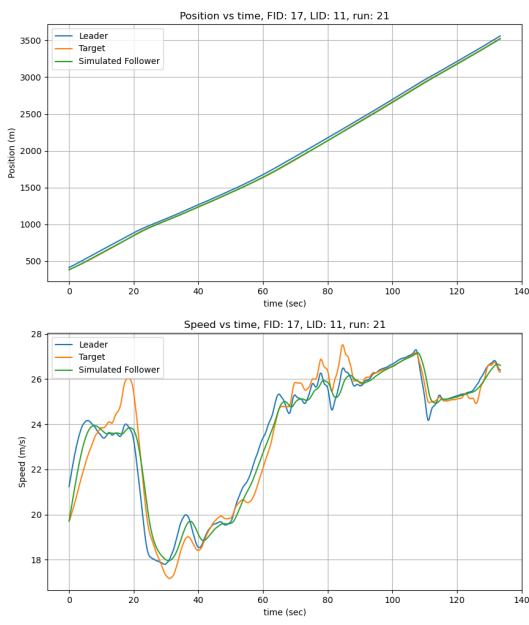


(a) Position and speed for CSP for vehicle 11 in run 21 I294L1 dataset.

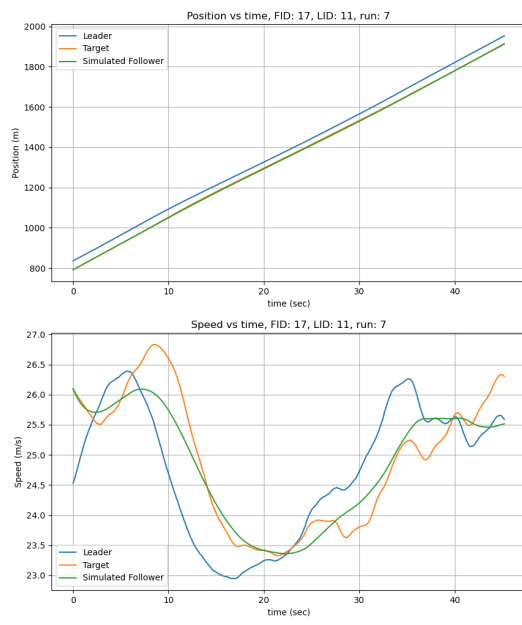


(b) Position and speed for CSP for vehicle 11 in run 7 I294L1 dataset.

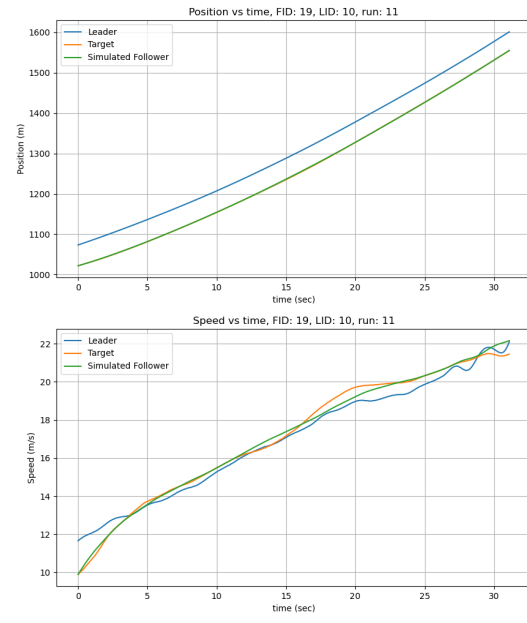
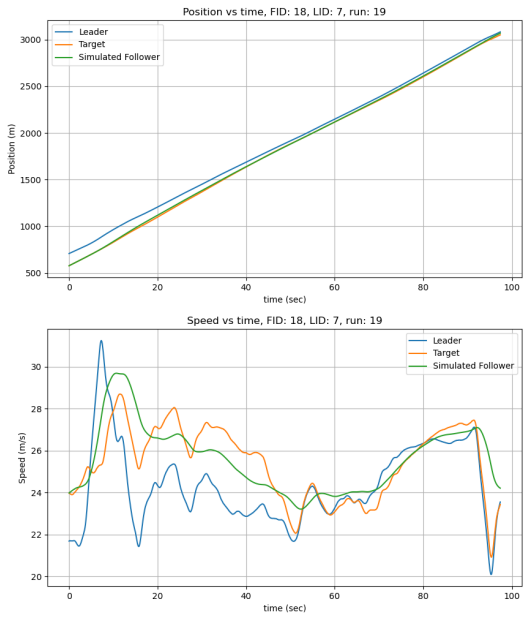


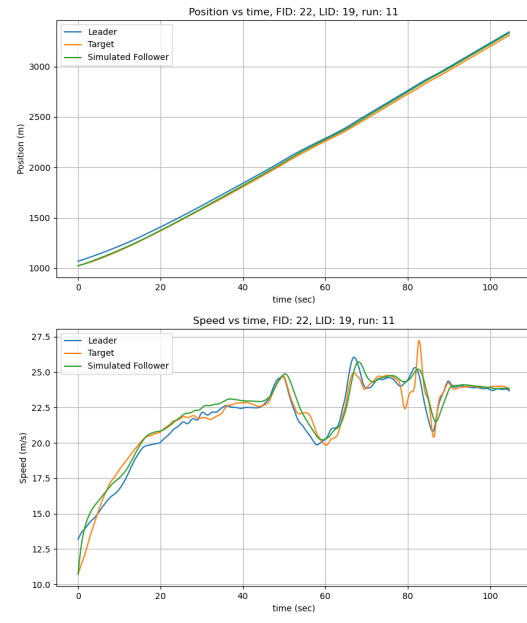
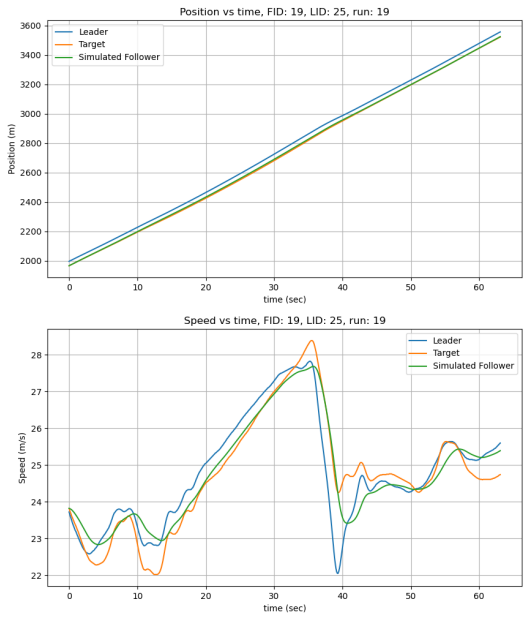


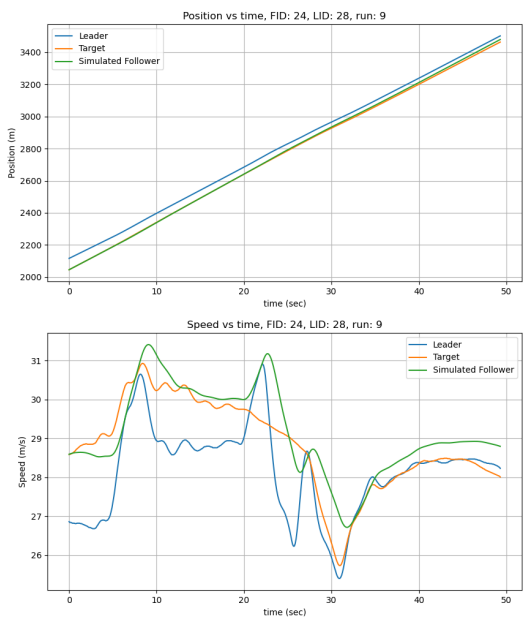
(a) Position and speed for CSP for vehicle 17 in run 21 I294L1 dataset.



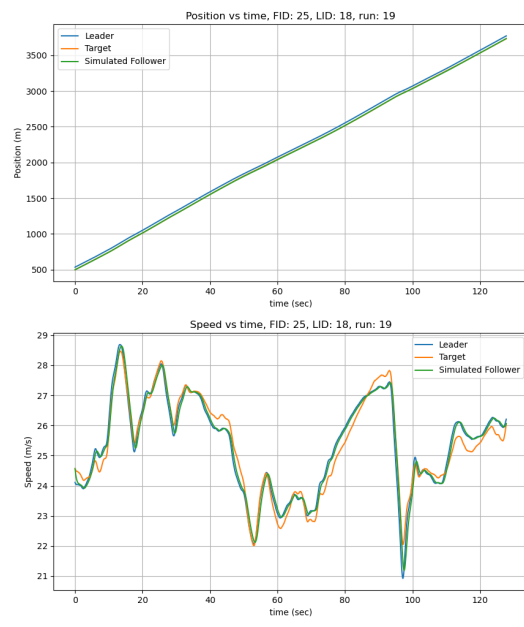
(b) Position and speed for CSP for vehicle 17 in run 7 I294L1 dataset.



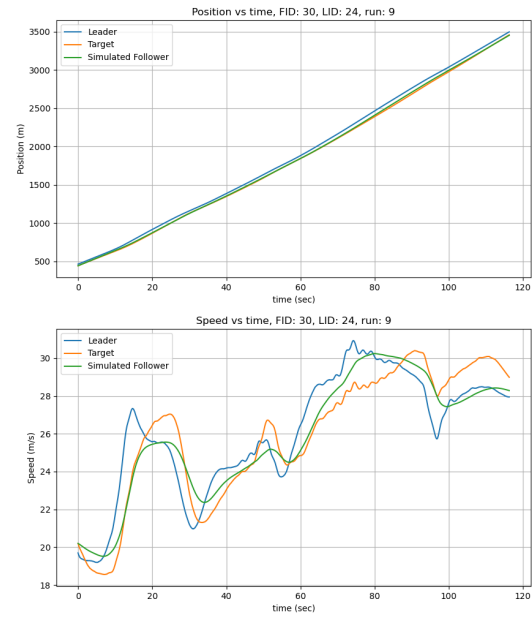
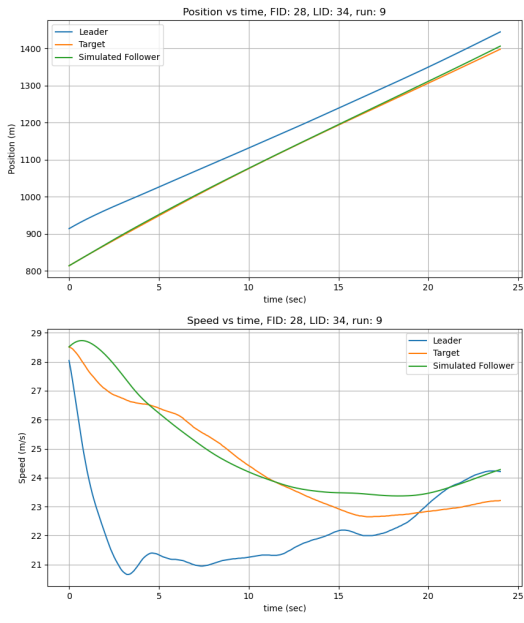


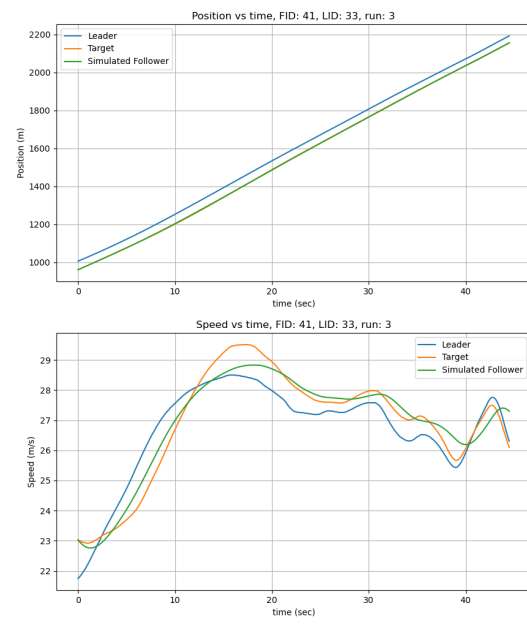
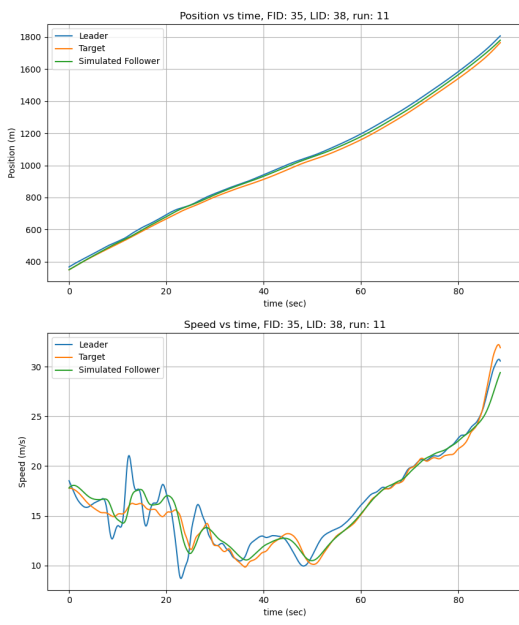


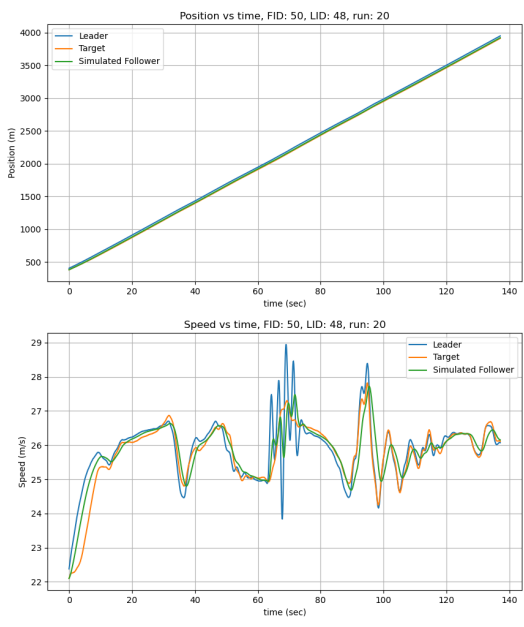
(a) Position and speed for CSP for vehicle 24 in run 9
I294L1 dataset.



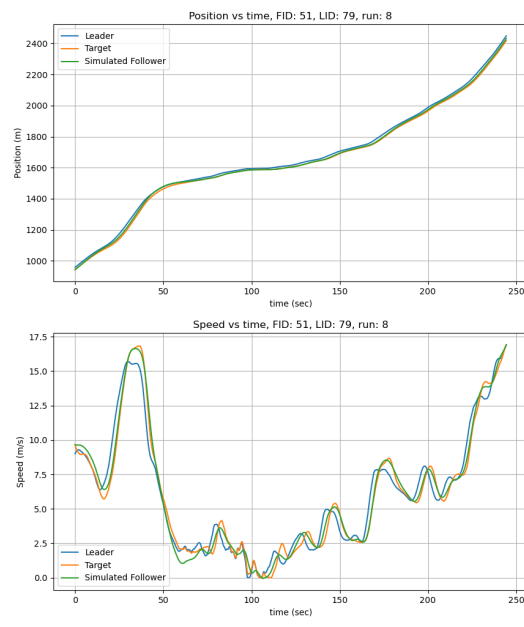
(b) Position and speed for CSP for vehicle 25 in run 19 I294L1 dataset.



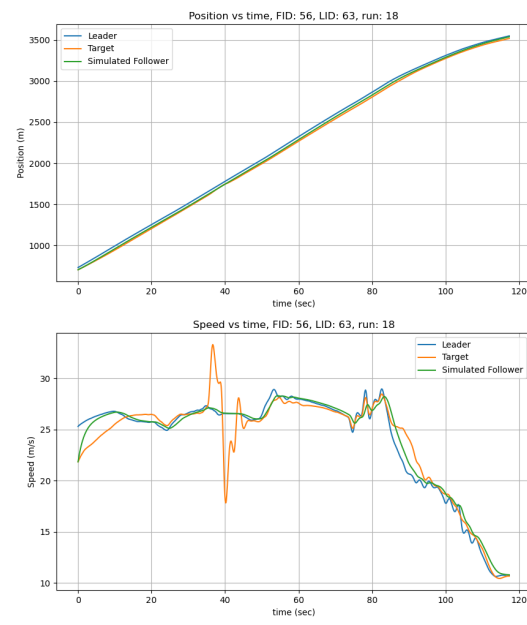
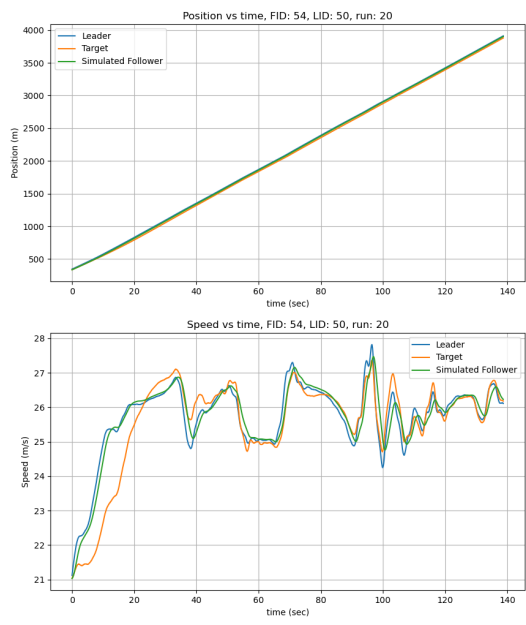


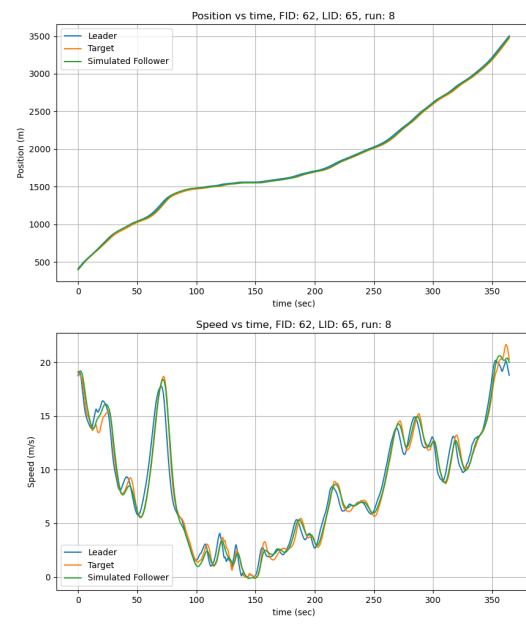
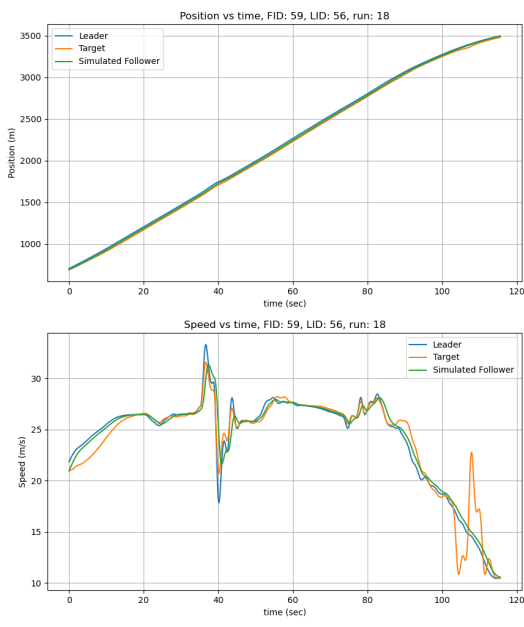


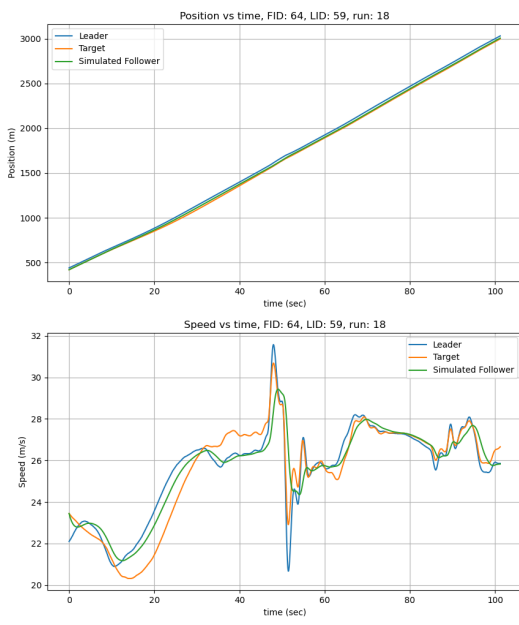
(a) Position and speed for CSP for vehicle 50 in run 20 I294L1 dataset.



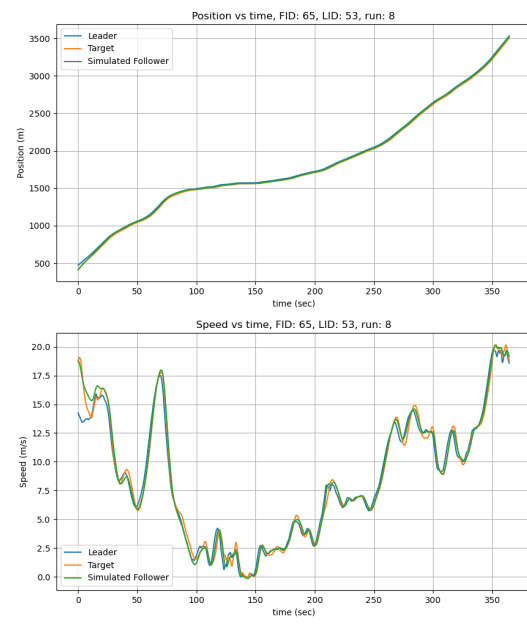
(b) Position and speed for CSP for vehicle 51 in run 8 I294L1 dataset.



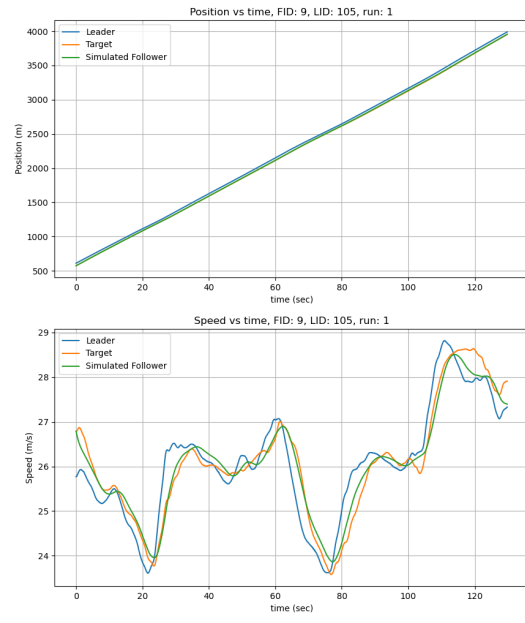
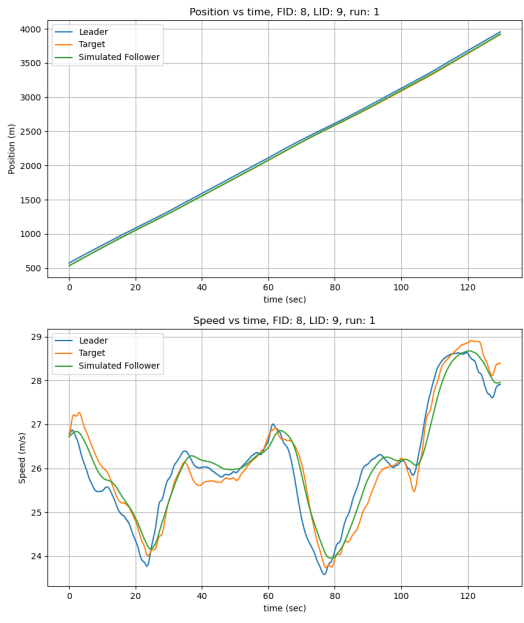




(a) Position and speed for CSP for vehicle 64 in run 18 I294L1 dataset.



(b) Position and speed for CSP for vehicle 65 in run 8 I294L1 dataset.



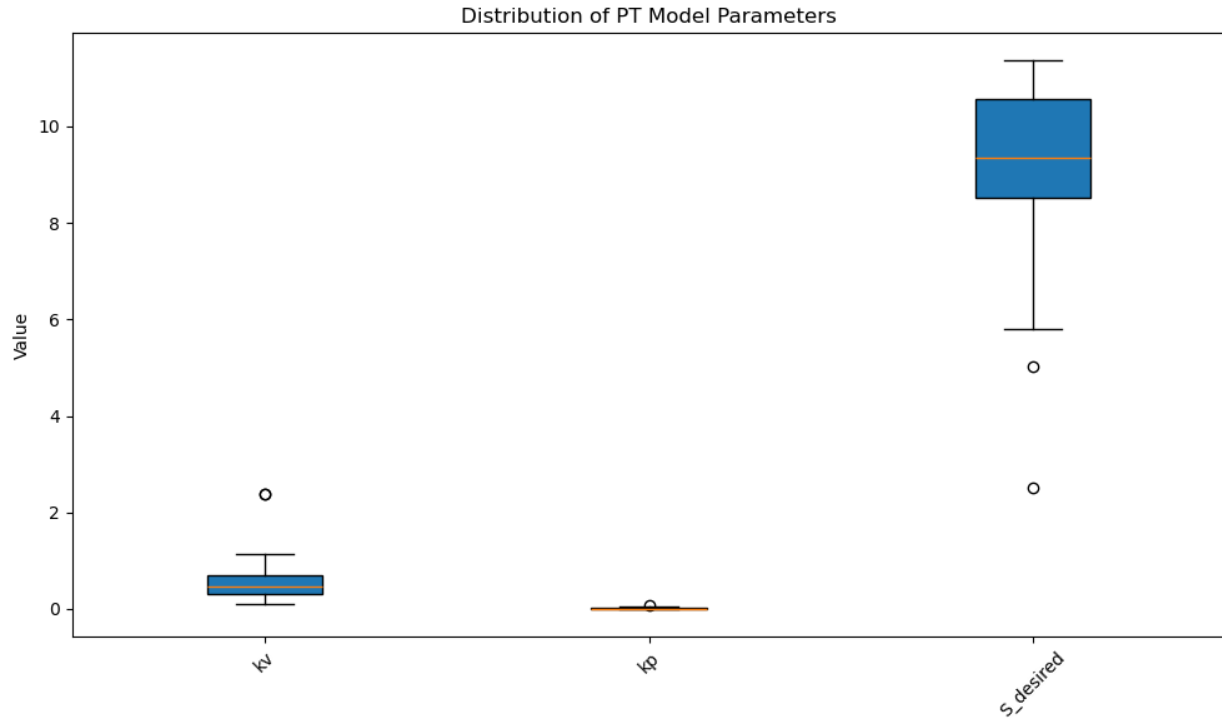


Fig. 14. Parameter ranges for CSP in I294L1 dataset.

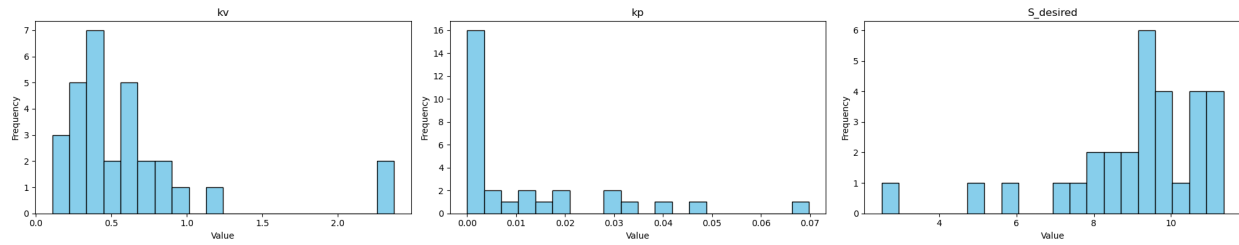
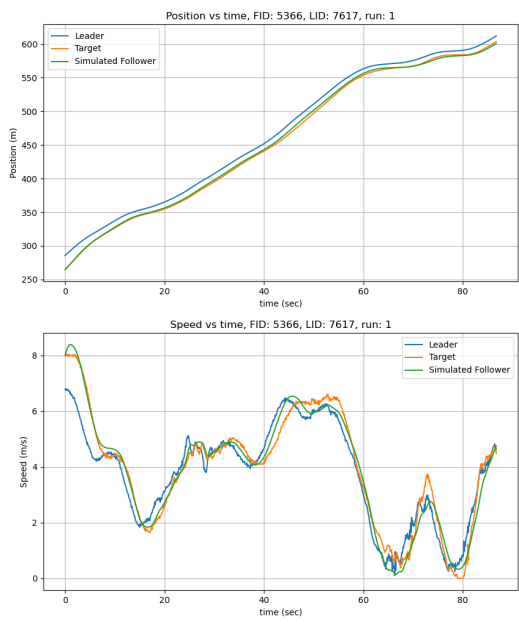
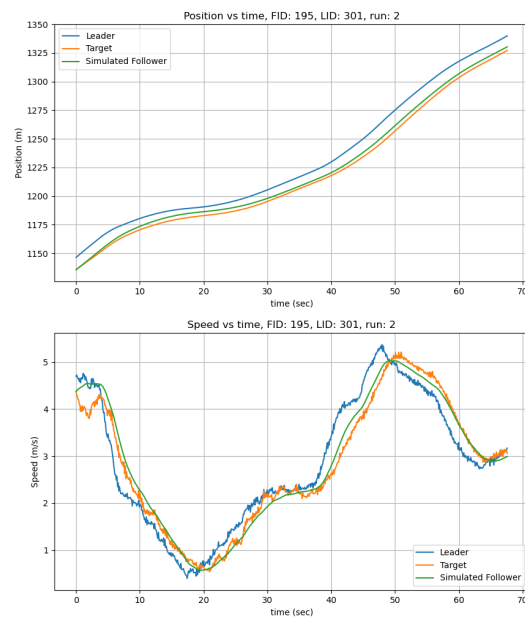


Fig. 15. Parameter histogram for CSP in I294L1 dataset.



(a) Position and speed for CSP for vehicle 5366 in I90/94 dataset.



(b) Position and speed for CSP for vehicle 195 in I90/94 dataset.

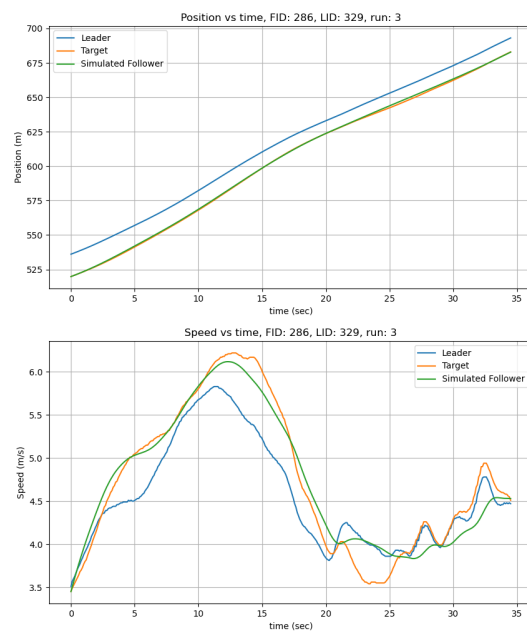


Fig. 17. Position and speed for CSP for vehicle 286 in I90/94 dataset.

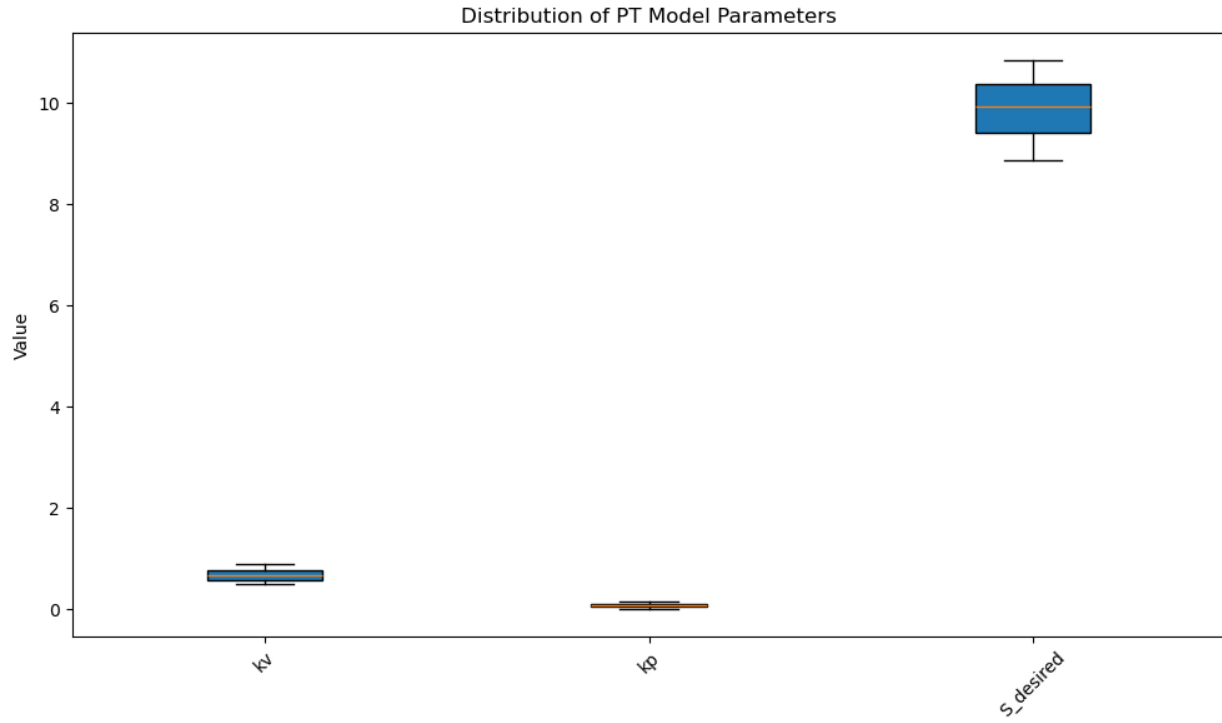


Fig. 18. Parameter ranges for CSP in I90/94.

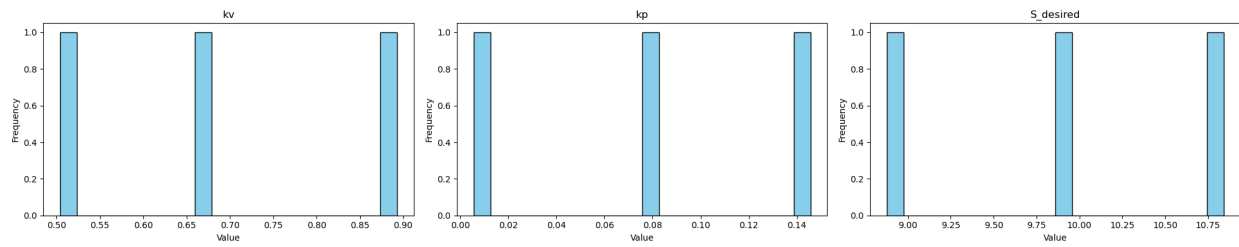
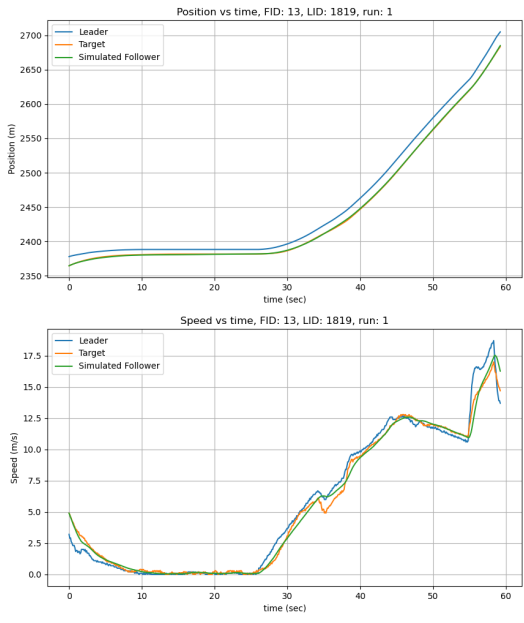
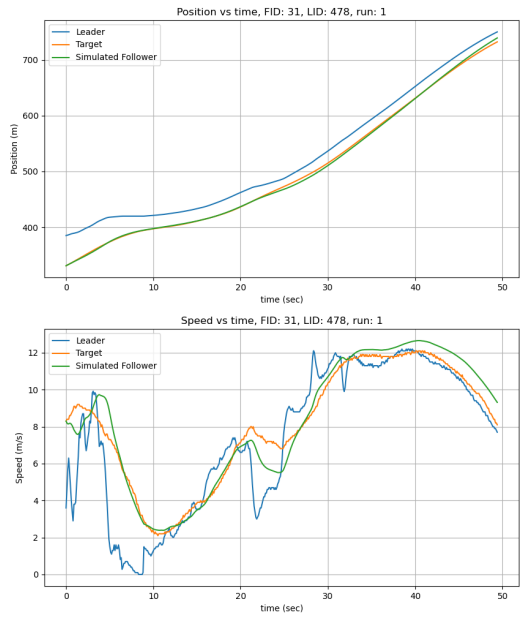


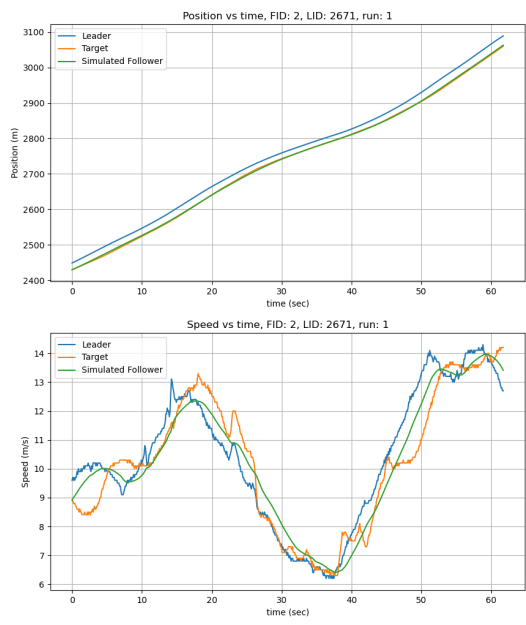
Fig. 19. Parameter histogram for CSP in I90/94.



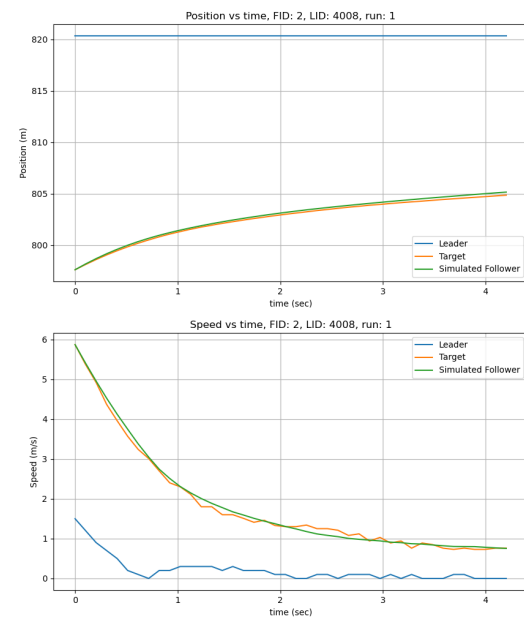
(a) Position and speed for CSP for vehicle 13 in Phoenix data H1A3 run 6.



(b) Position and speed for CSP for vehicle 31 in Phoenix data H1A3 run 1.



(a) Position and speed for CSP for vehicle 2 in Phoenix data H1A3 run 9 ES.



(b) Position and speed for CSP for vehicle 2 in Phoenix data H1A3 run 9 NS.

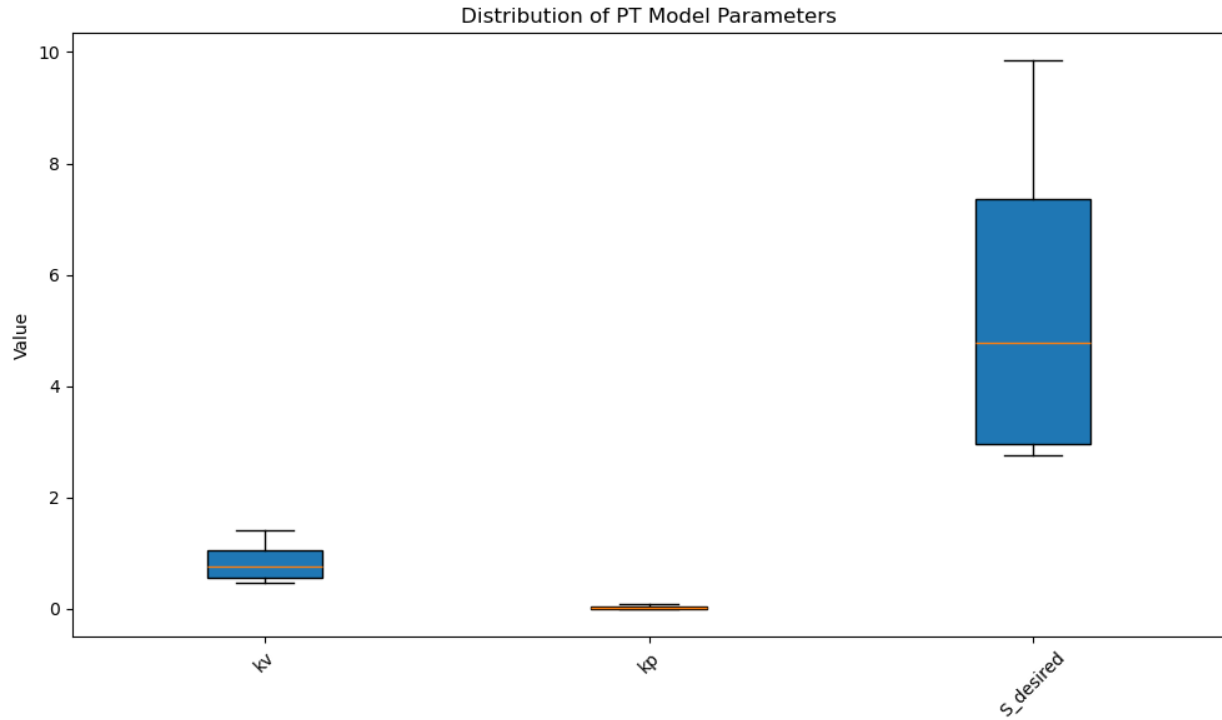


Fig. 22. Parameter ranges for CSP in Phoenix.

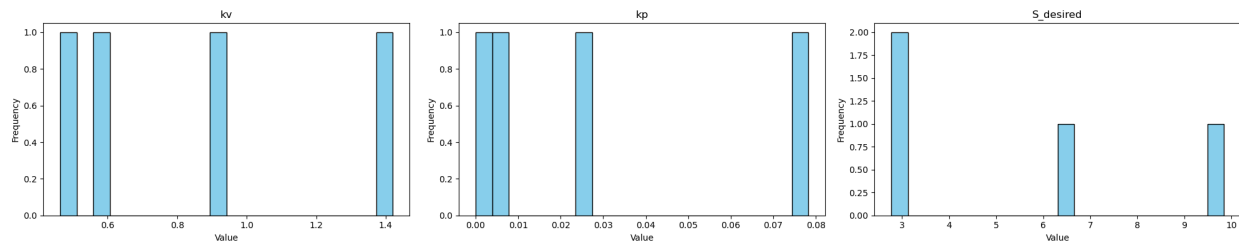
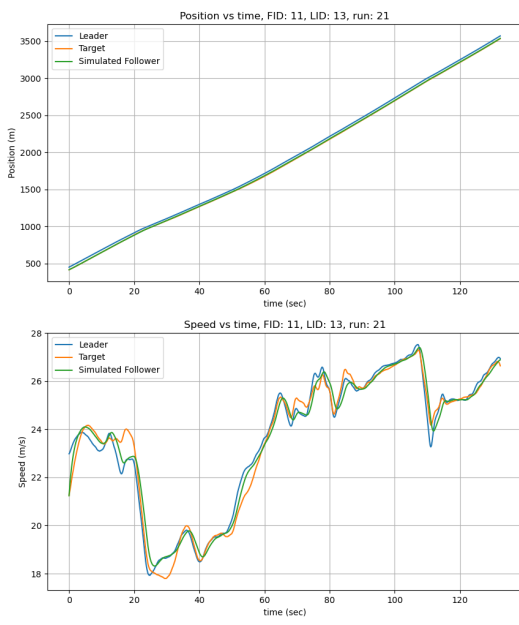
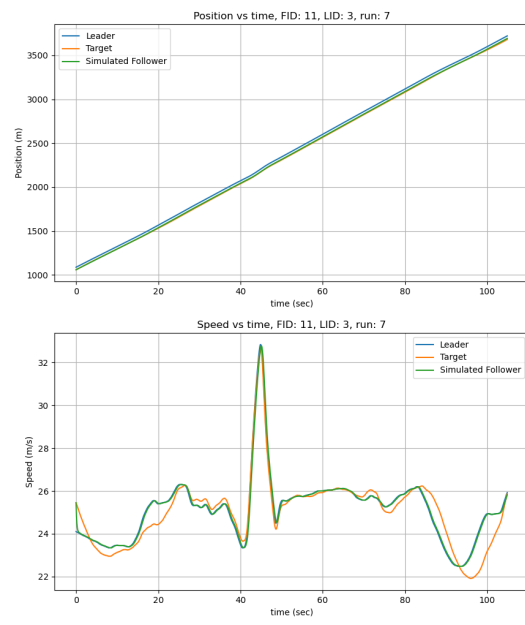


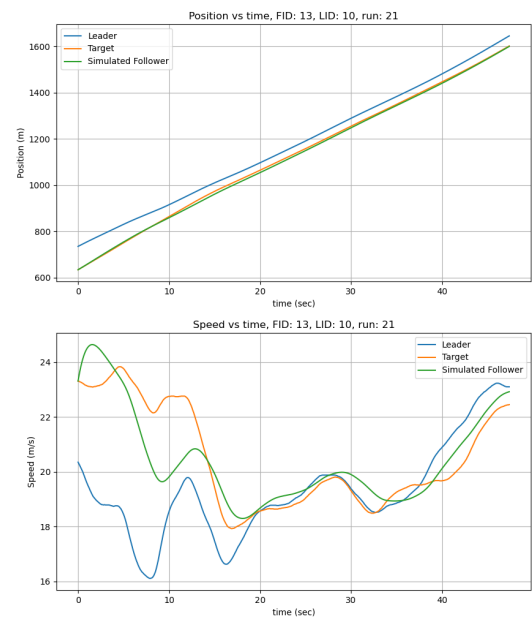
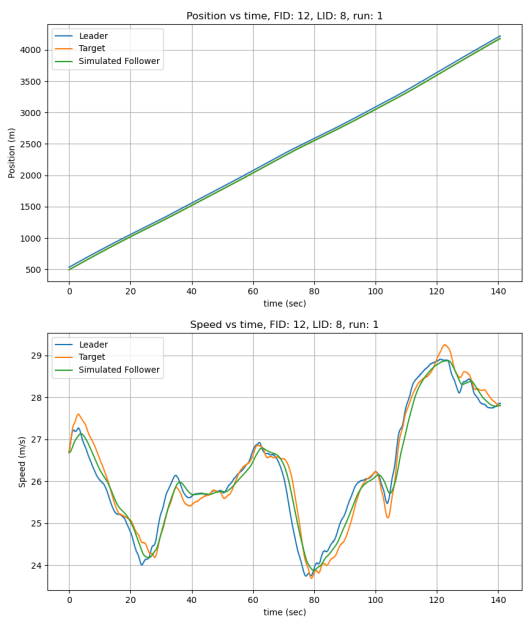
Fig. 23. Parameter histogram for CSP in Phoenix.



(a) Position and speed for CTH for vehicle 11 in run 21 I294L1 dataset.

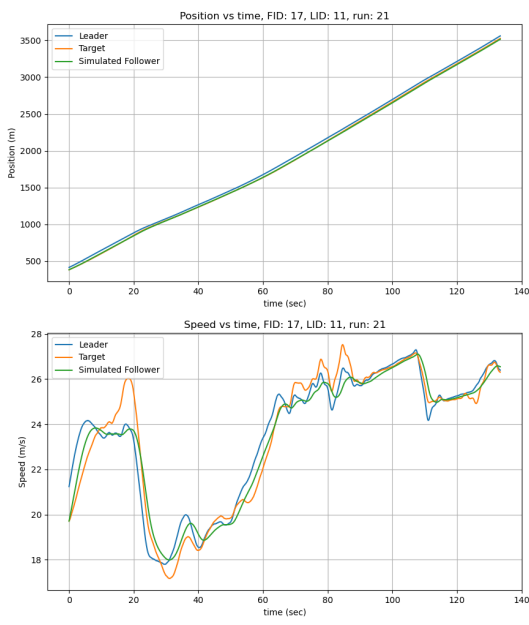


(b) Position and speed for CTH for vehicle 11 in run 7 I294L1 dataset.

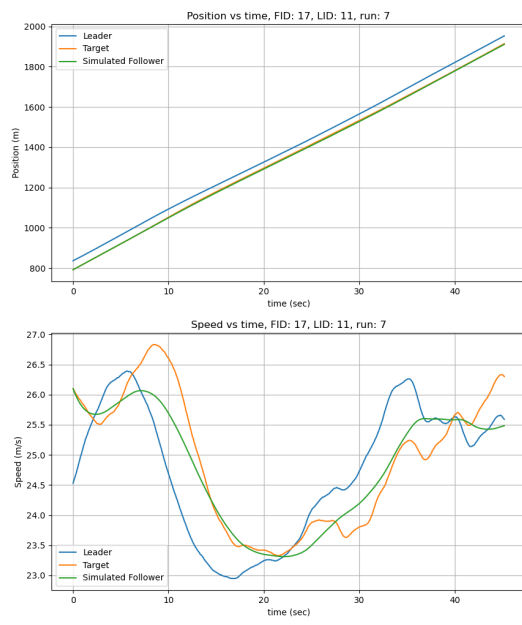


(a) Position and speed for CTH for vehicle 12 in run 1
I294L1 dataset.

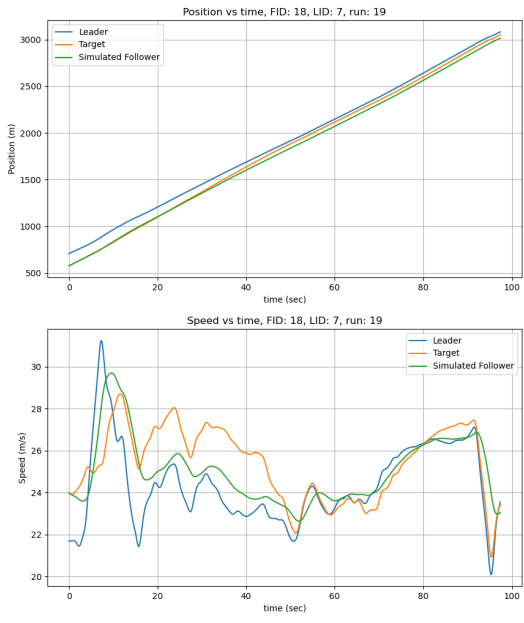
(b) Position and speed for CTH for vehicle 13 in run
21 I294L1 dataset.



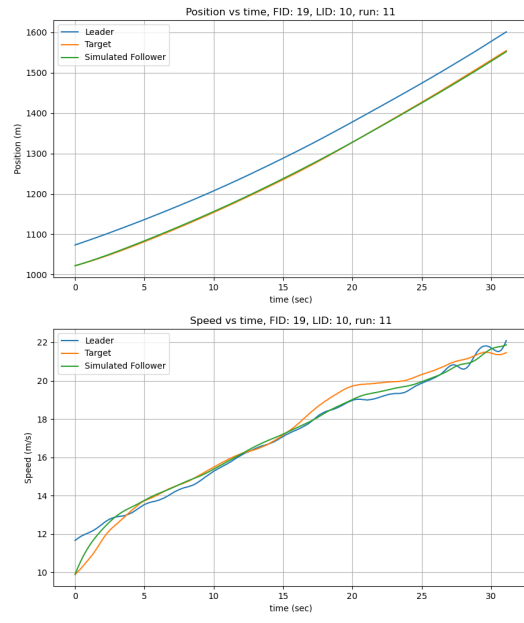
(a) Position and speed for CTH for vehicle 17 in run 21 I294L1 dataset.



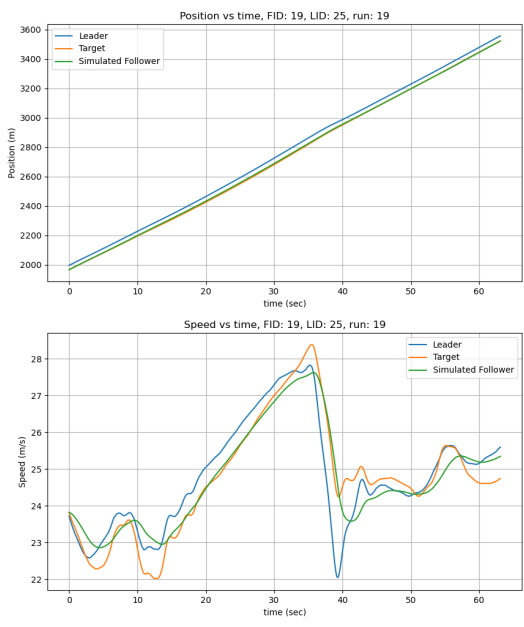
(b) Position and speed for CTH for vehicle 17 in run 7 I294L1 dataset.



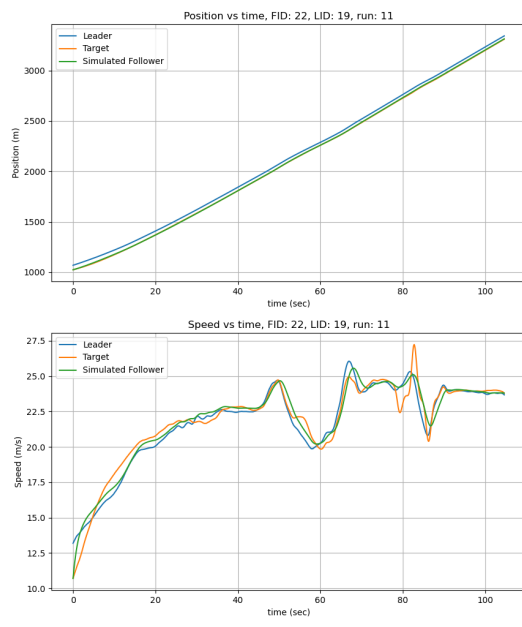
(a) Position and speed for CTH for vehicle 18 in run 19 I294L1 dataset.



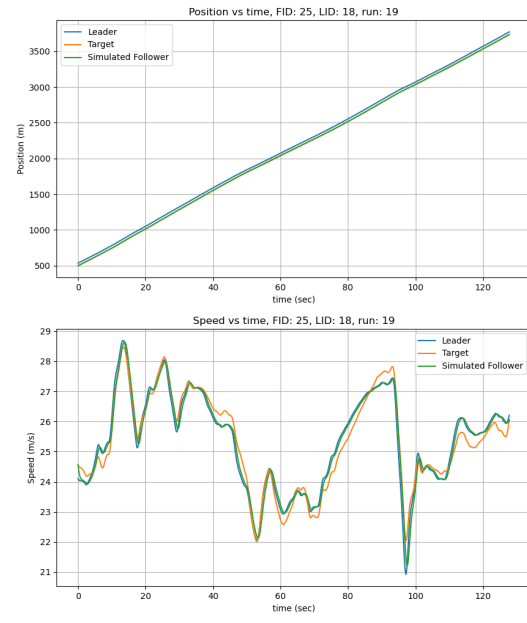
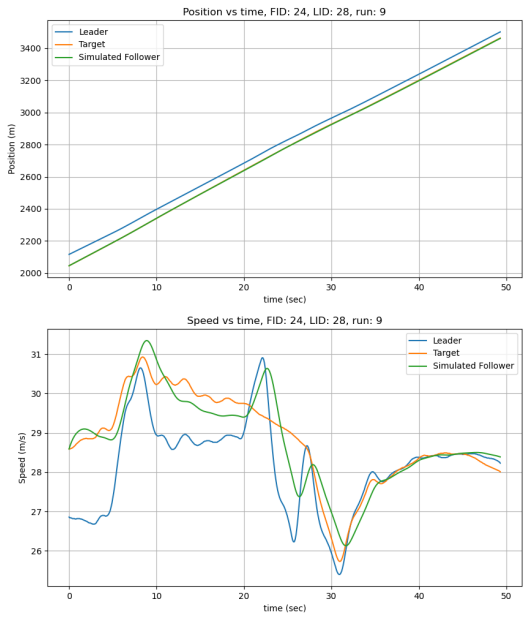
(b) Position and speed for CTH for vehicle 19 in run 11 I294L1 dataset.

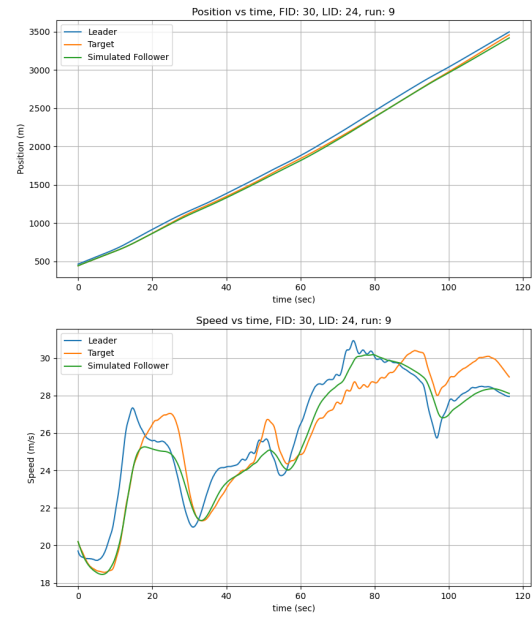
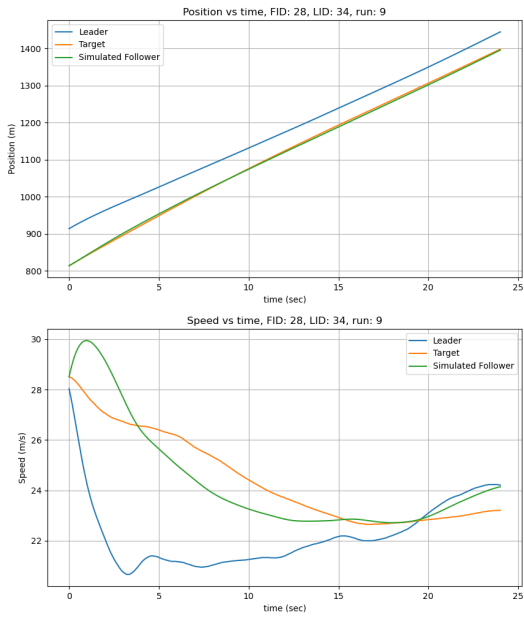


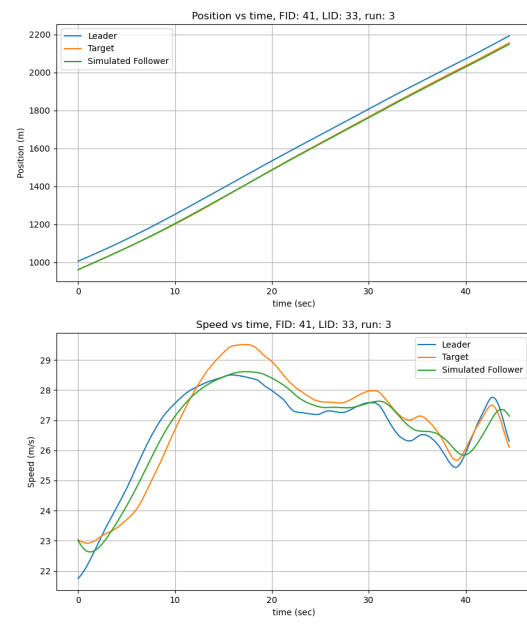
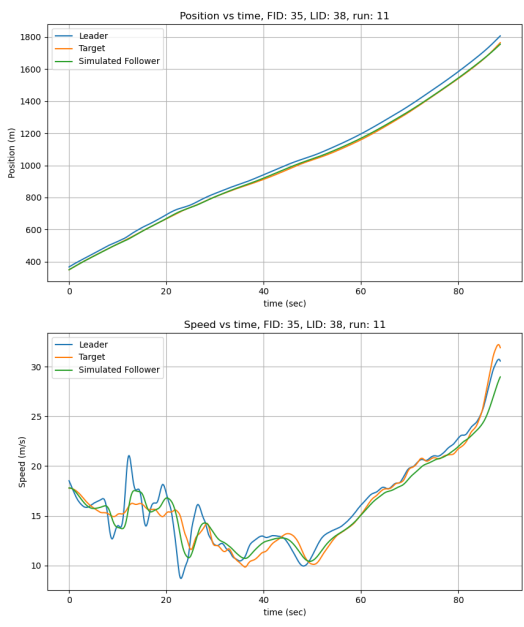
(a) Position and speed for CTH for vehicle 19 in run 19 I294L1 dataset.

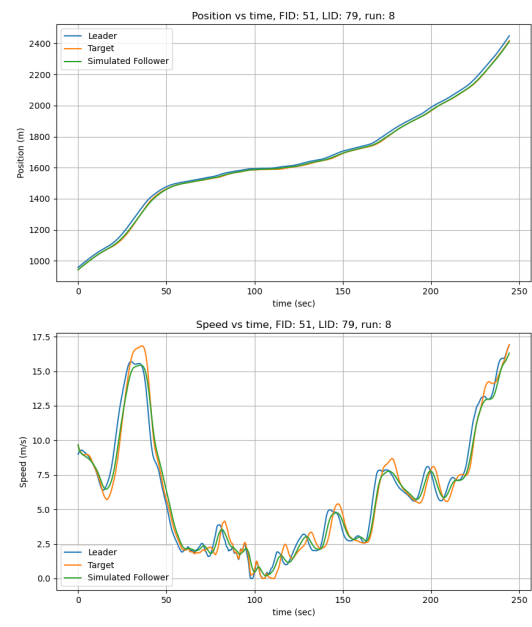
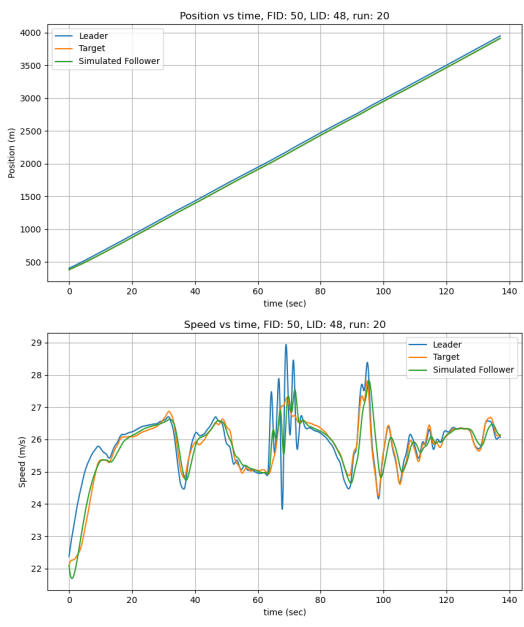


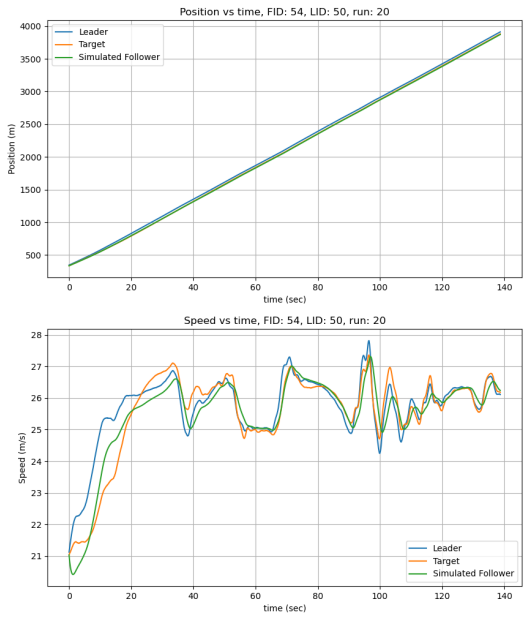
(b) Position and speed for CTH for vehicle 22 in run 11 I294L1 dataset.



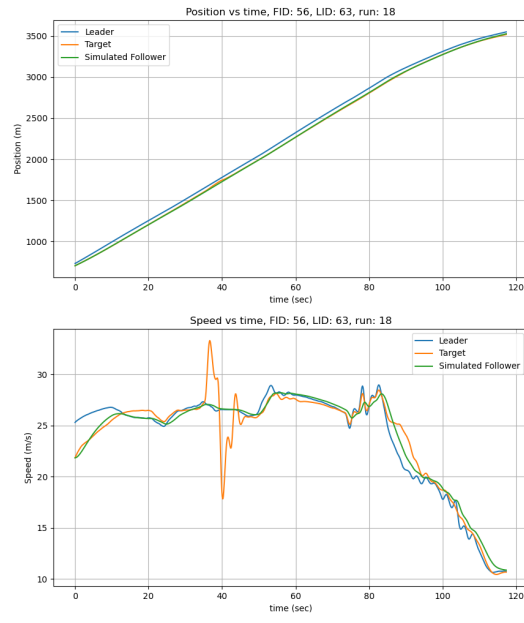




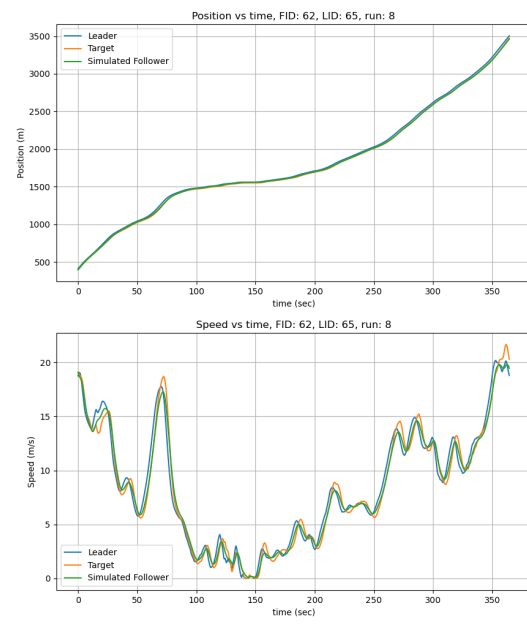
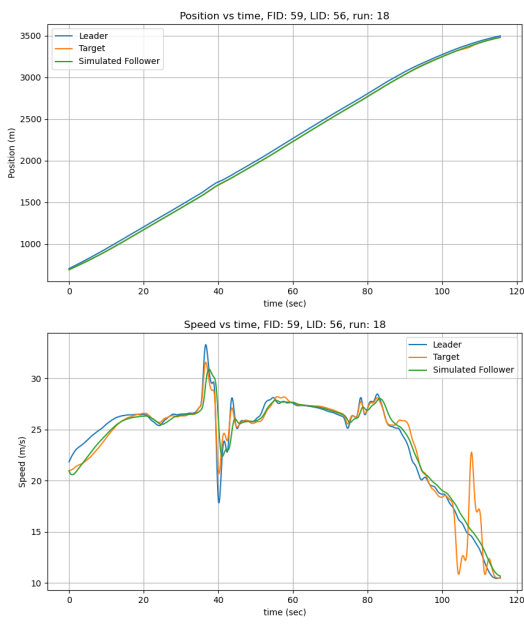


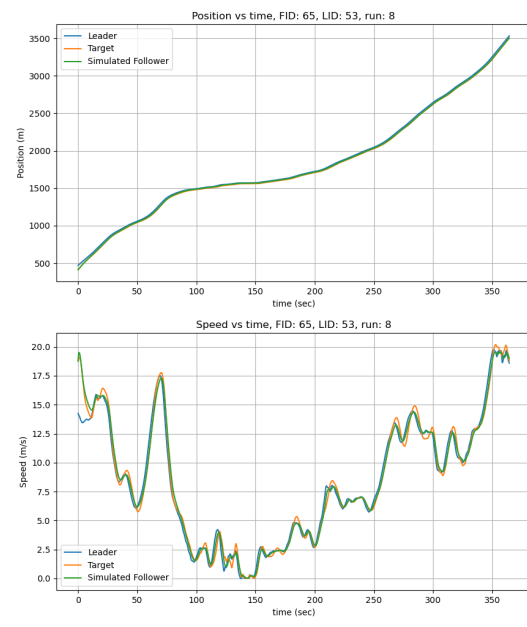
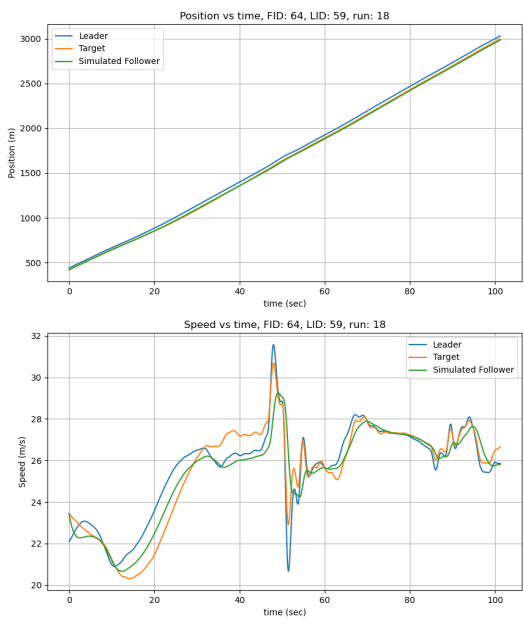


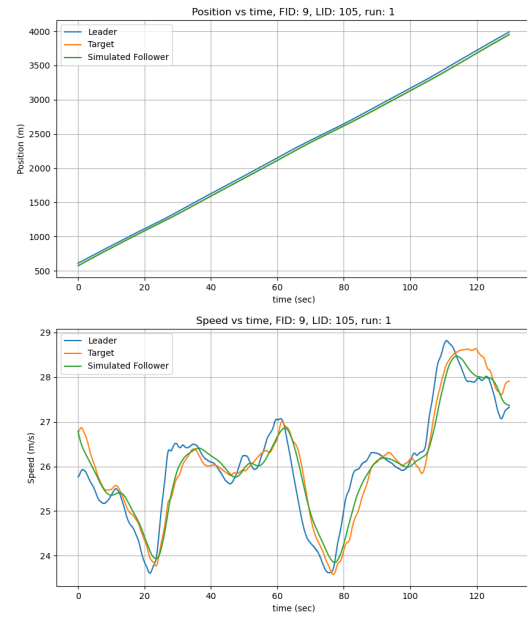
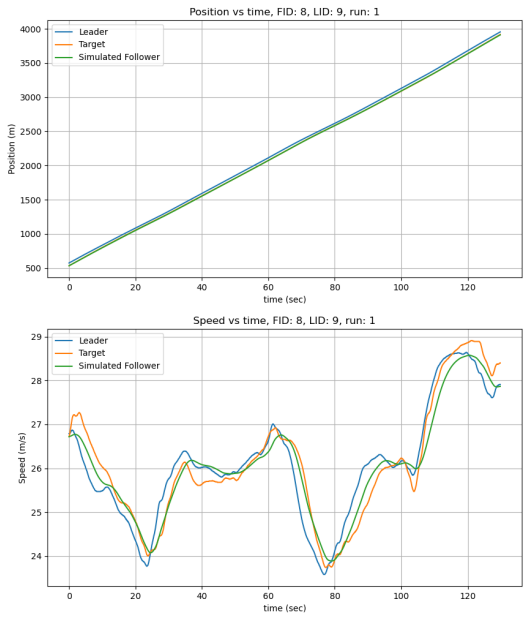
(a) Position and speed for CTH for vehicle 54 in run 20 I294L1 dataset.



(b) Position and speed for CTH for vehicle 56 in run 18 I294L1 dataset.







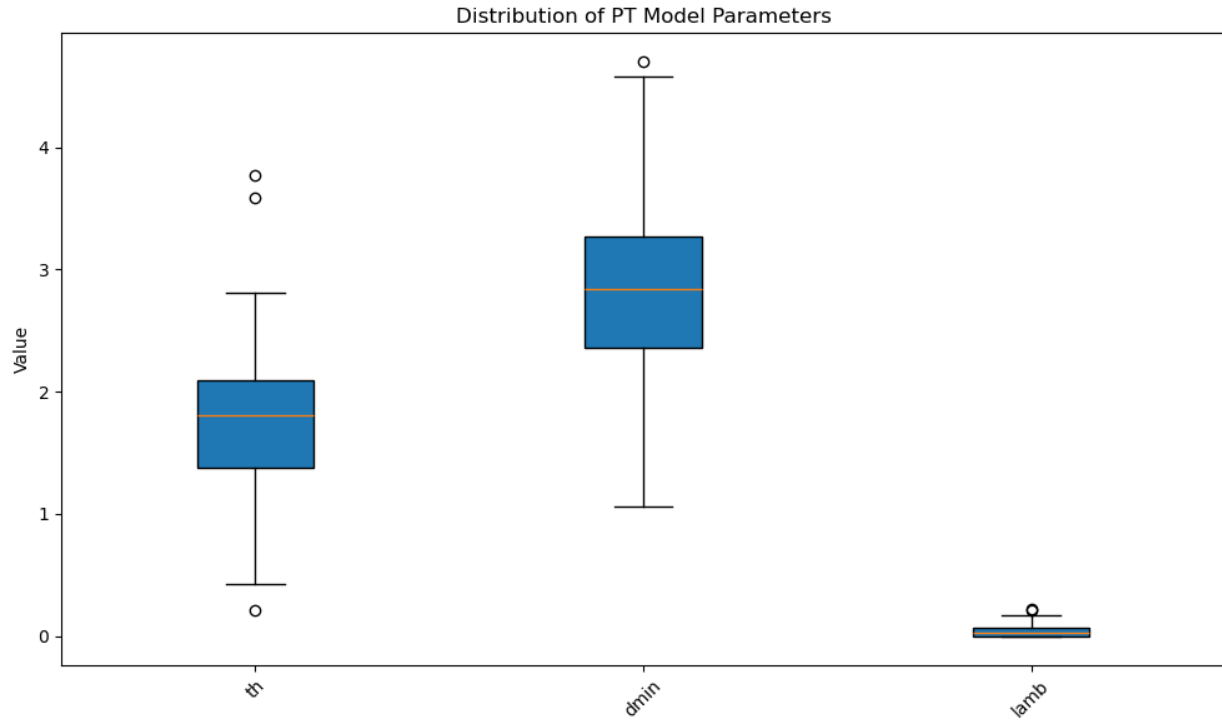


Fig. 37. Parameter ranges for CTH in I294L1 dataset.

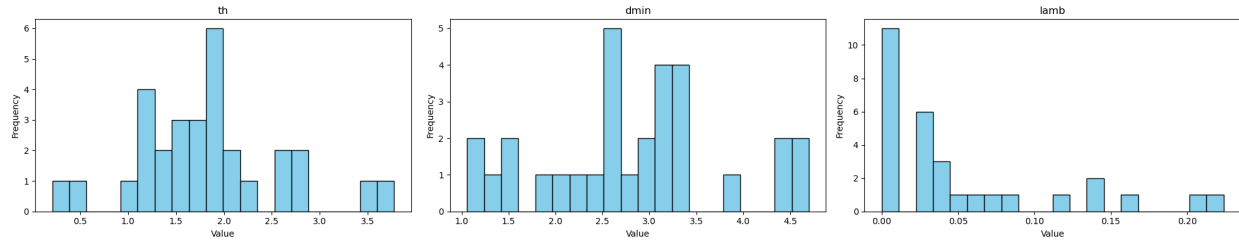
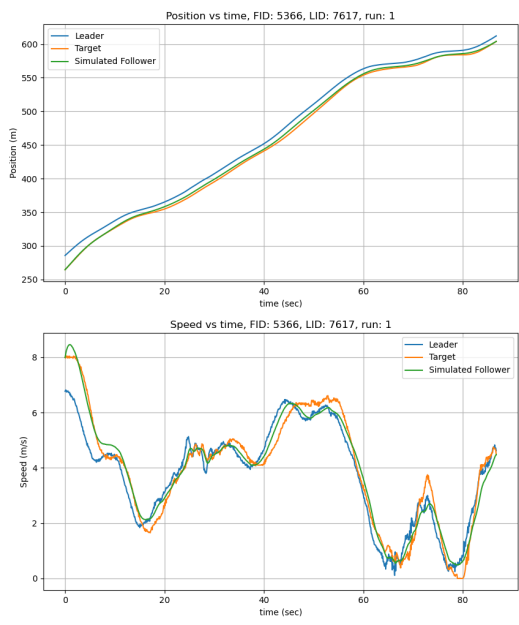
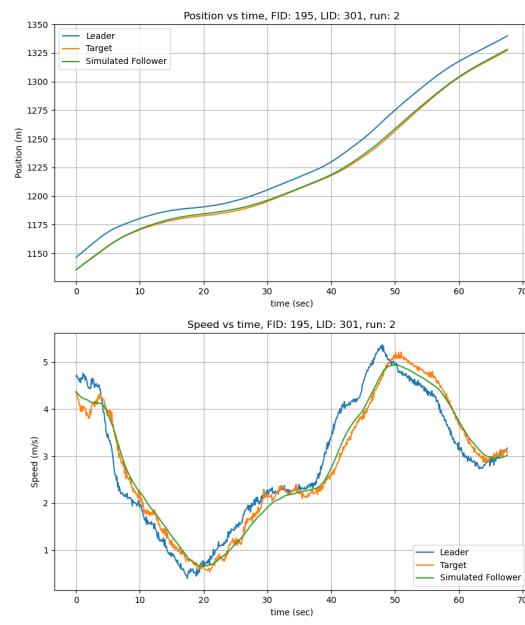


Fig. 38. Parameter histogram for CTH in I294L1 dataset.



(a) Position and speed for CTH for vehicle 5366 in I90/94 dataset.



(b) Position and speed for CTH for vehicle 195 in I90/94 dataset.

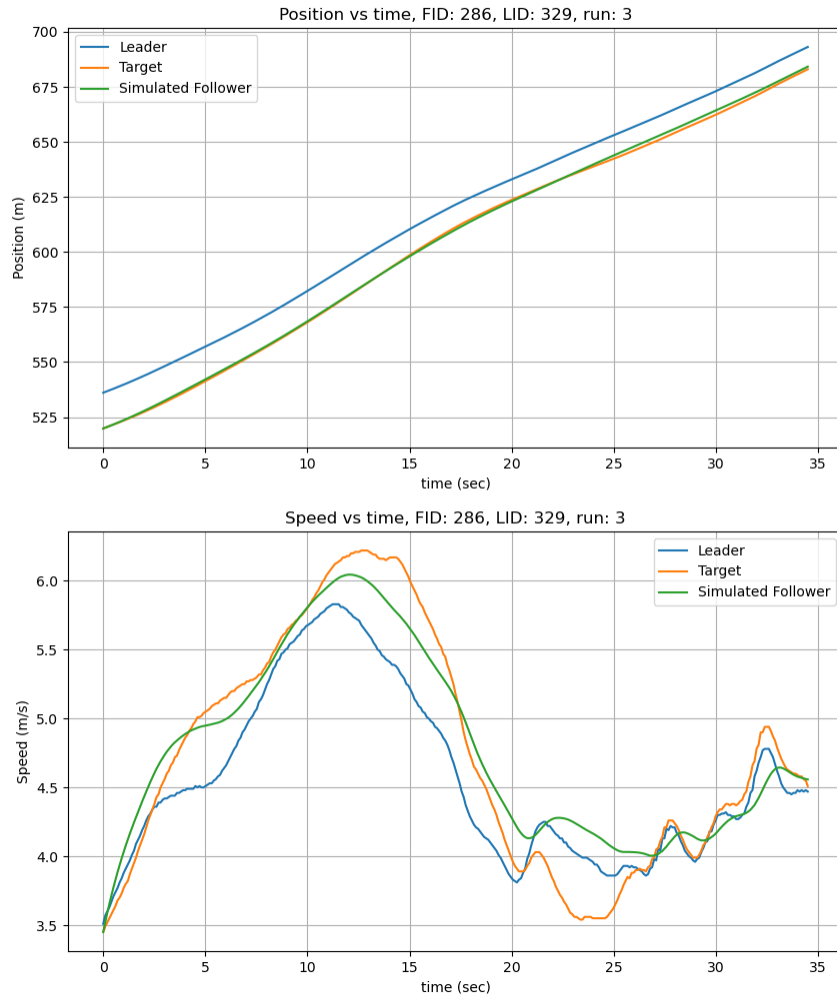


Fig. 40. Position and speed for CTH for vehicle 286 in I90/94 dataset.

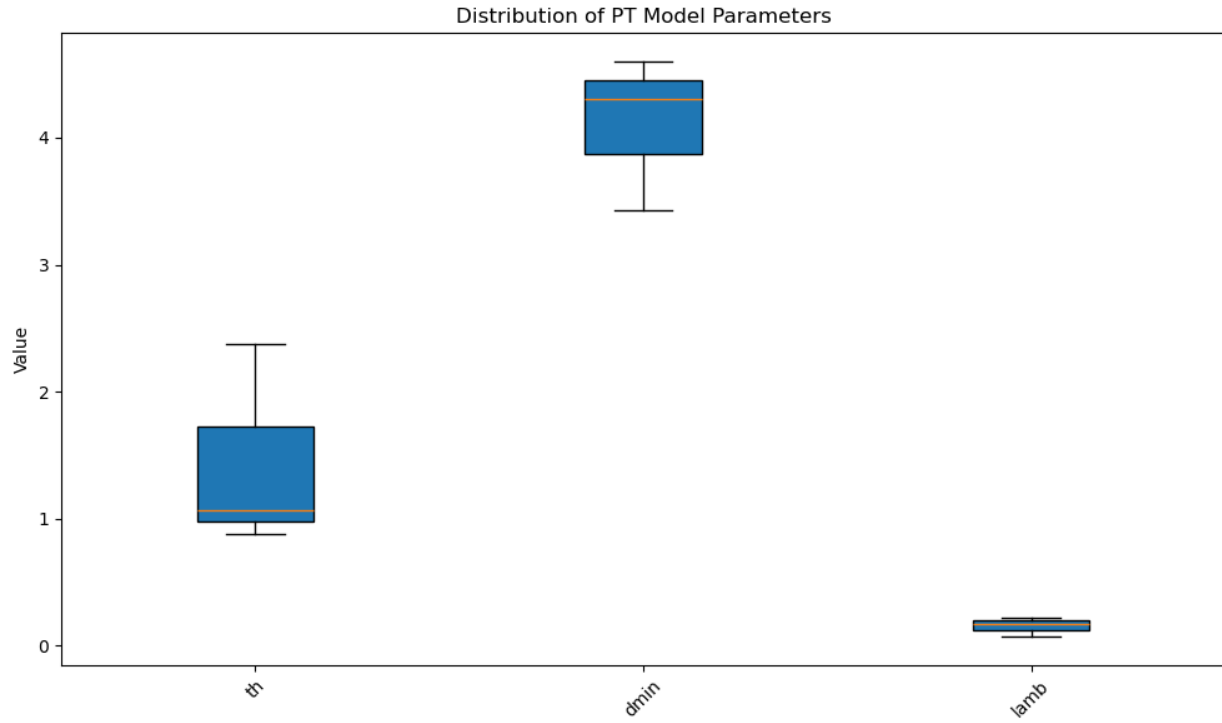


Fig. 41. Parameter ranges for CTH in I90/94.

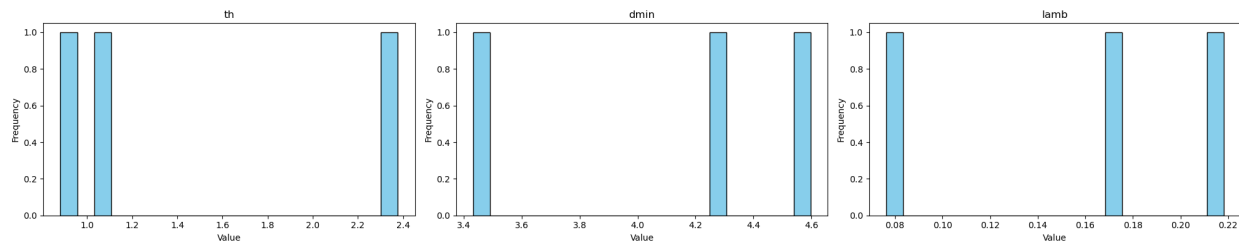
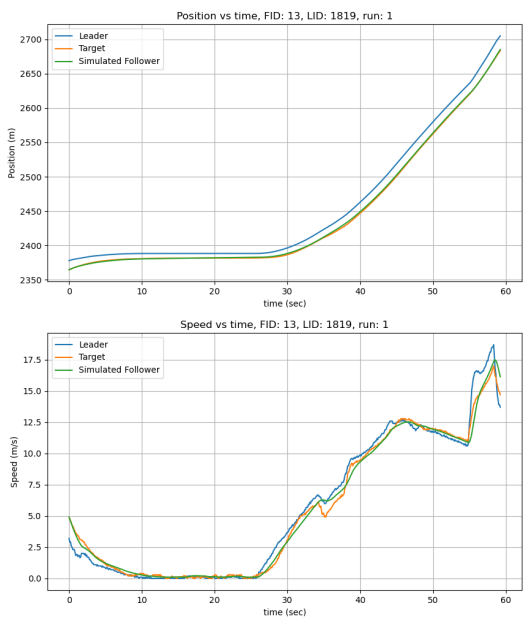
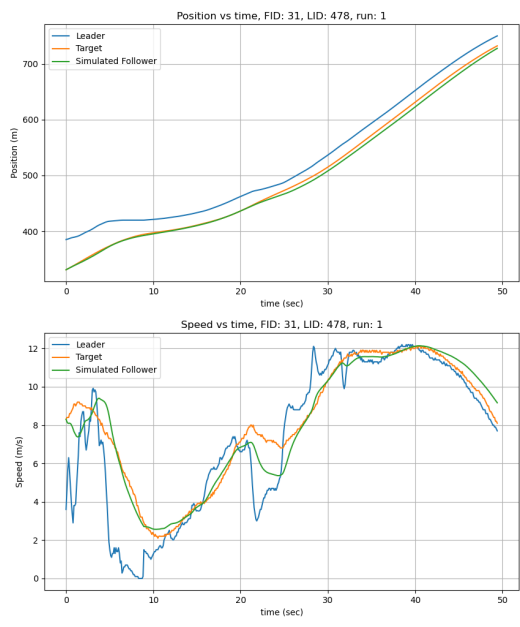


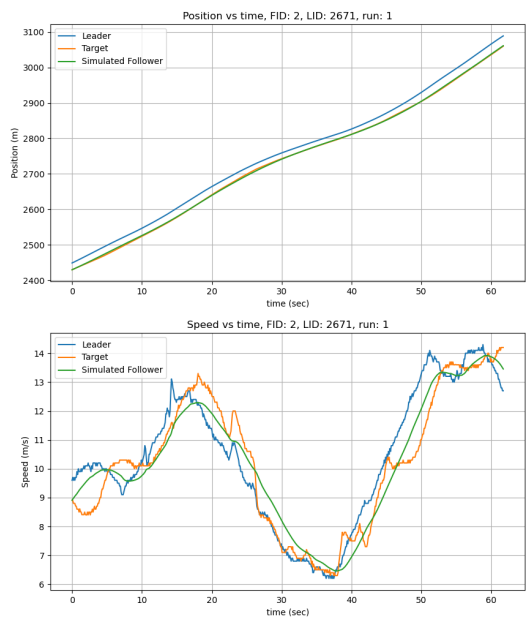
Fig. 42. Parameter histogram for CTH in I90/94.



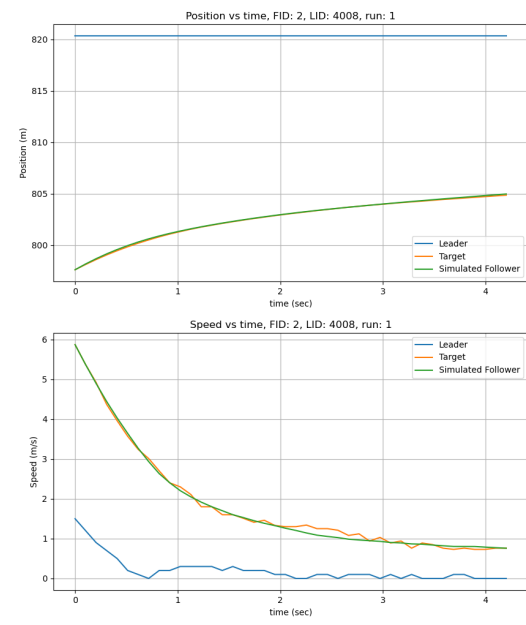
(a) Position and speed for CTH for vehicle 13 in Phoenix data H1A3 run 6.



(b) Position and speed for CTH for vehicle 31 in Phoenix data H1A3 run 1.



(a) Position and speed for CTH for vehicle 2 in Phoenix data H1A3 run 9 ES.



(b) Position and speed for CTH for vehicle 2 in Phoenix data H1A3 run 9 NS.

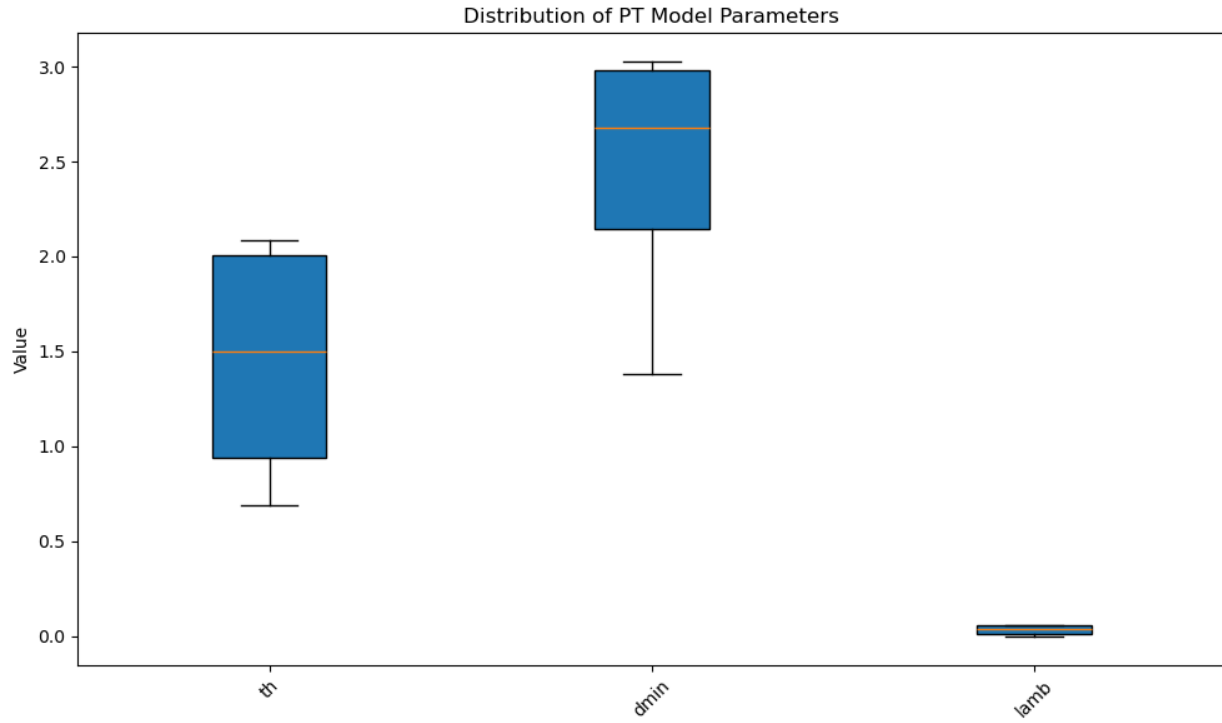


Fig. 45. Parameter ranges for CTH in Phoenix.

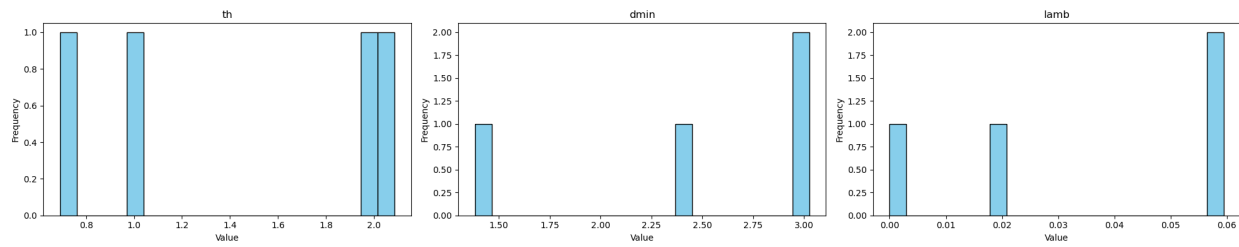
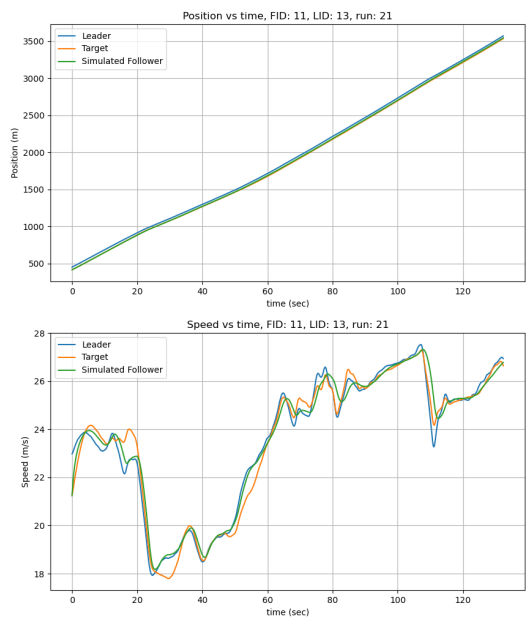
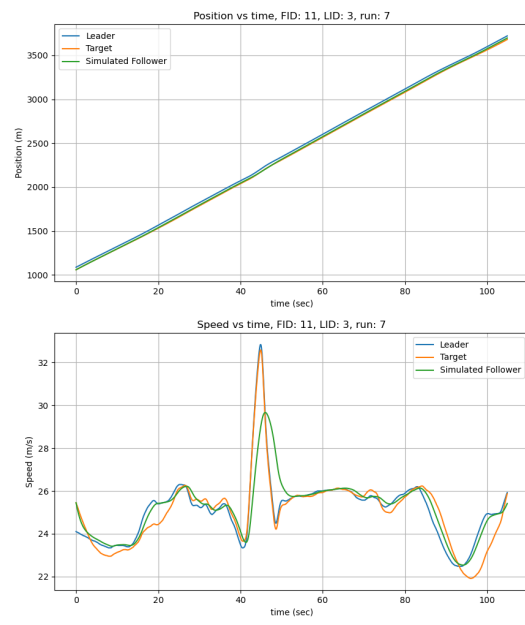


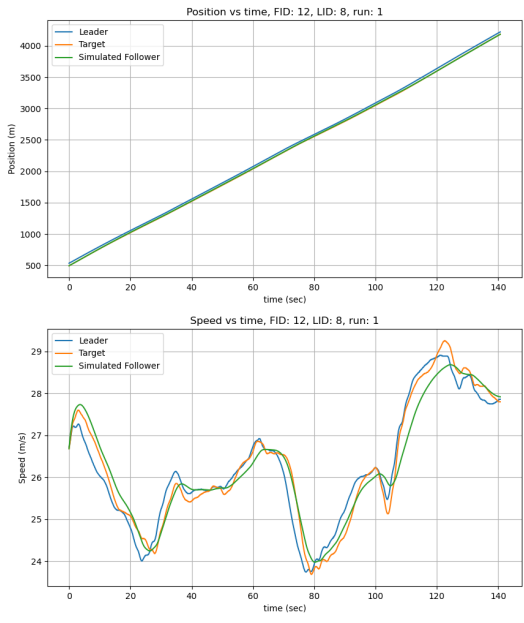
Fig. 46. Parameter histogram for CTH in Phoenix.



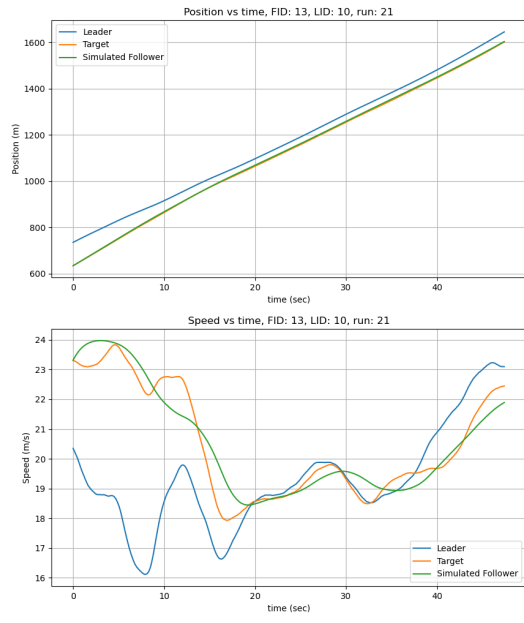
(a) Position and speed for TFS for vehicle 11 in run 21 I294L1 dataset.



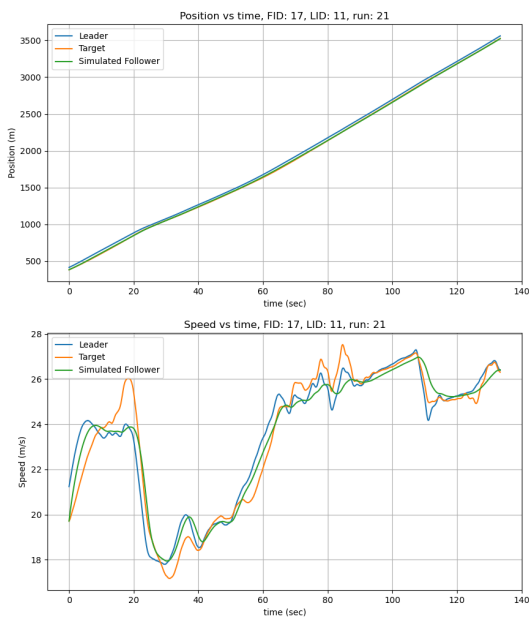
(b) Position and speed for TFS for vehicle 11 in run 7 I294L1 dataset.



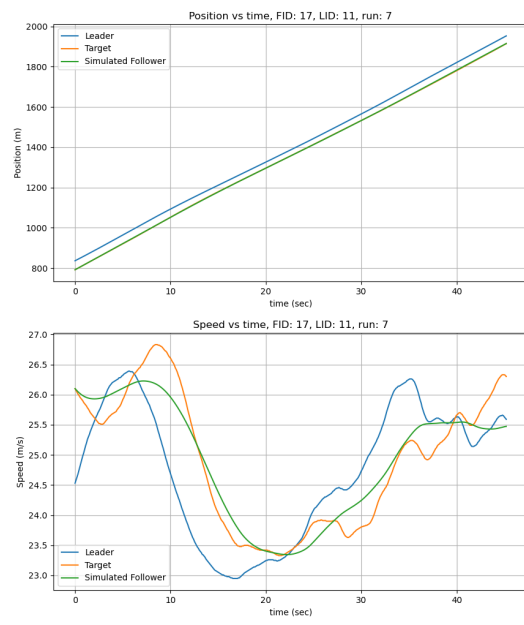
(a) Position and speed for TFS for vehicle 12 in run 1
I294L1 dataset.



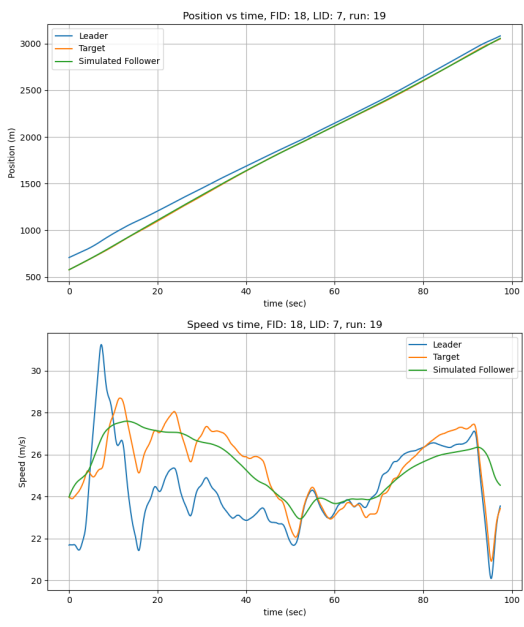
(b) Position and speed for TFS for vehicle 13 in run
21 I294L1 dataset.



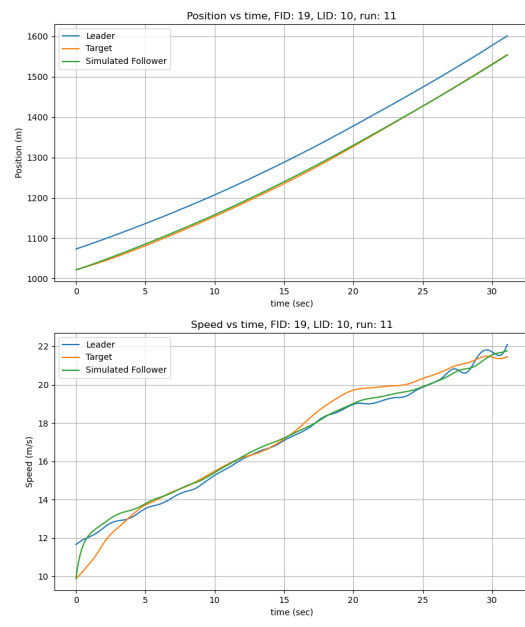
(a) Position and speed for TFS for vehicle 17 in run 21 I294L1 dataset.



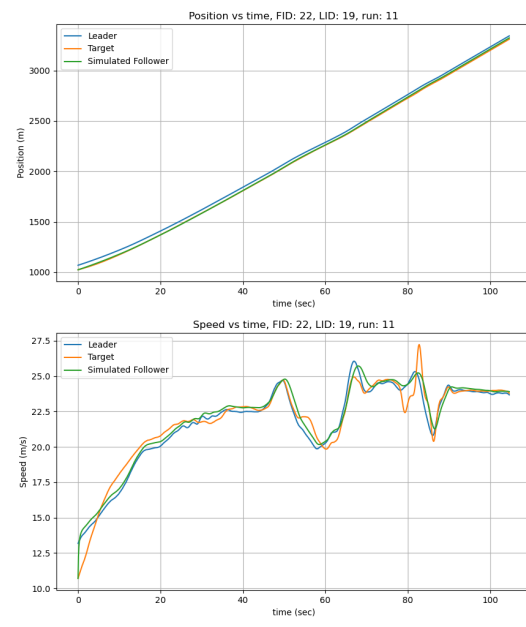
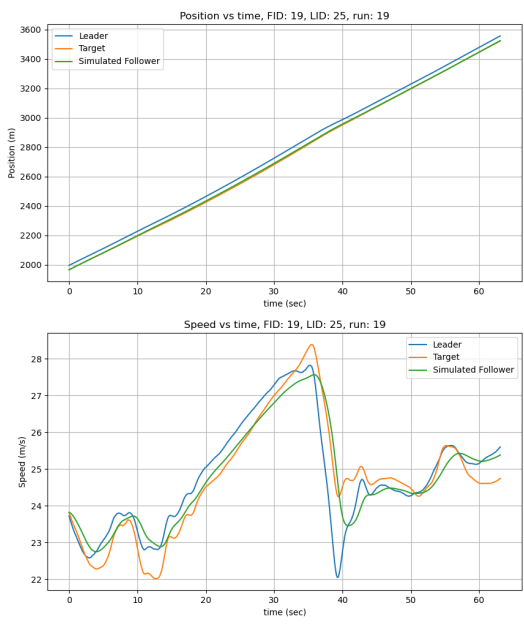
(b) Position and speed for TFS for vehicle 17 in run 7 I294L1 dataset.

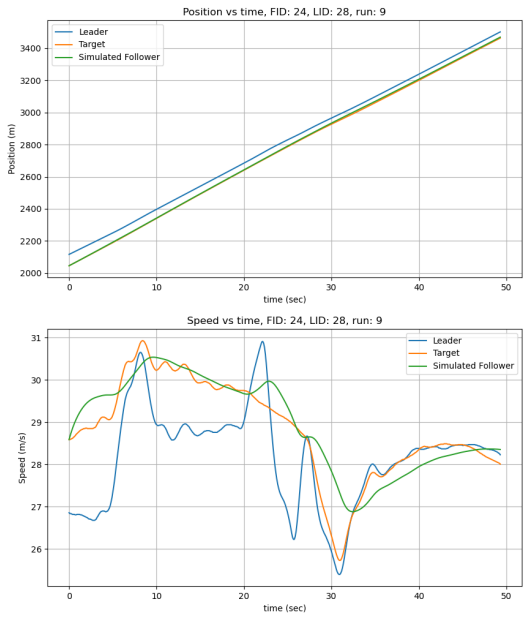


(a) Position and speed for TFS for vehicle 18 in run 19 I294L1 dataset.

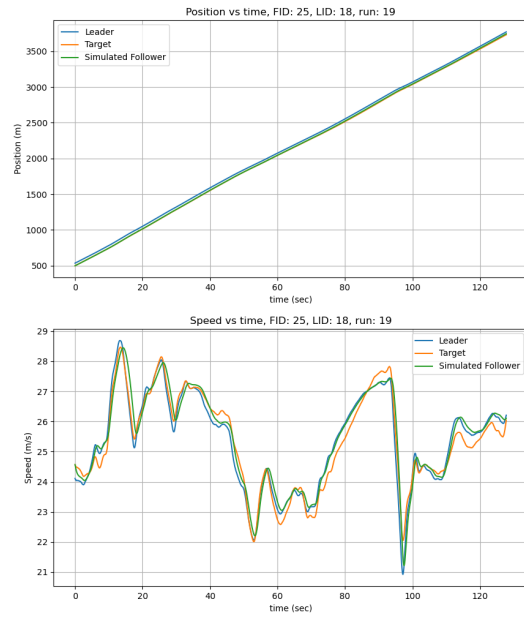


(b) Position and speed for TFS for vehicle 19 in run 11 I294L1 dataset.

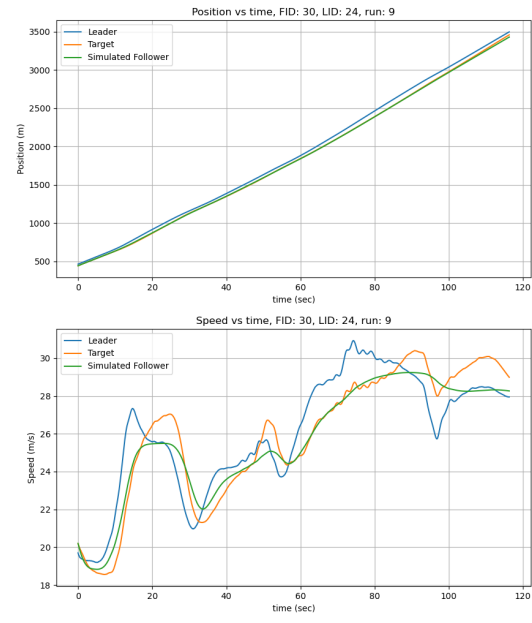
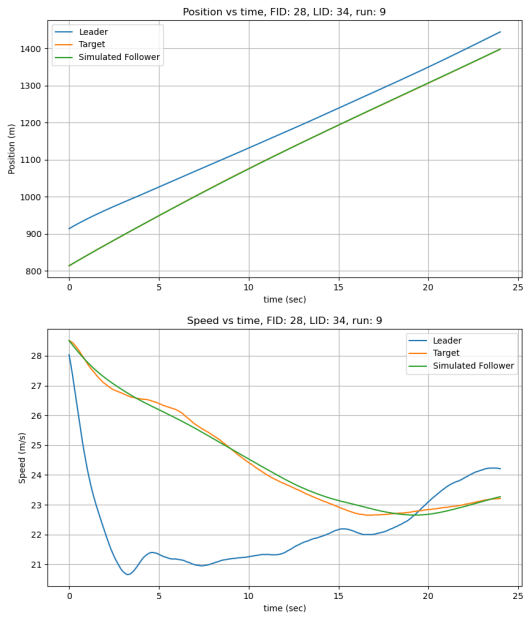




(a) Position and speed for TFS for vehicle 24 in run 9 I294L1 dataset.

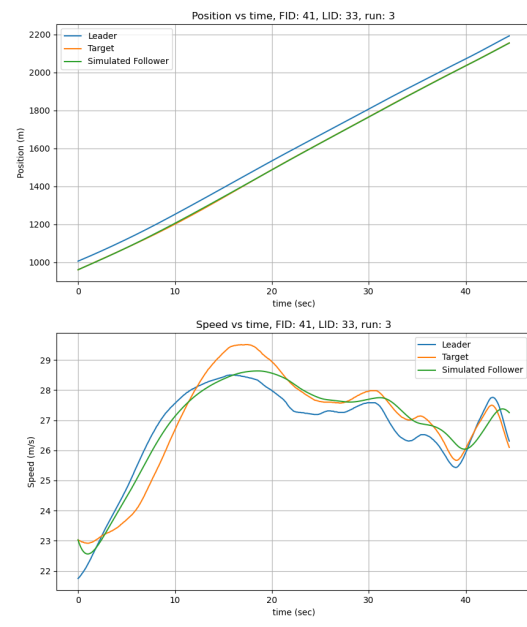
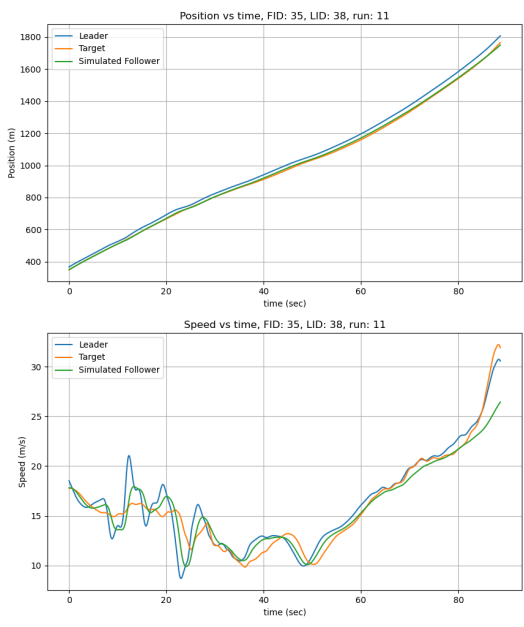


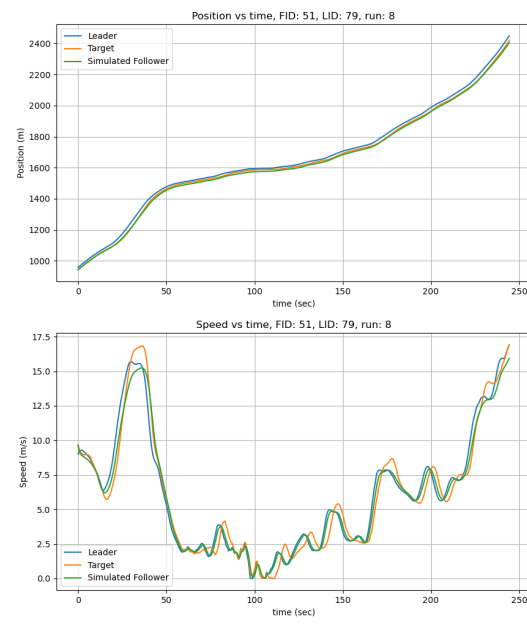
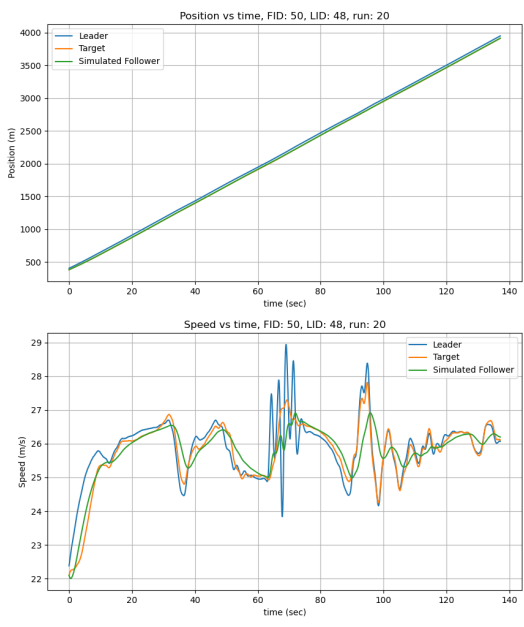
(b) Position and speed for TFS for vehicle 25 in run 19 I294L1 dataset.

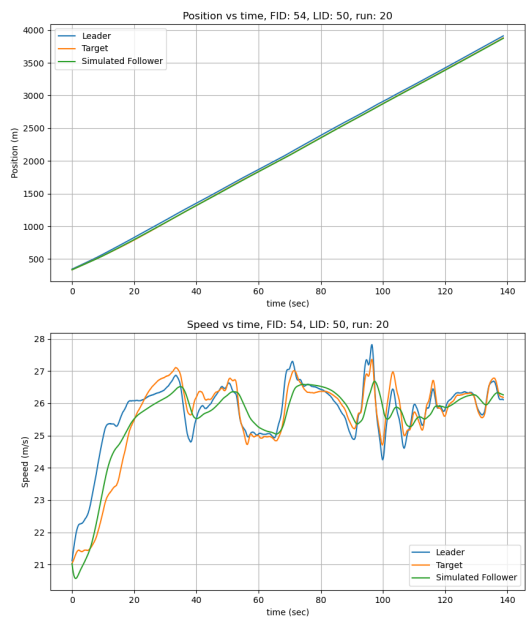


(a) Position and speed for TFS for vehicle 28 in run 9
I294L1 dataset.

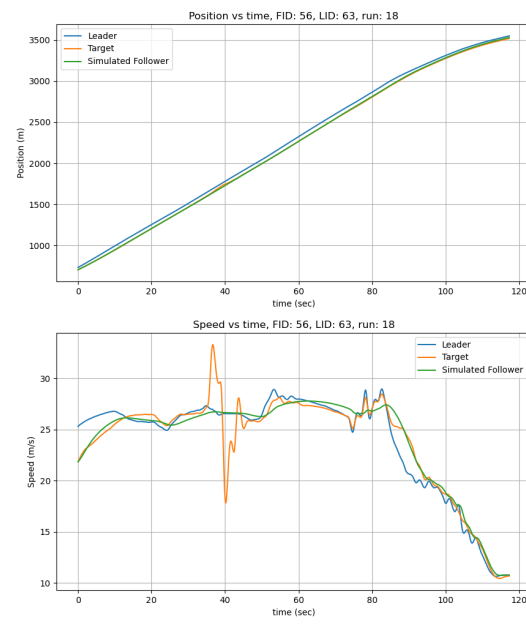
(b) Position and speed for TFS for vehicle 30 in run 9
I294L1 dataset.



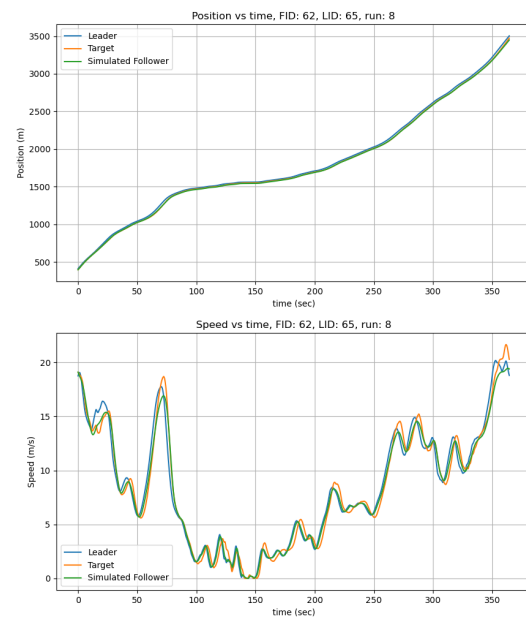
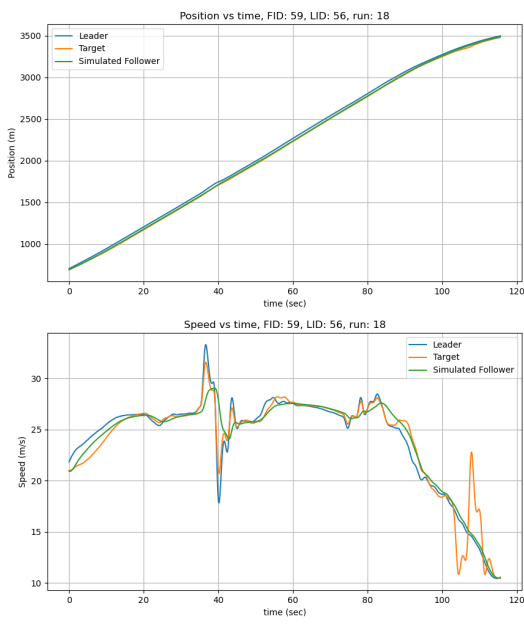


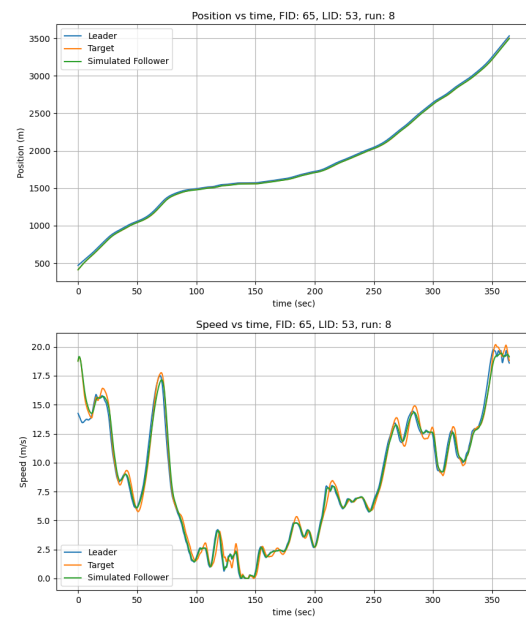
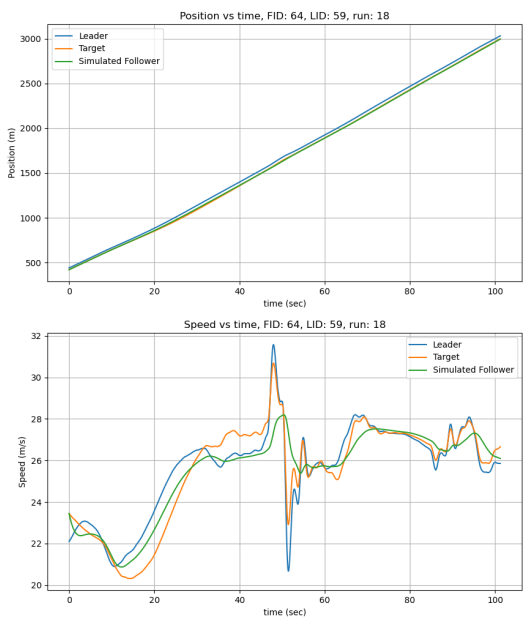


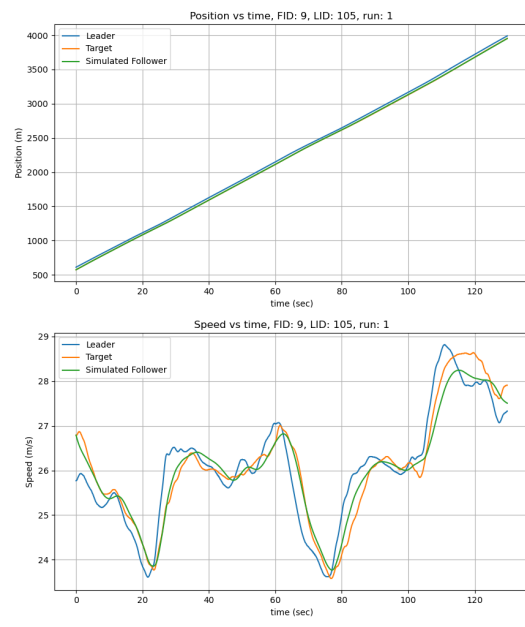
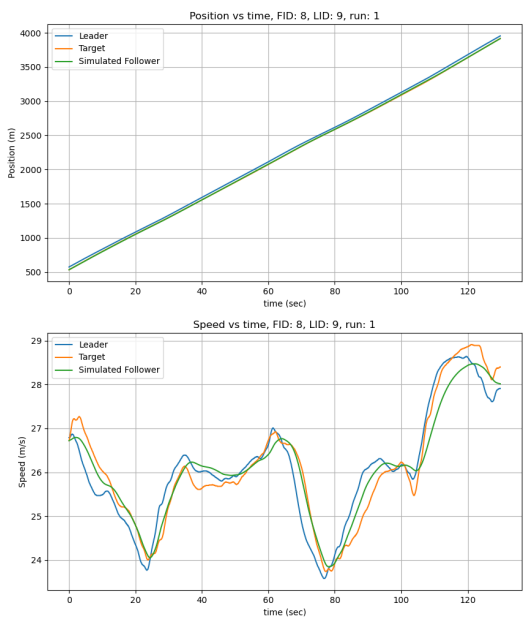
(a) Position and speed for TFS for vehicle 54 in run 20 I294L1 dataset.



(b) Position and speed for TFS for vehicle 56 in run 18 I294L1 dataset.







(a) Position and speed for TFS for vehicle 8 in run 1
I294L1 dataset.

(b) Position and speed for TFS for vehicle 9 in run 1
I294L1 dataset.

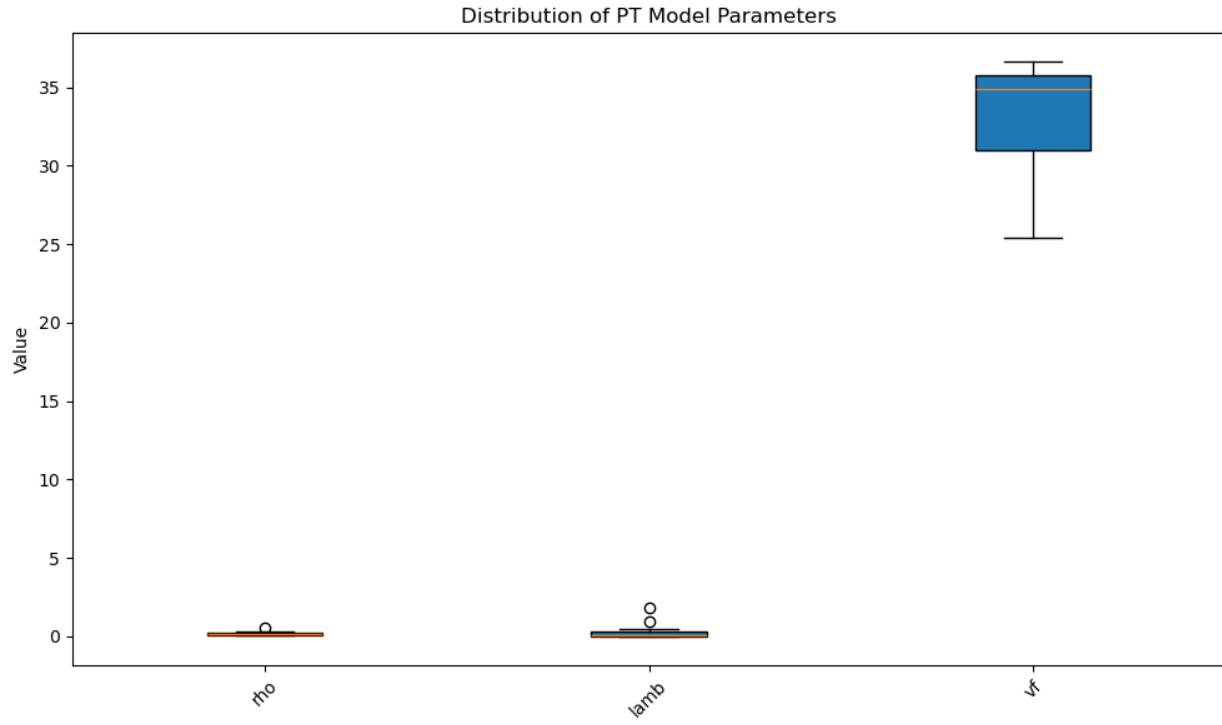


Fig. 60. Parameter ranges for TFS in I294L1 dataset.

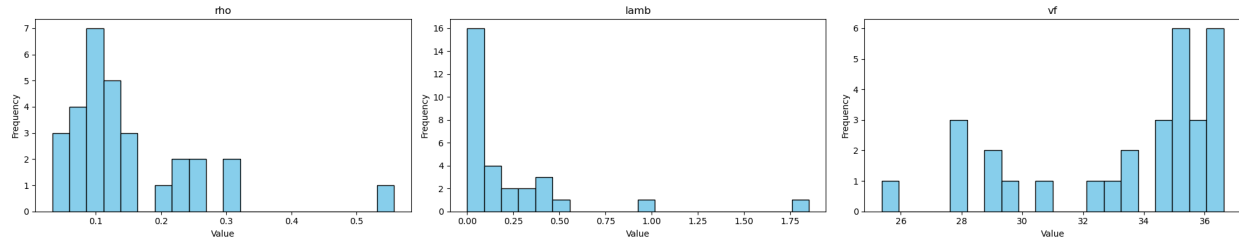
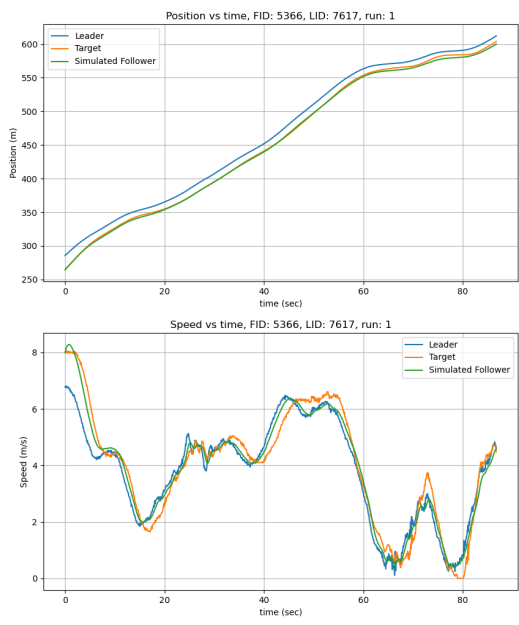
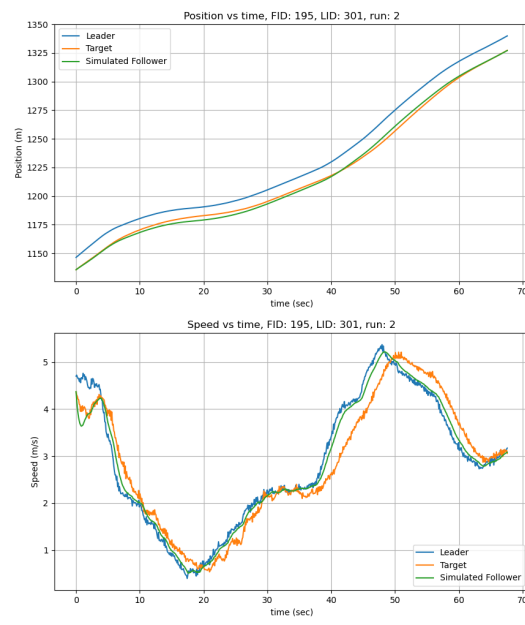


Fig. 61. Parameter histogram for TFS in I294L1 dataset.



(a) Position and speed for TFS for vehicle 5366 in I90/94 dataset.



(b) Position and speed for TFS for vehicle 195 in I90/94 dataset.

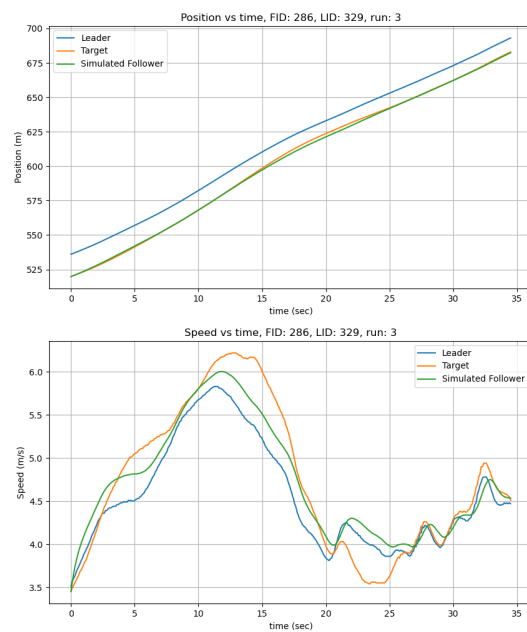


Fig. 63. Position and speed for TFS for vehicle 286 in I90/94 dataset.

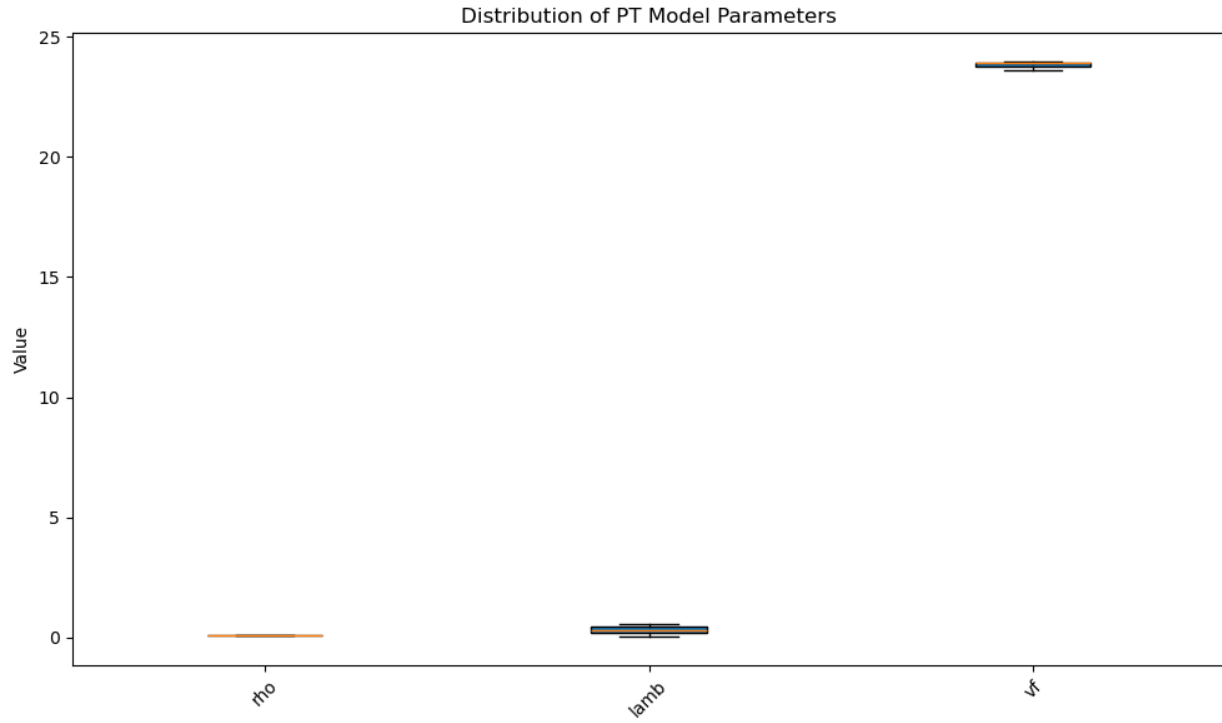


Fig. 64. Parameter ranges for TFS in I90/94.

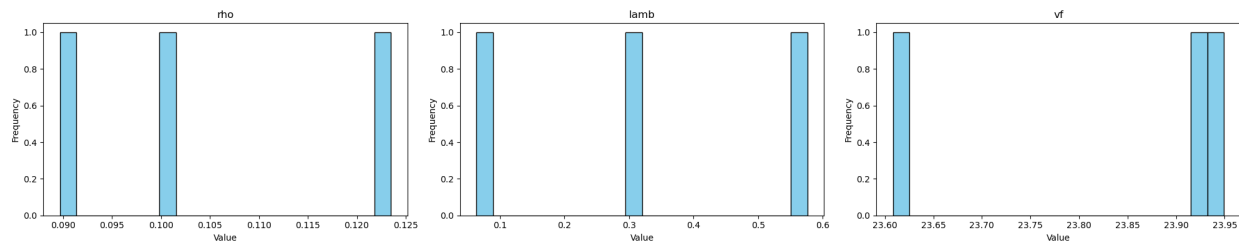
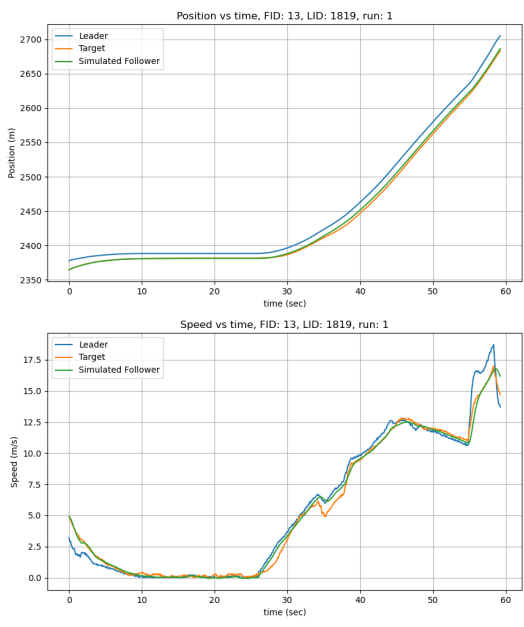
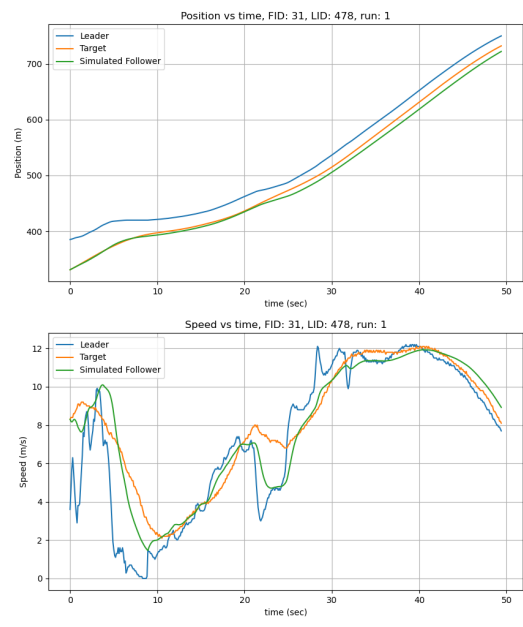


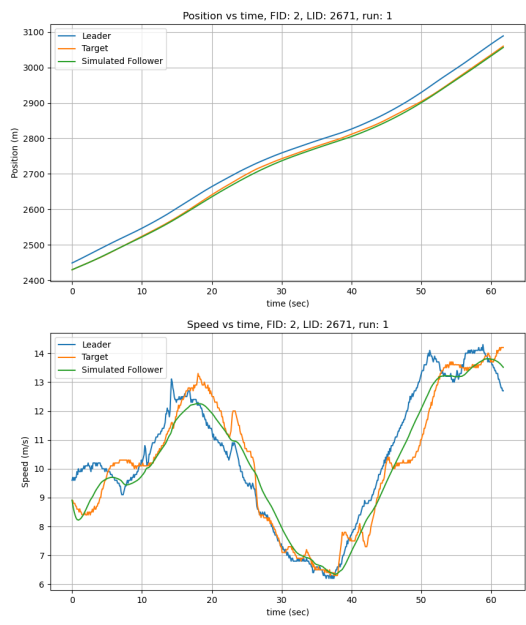
Fig. 65. Parameter histogram for TFS in I90/94.



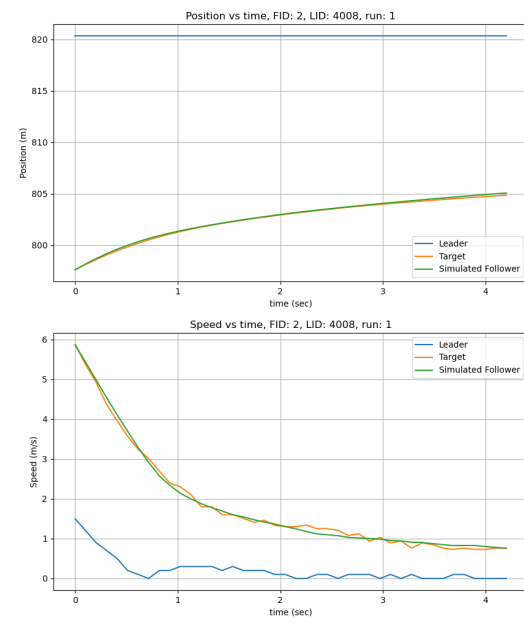
(a) Position and speed for TFS for vehicle 13 in Phoenix data H1A3 run 6.



(b) Position and speed for TFS for vehicle 31 in Phoenix data H1A3 run 1.



(a) Position and speed for TFS for vehicle 2 in Phoenix data H1A3 run 9 ES.



(b) Position and speed for TFS for vehicle 2 in Phoenix data H1A3 run 9 NS.

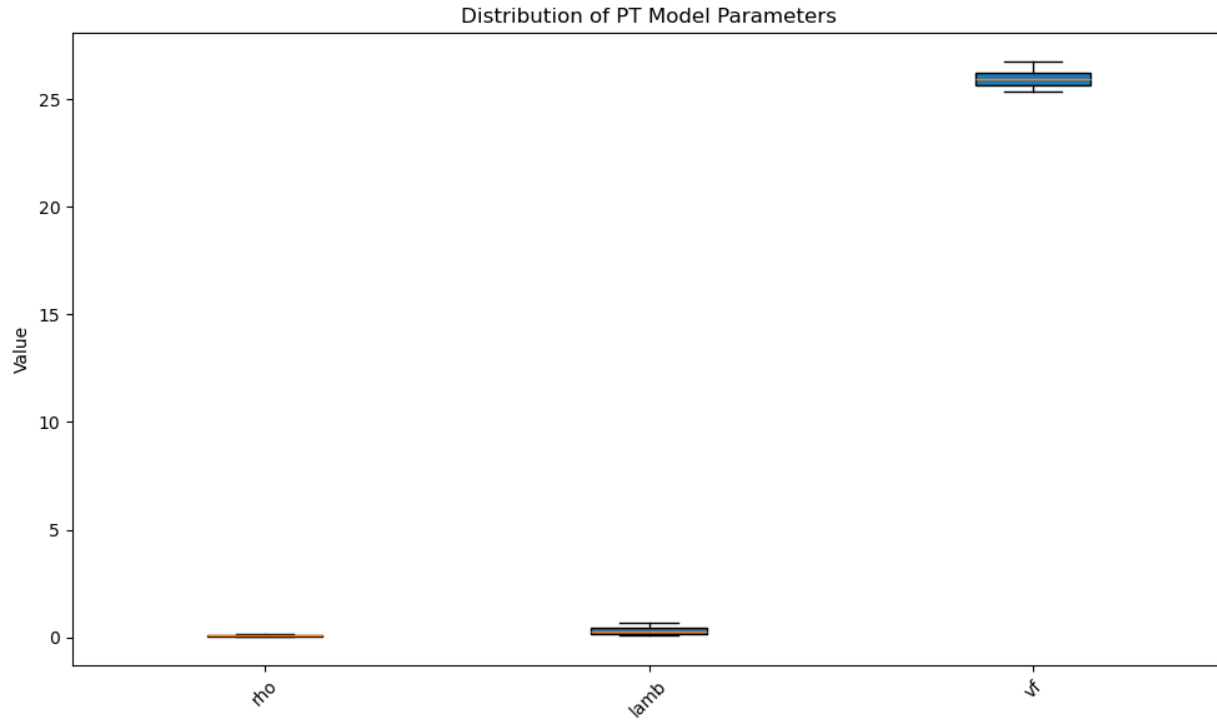


Fig. 68. Parameter ranges for TFS in Phoenix.

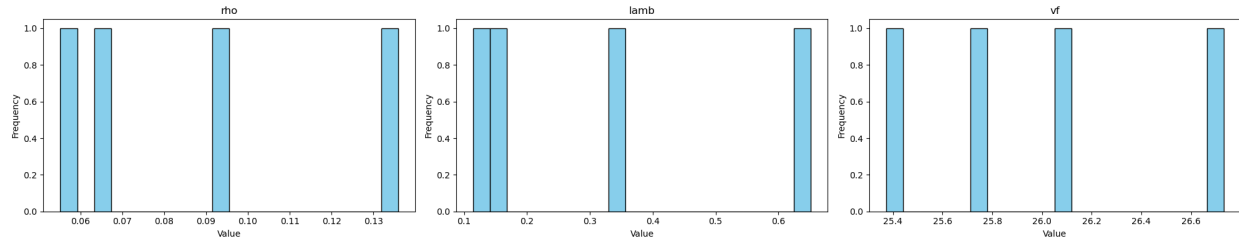
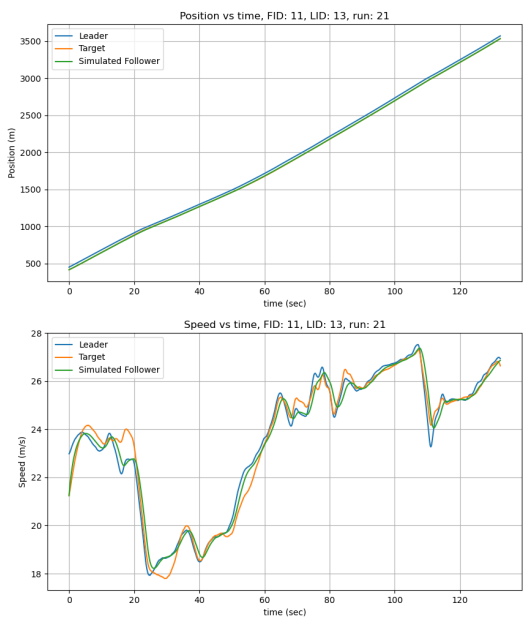
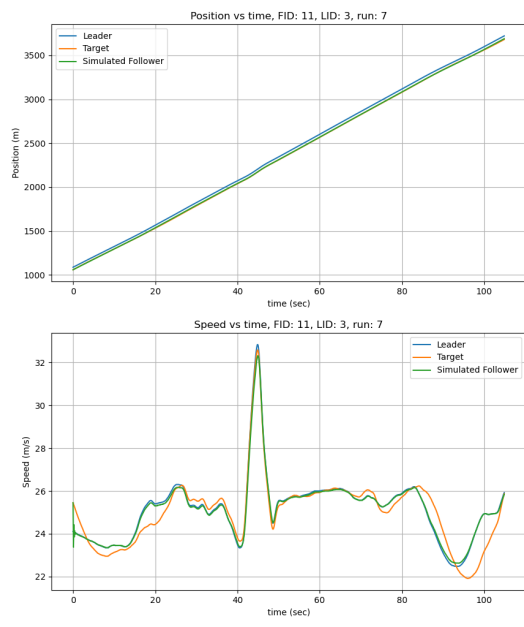


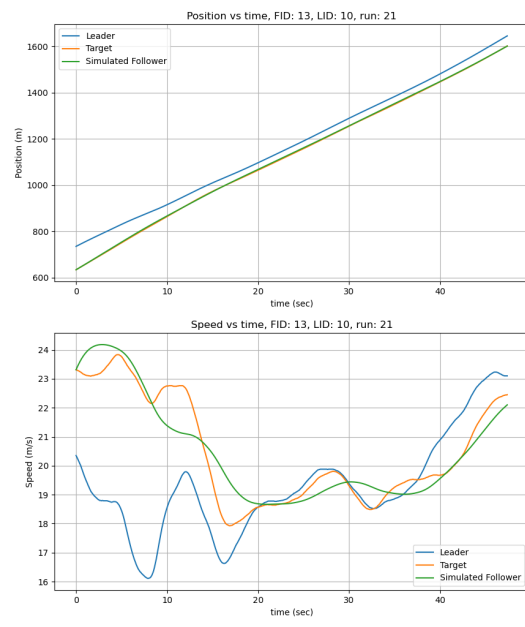
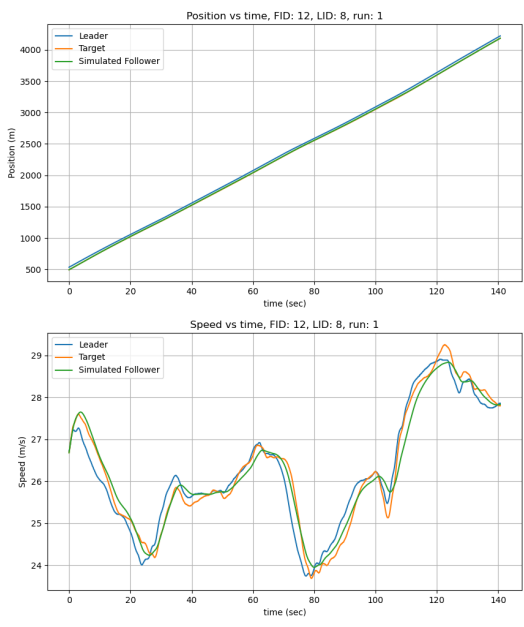
Fig. 69. Parameter histogram for TFS in Phoenix.

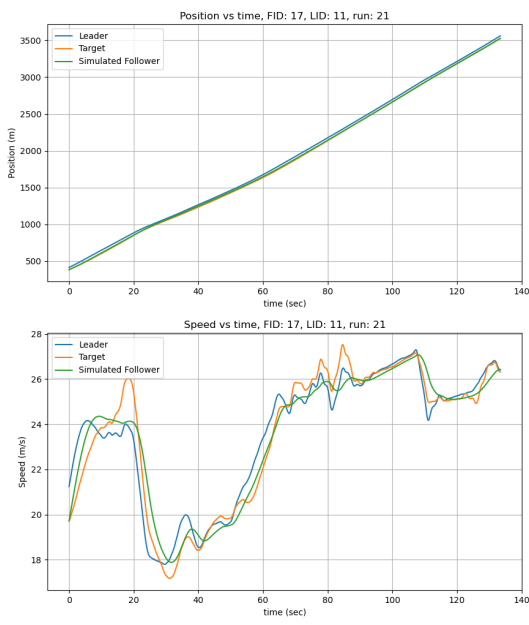


(a) Position and speed for CSF for vehicle 11 in run 21 I294L1 dataset.

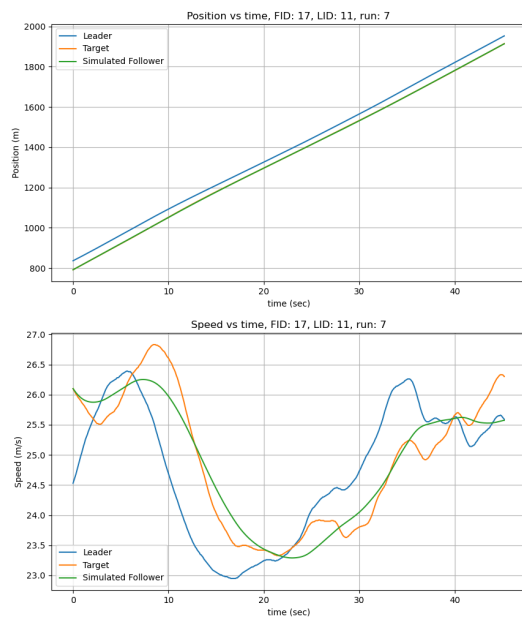


(b) Position and speed for CSF for vehicle 11 in run 7 I294L1 dataset.

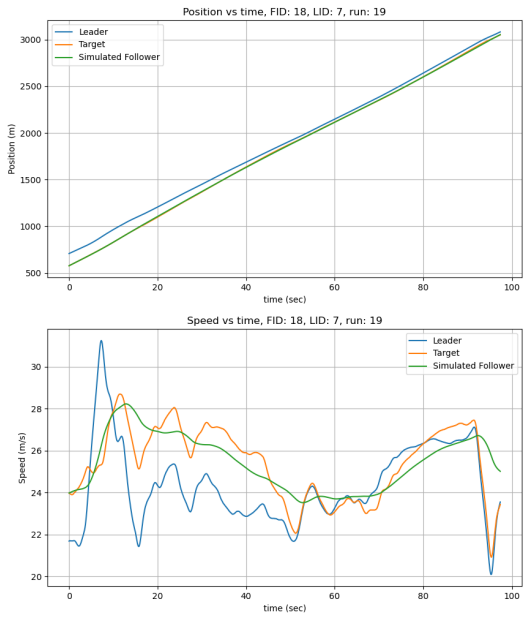




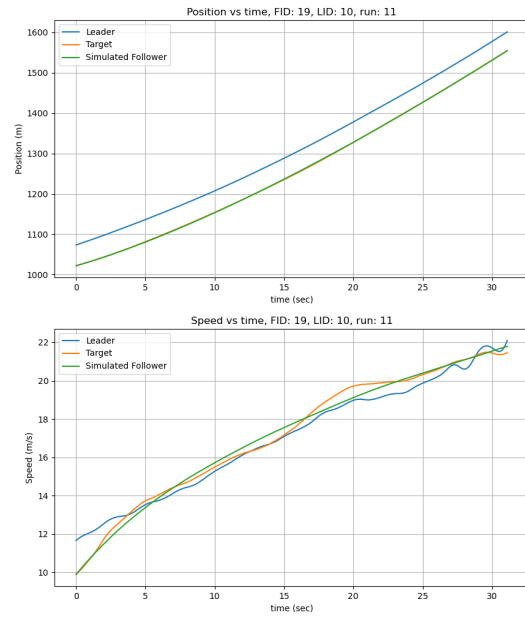
(a) Position and speed for CSF for vehicle 17 in run 21 I294L1 dataset.



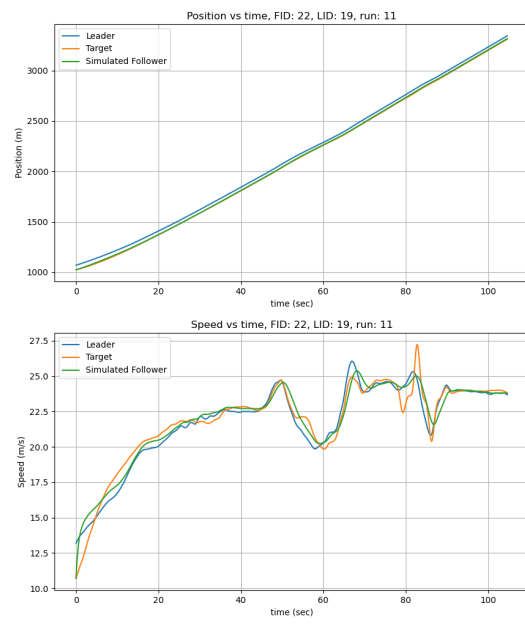
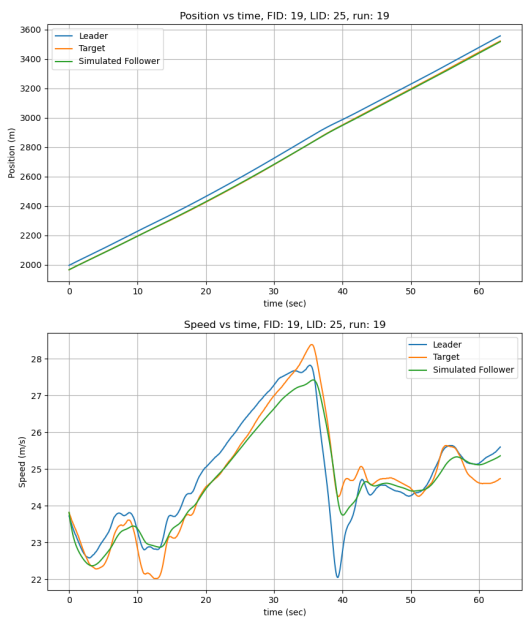
(b) Position and speed for CSF for vehicle 17 in run 7 I294L1 dataset.

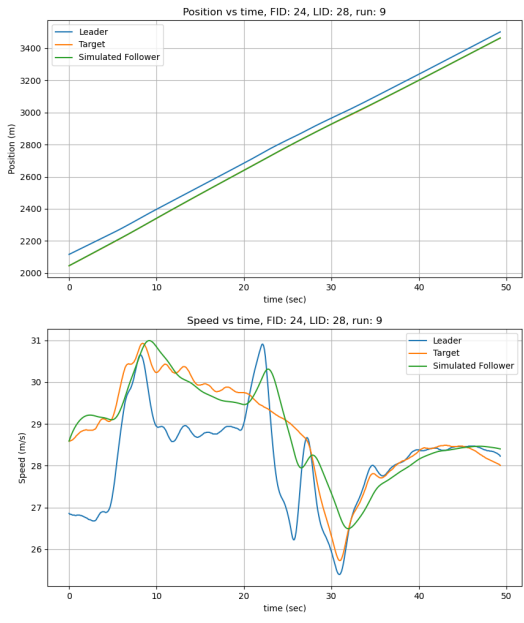


(a) Position and speed for CSF for vehicle 18 in run 19 I294L1 dataset.

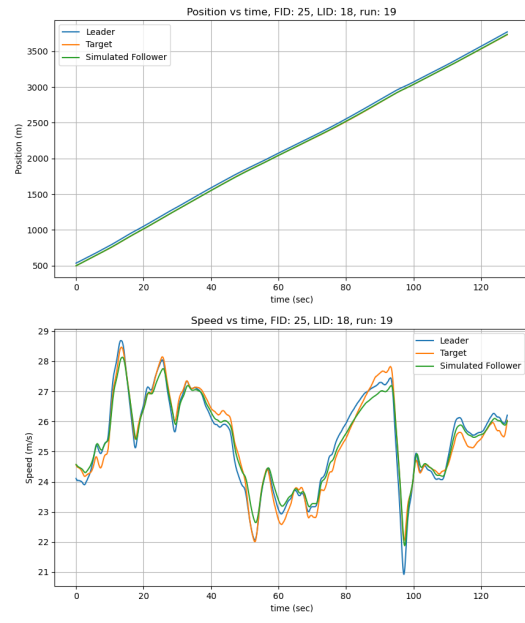


(b) Position and speed for CSF for vehicle 19 in run 11 I294L1 dataset.

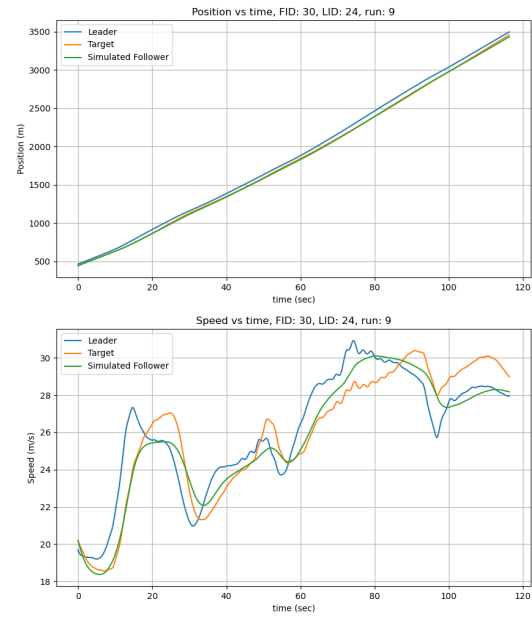
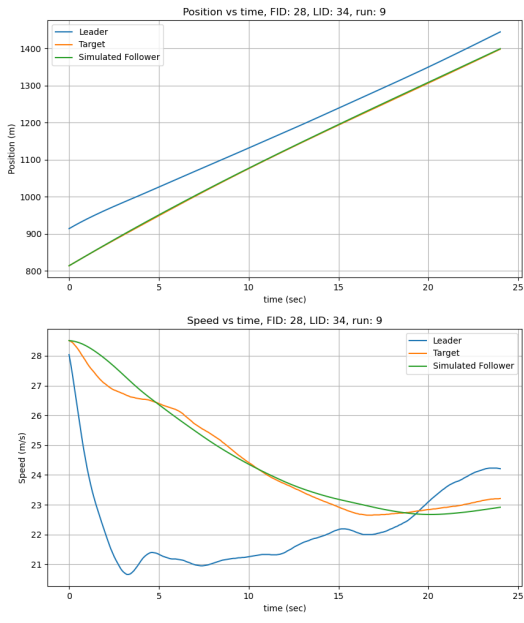


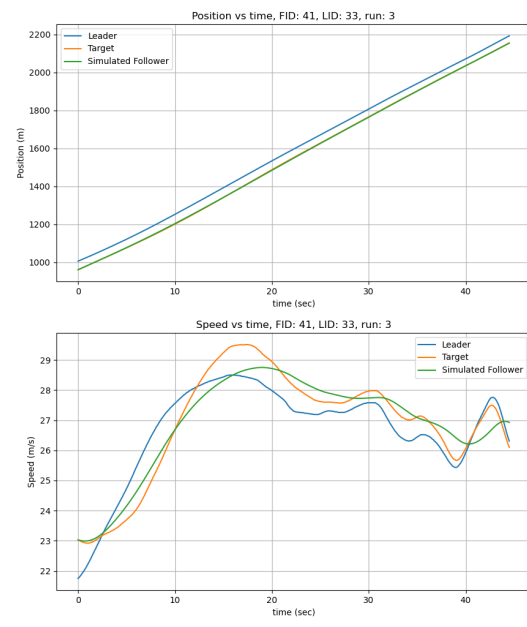
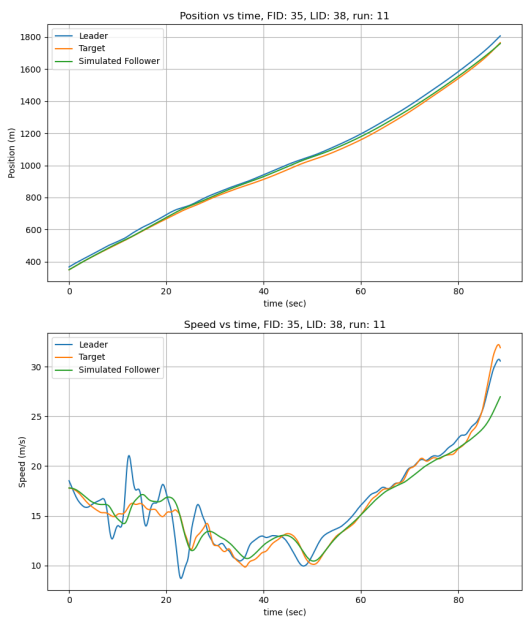


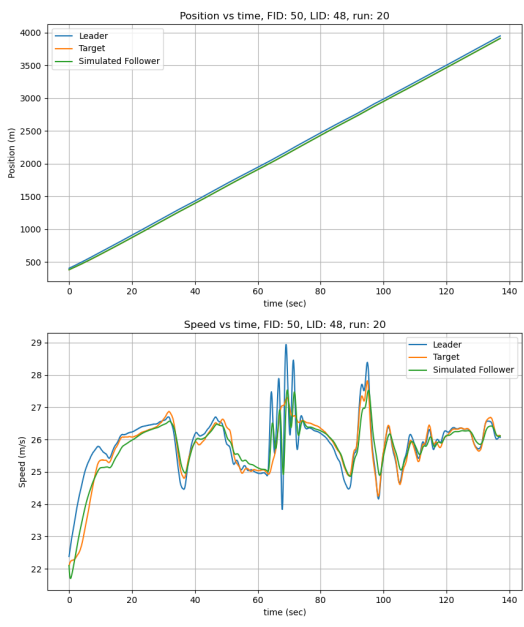
(a) Position and speed for CSF for vehicle 24 in run 9
I294L1 dataset.



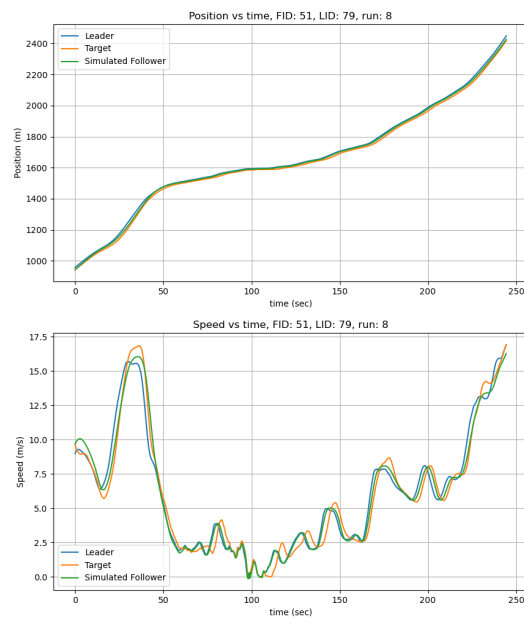
(b) Position and speed for CSF for vehicle 25 in run 19 I294L1 dataset.



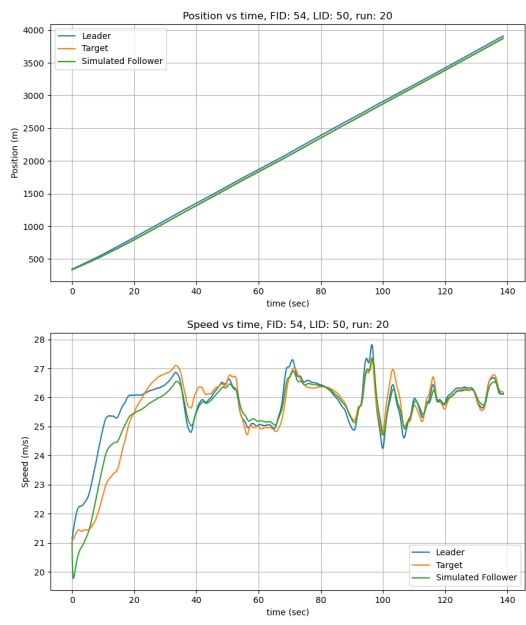




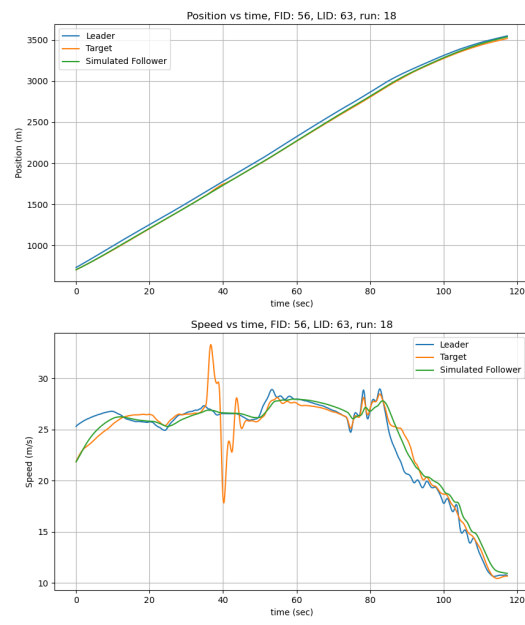
(a) Position and speed for CSF for vehicle 50 in run 20 I294L1 dataset.



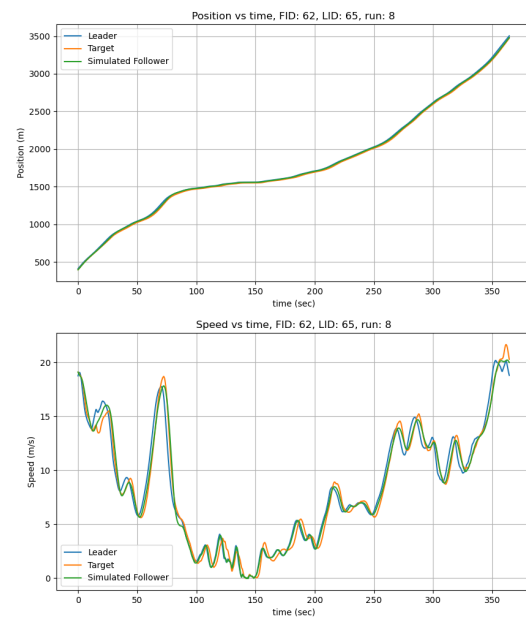
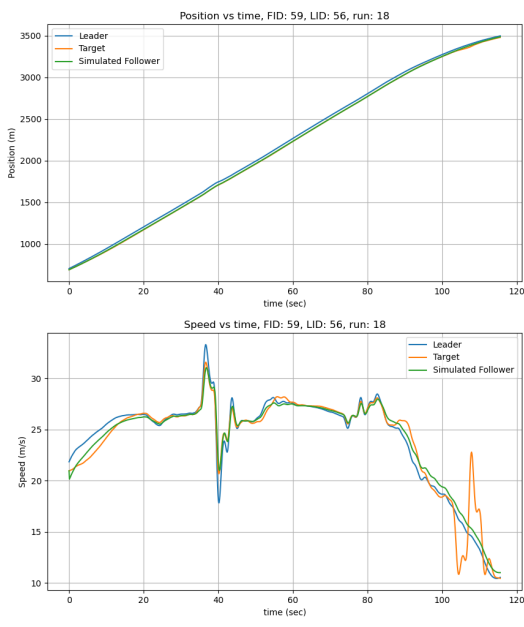
(b) Position and speed for CSF for vehicle 51 in run 8 I294L1 dataset.

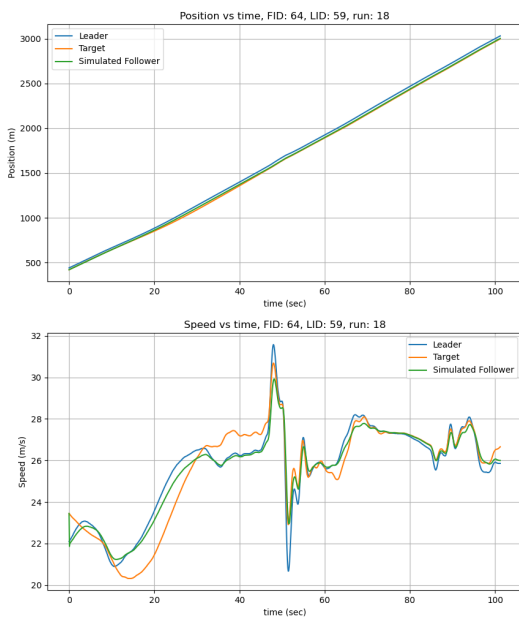


(a) Position and speed for CSF for vehicle 54 in run 20 I294L1 dataset.

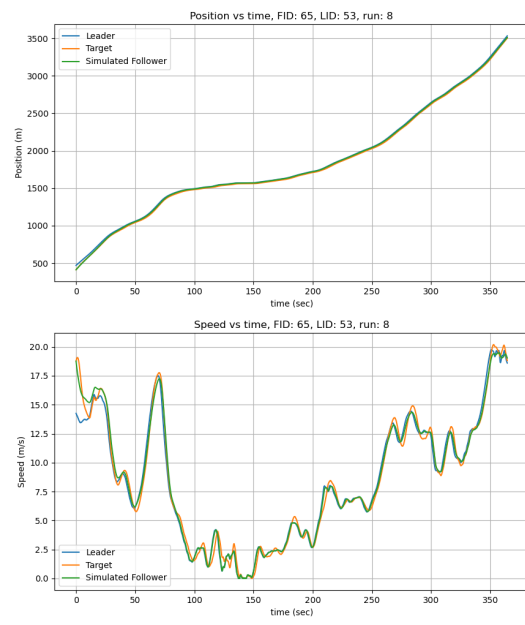


(b) Position and speed for CSF for vehicle 56 in run 18 I294L1 dataset.

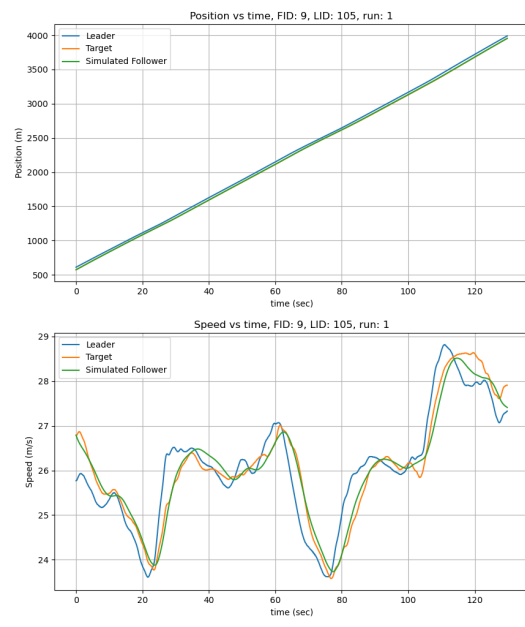
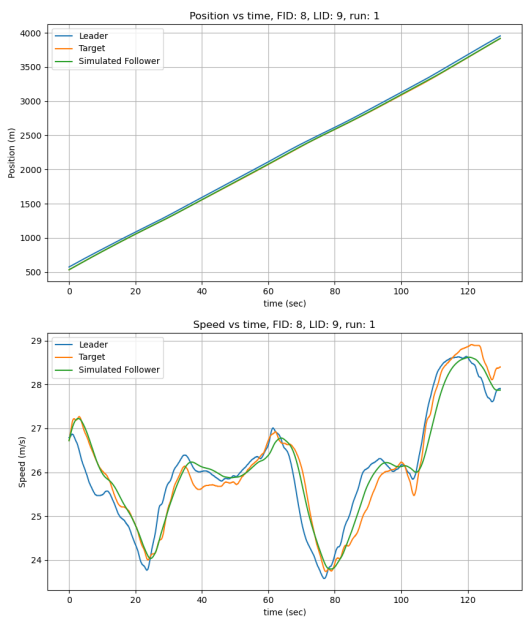




(a) Position and speed for CSF for vehicle 64 in run 18 I294L1 dataset.



(b) Position and speed for CSF for vehicle 65 in run 8 I294L1 dataset.



(a) Position and speed for CSF for vehicle 8 in run 1
I294L1 dataset.

(b) Position and speed for CSF for vehicle 9 in run 1
I294L1 dataset.

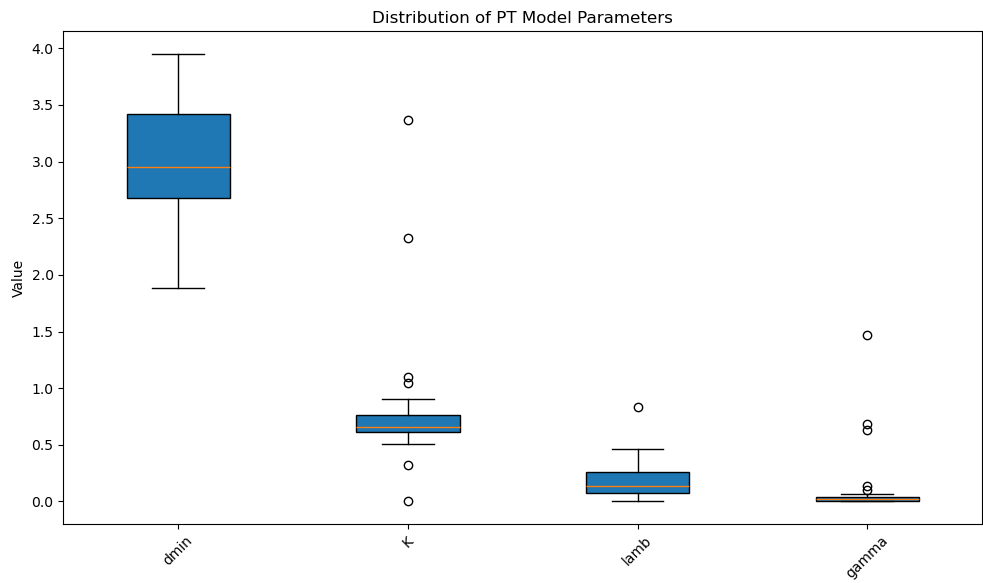


Fig. 83. Parameter ranges for CSF in I294L1 dataset.

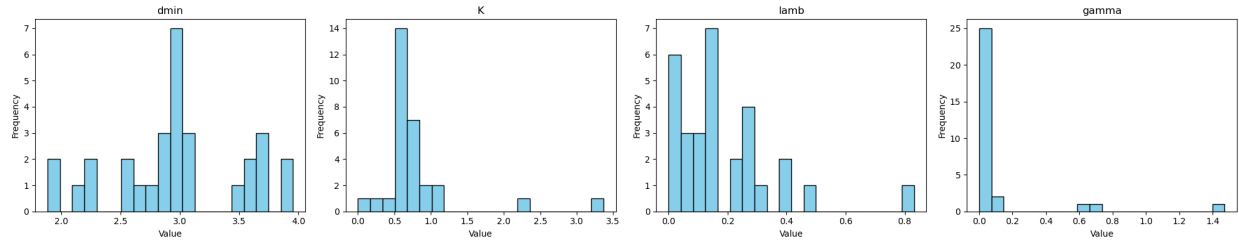
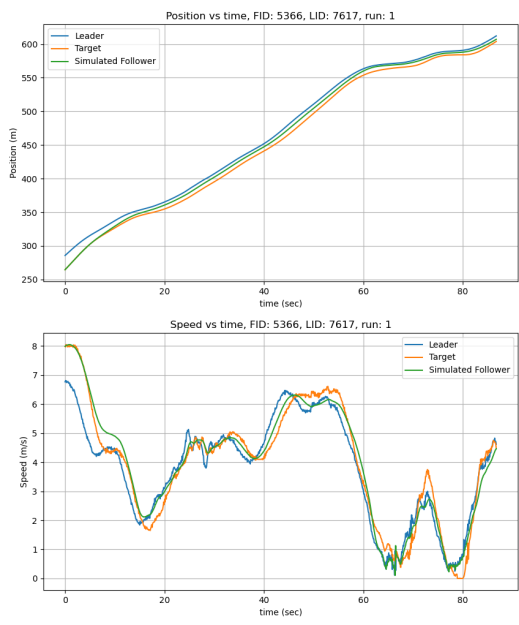
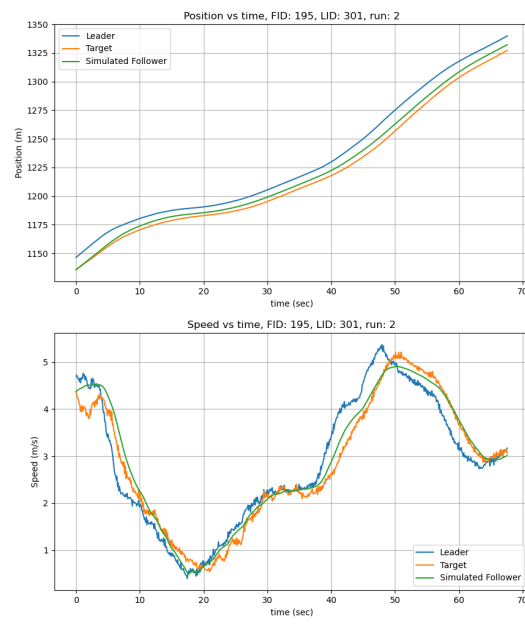


Fig. 84. Parameter histogram for CSF in I294L1 dataset.



(a) Position and speed for CSF for vehicle 5366 in I90/94 dataset.



(b) Position and speed for CSF for vehicle 195 in I90/94 dataset.

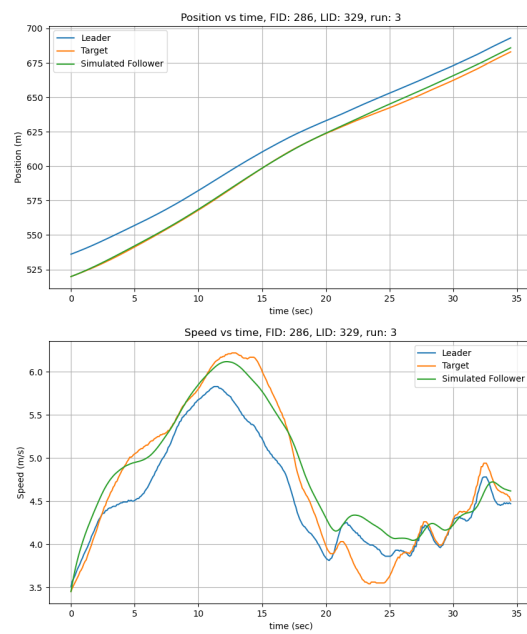


Fig. 86. Position and speed for CSF for vehicle 286 in I90/94 dataset.

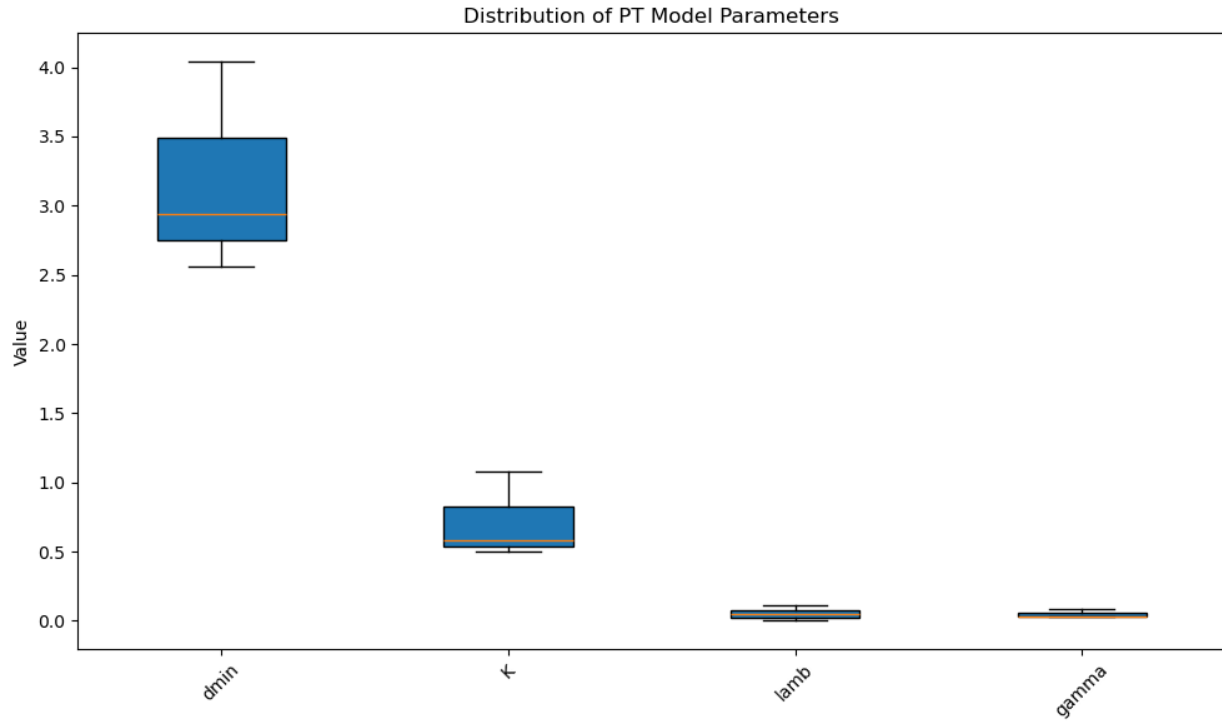


Fig. 87. Parameter ranges for CSF in I90/94.

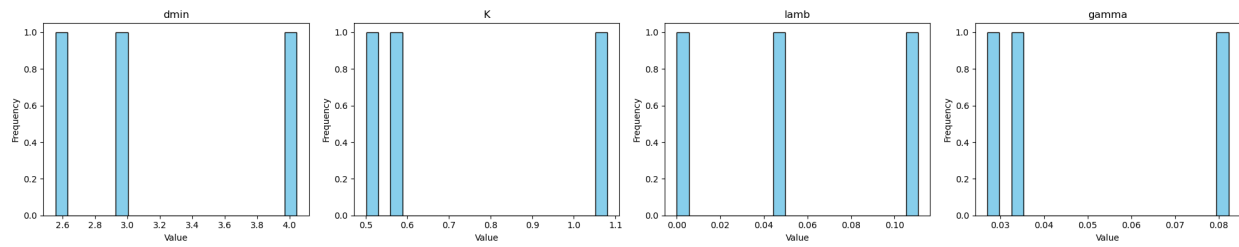
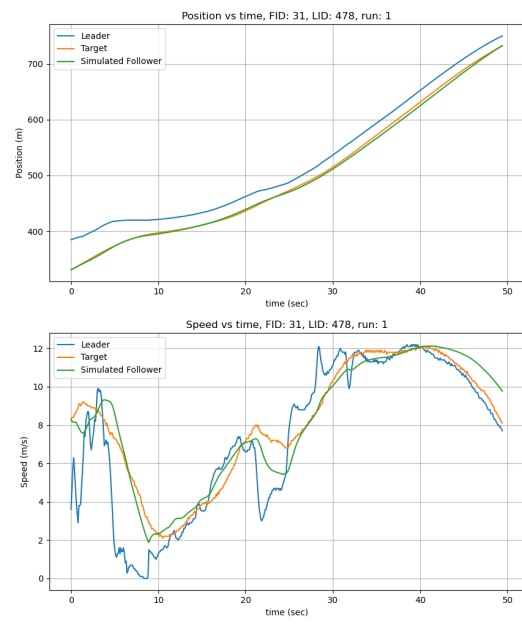
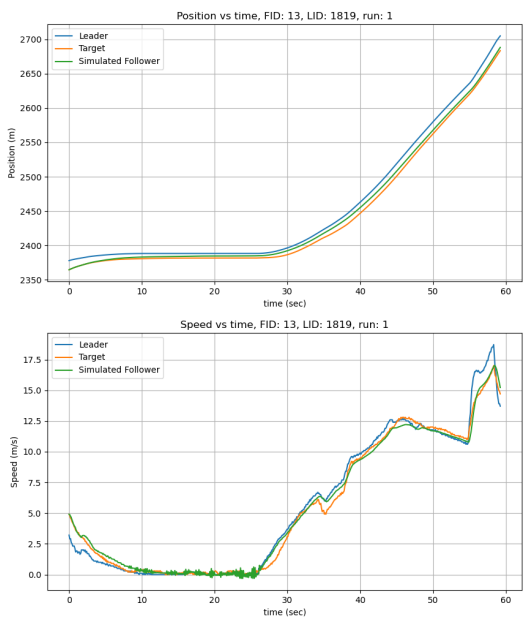
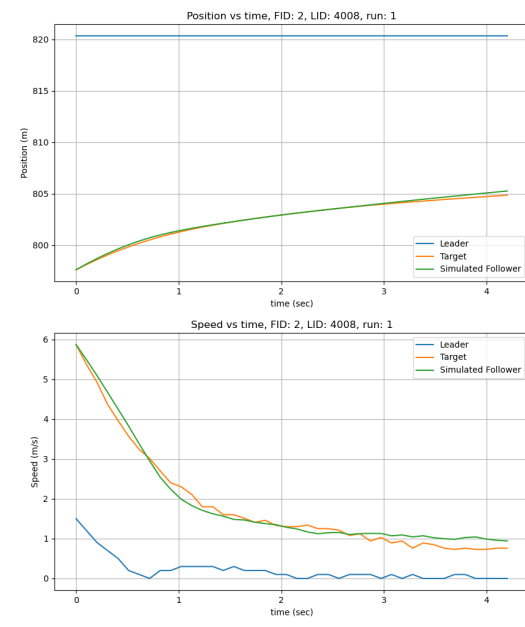
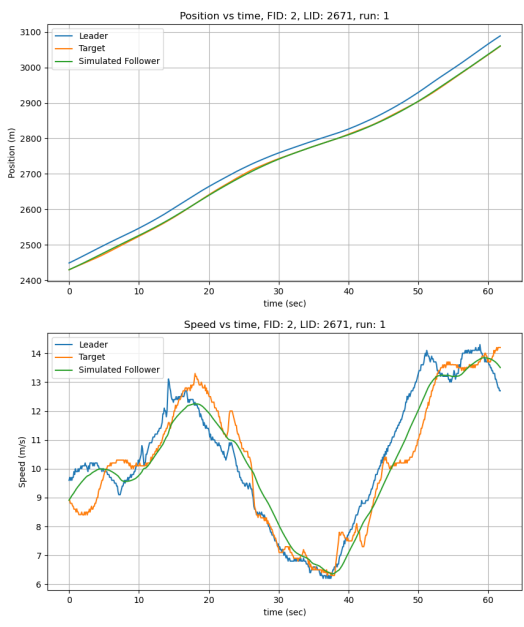


Fig. 88. Parameter histogram for CSF in I90/94.





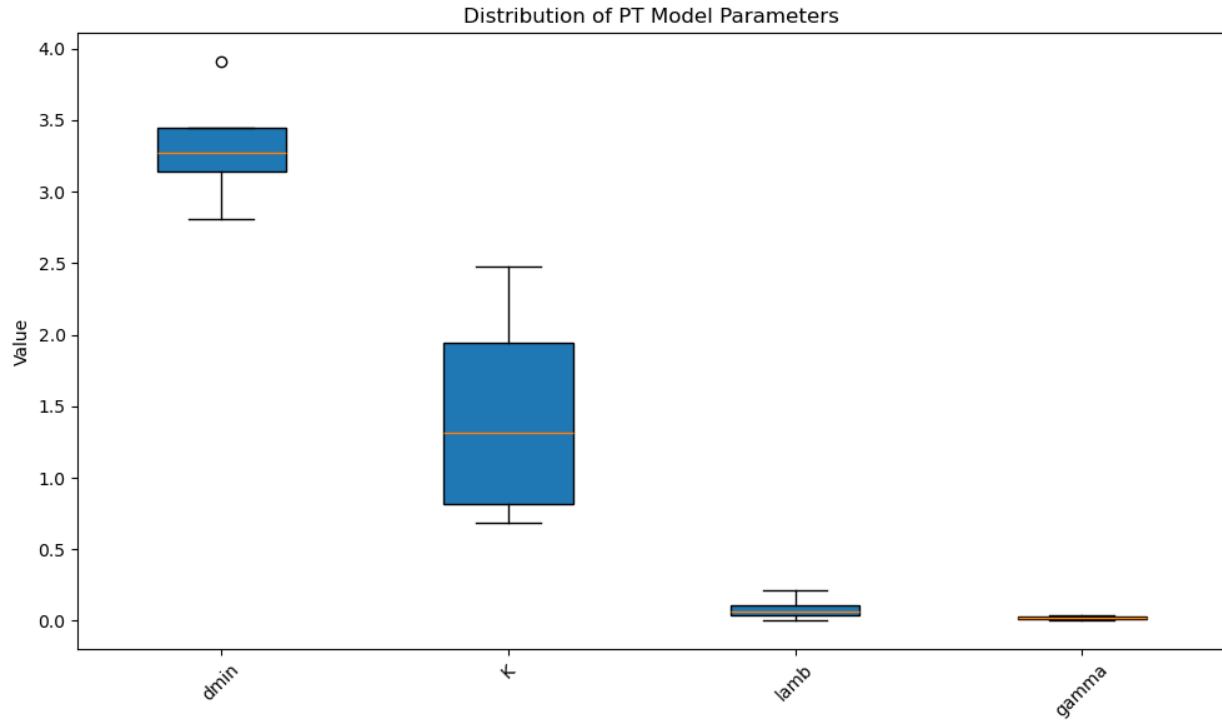


Fig. 91. Parameter ranges for CSF in Phoenix.

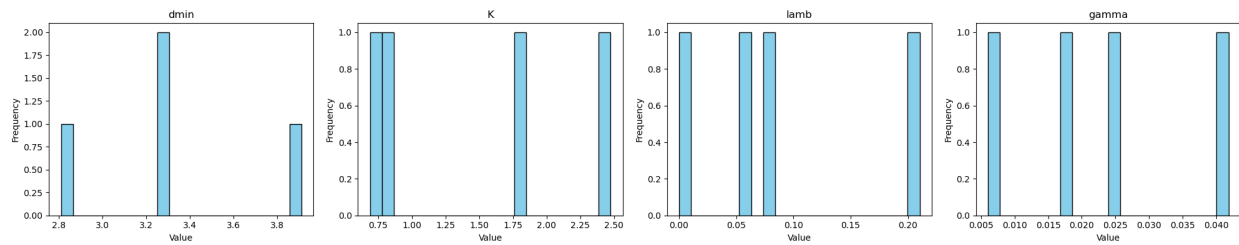
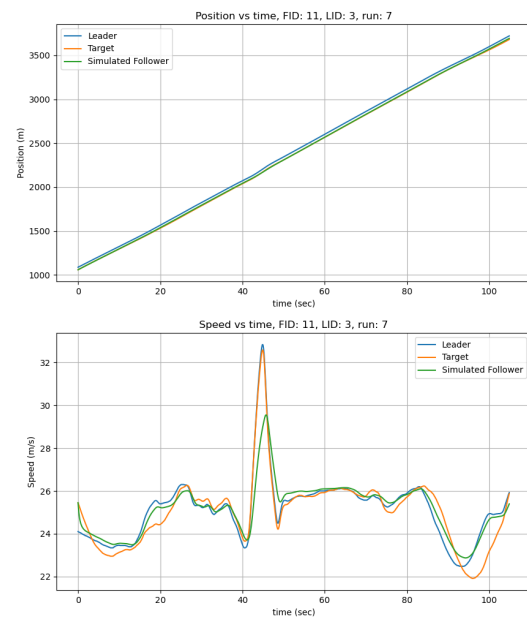
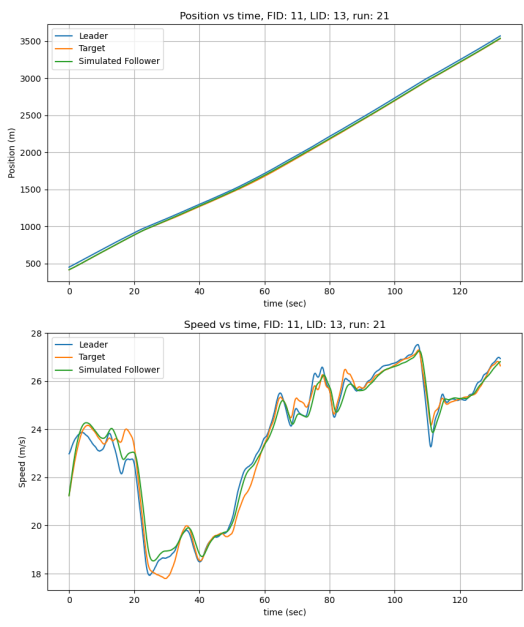
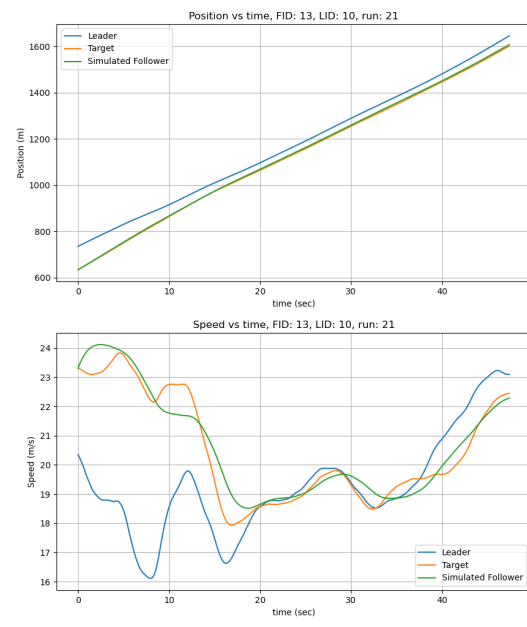
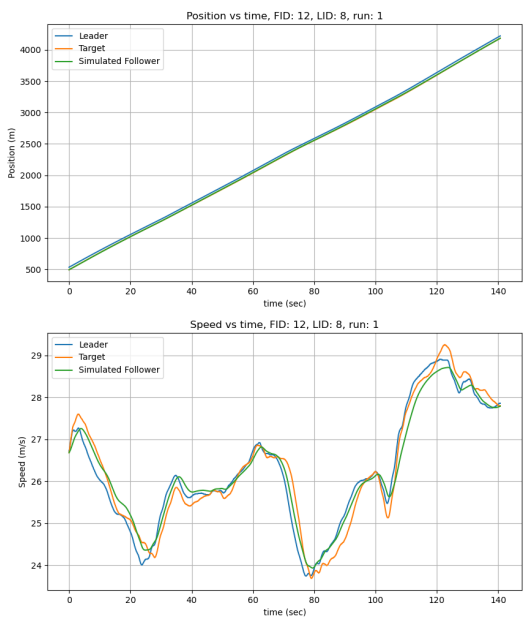
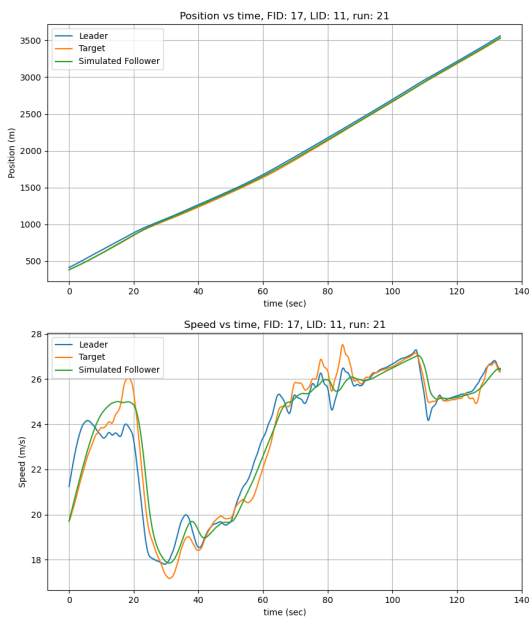


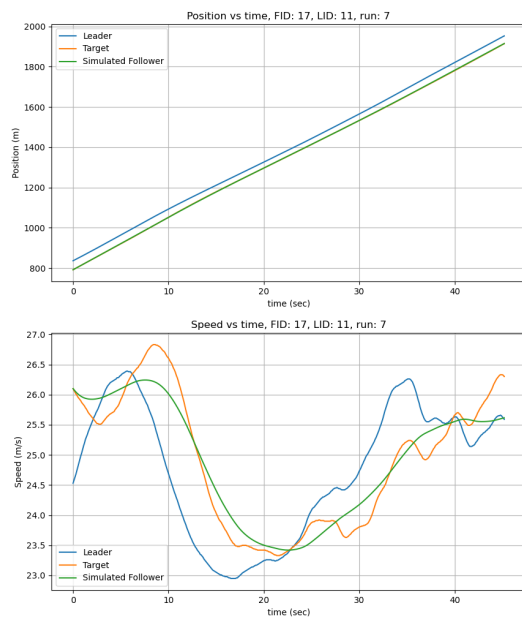
Fig. 92. Parameter histogram for CSF in Phoenix.



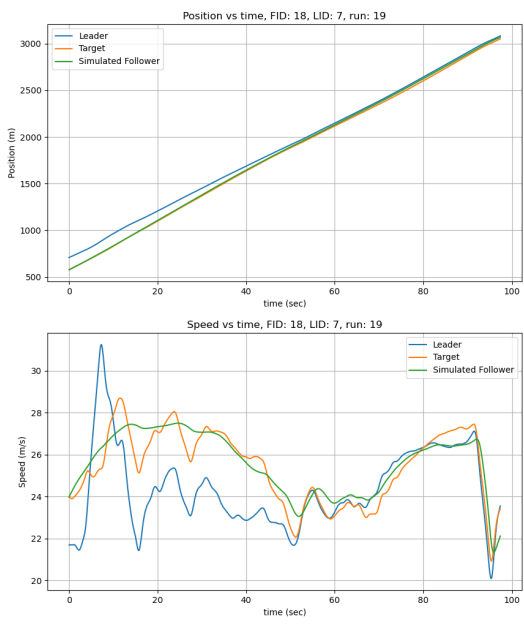




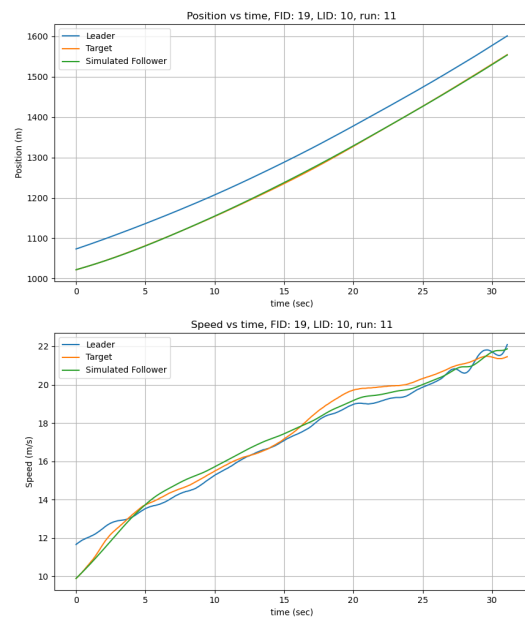
(a) Position and speed for IDM for vehicle 17 in run 21 I294L1 dataset.



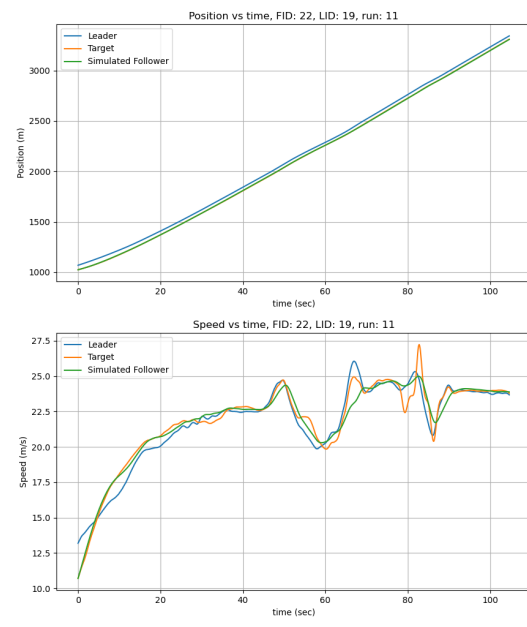
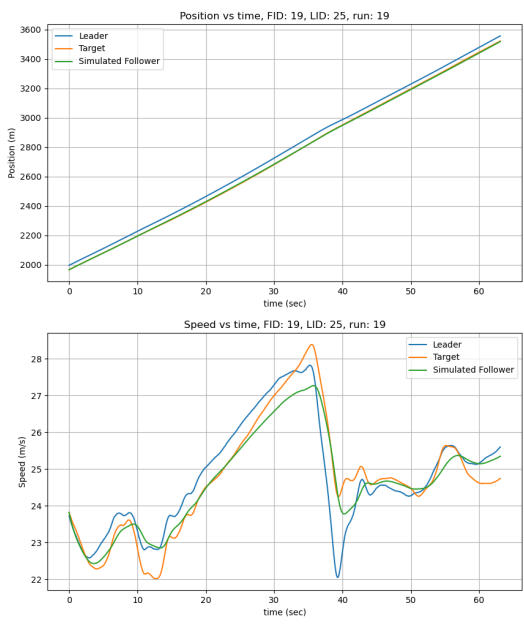
(b) Position and speed for IDM for vehicle 17 in run 7 I294L1 dataset.

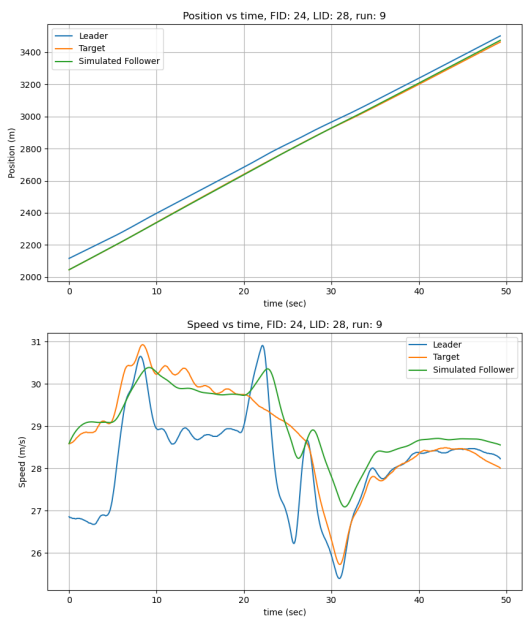


(a) Position and speed for IDM for vehicle 18 in run 19 I294L1 dataset.

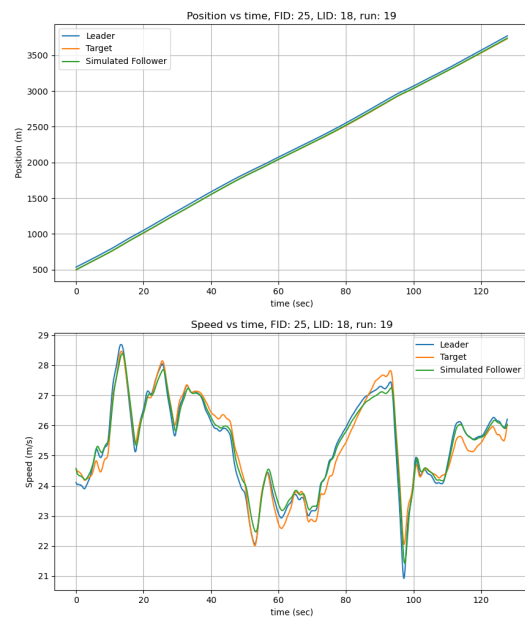


(b) Position and speed for IDM for vehicle 19 in run 11 I294L1 dataset.

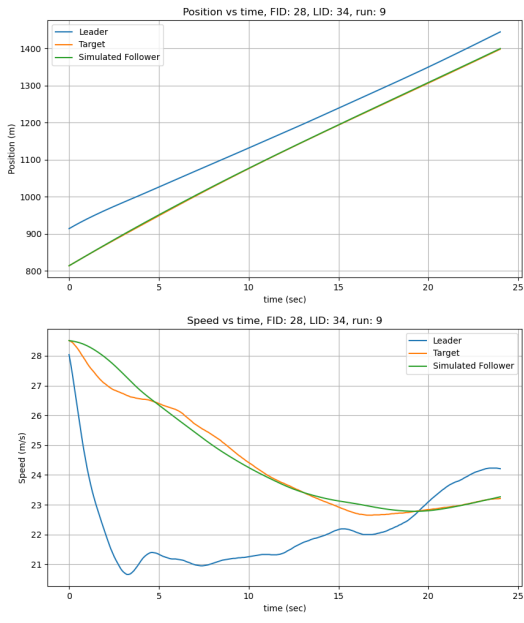




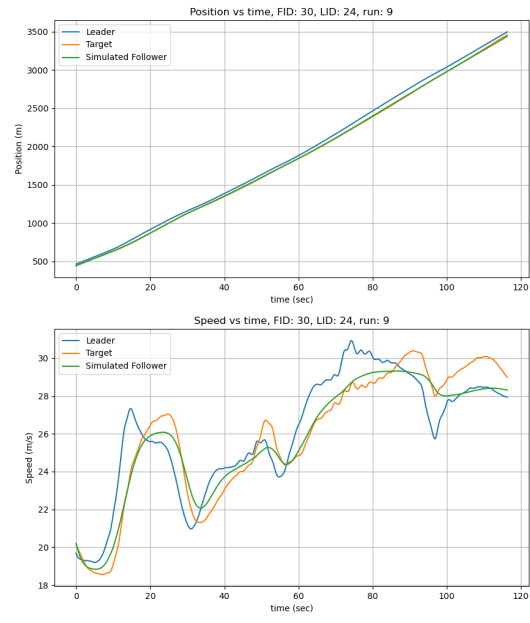
(a) Position and speed for IDM for vehicle 24 in run 9
I294L1 dataset.



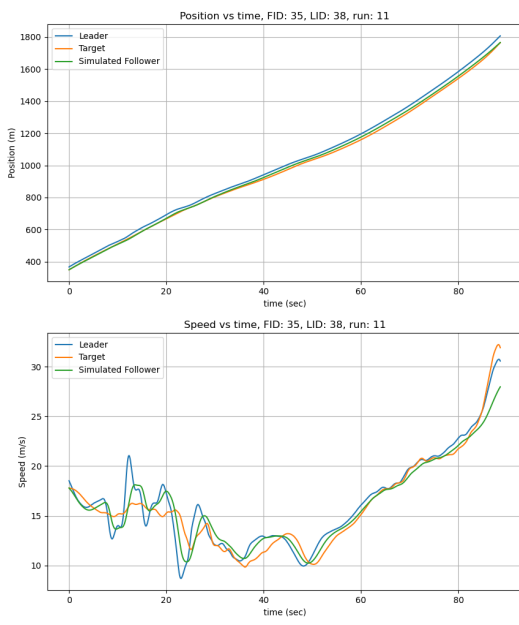
(b) Position and speed for IDM for vehicle 25 in run 19 I294L1 dataset.



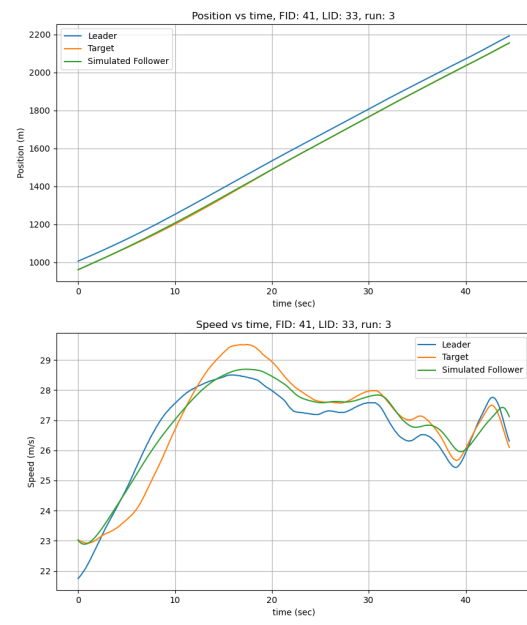
(a) Position and speed for IDM for vehicle 28 in run 9
I294L1 dataset.



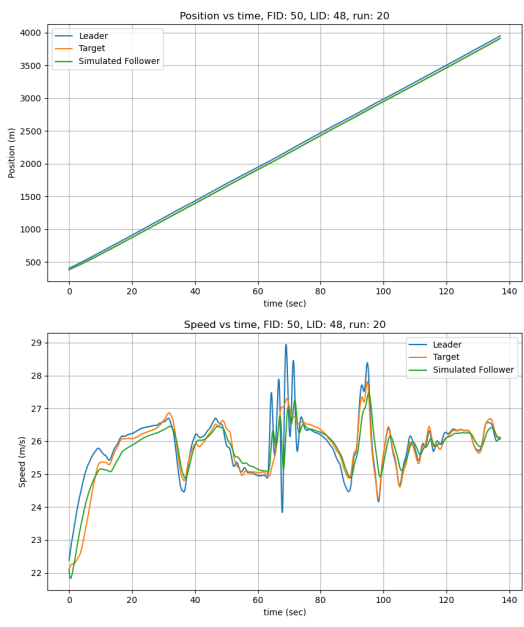
(b) Position and speed for IDM for vehicle 30 in run 9
I294L1 dataset.



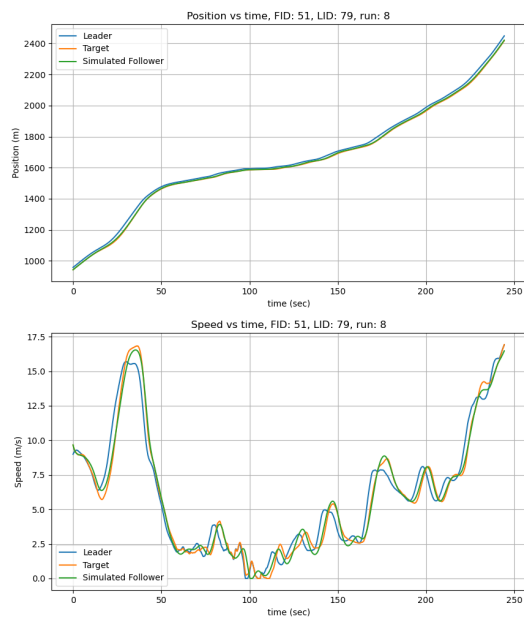
(a) Position and speed for IDM for vehicle 35 in run 11 I294L1 dataset.



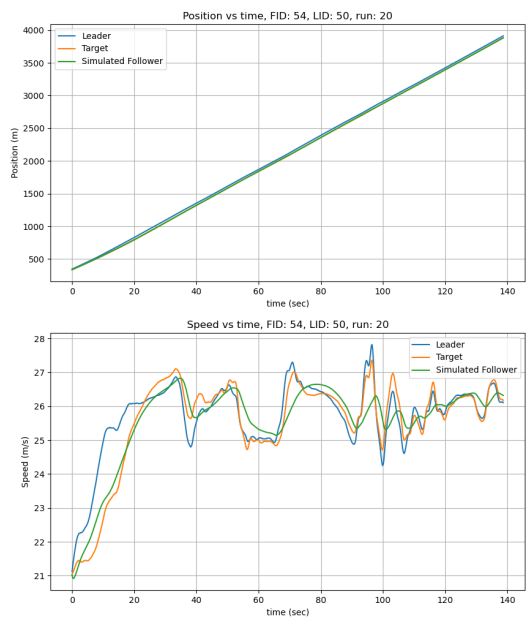
(b) Position and speed for IDM for vehicle 41 in run 3 I294L1 dataset.



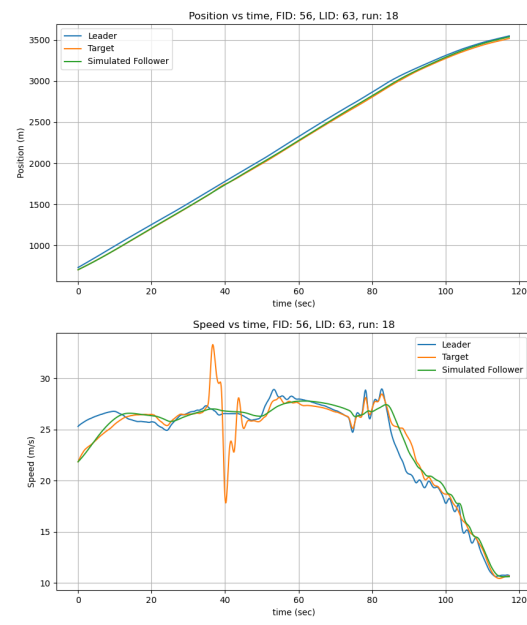
(a) Position and speed for IDM for vehicle 50 in run 20 I294L1 dataset.



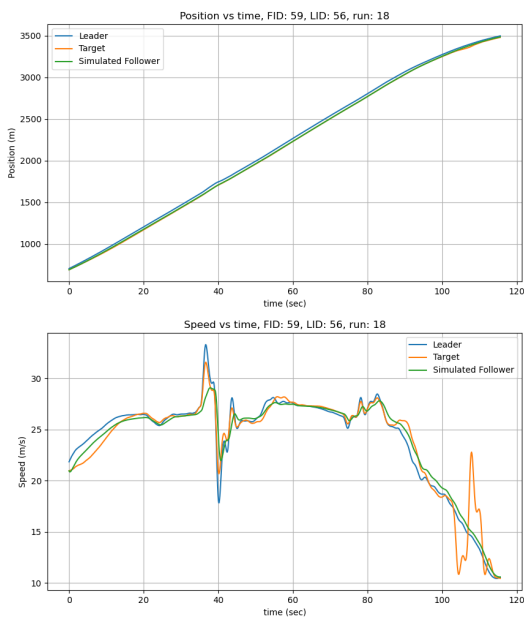
(b) Position and speed for IDM for vehicle 51 in run 8 I294L1 dataset.



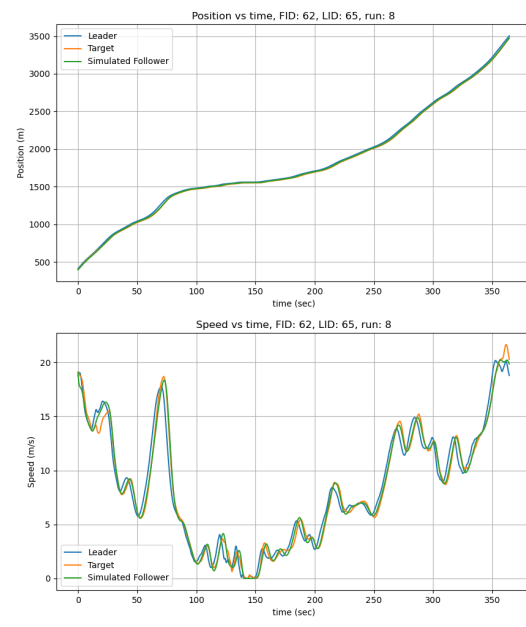
(a) Position and speed for IDM for vehicle 54 in run 20 I294L1 dataset.



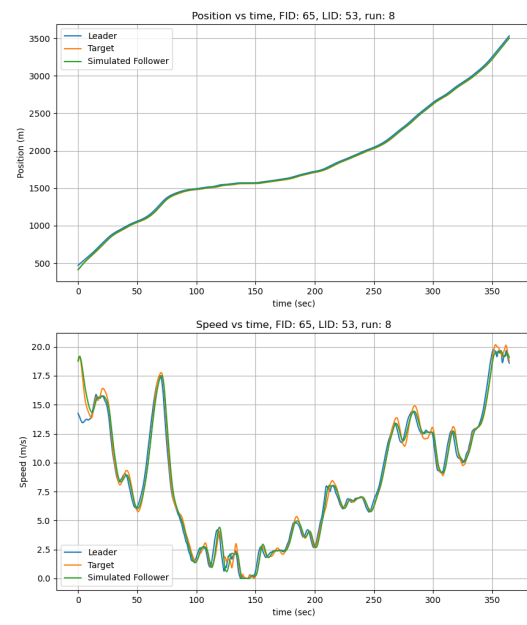
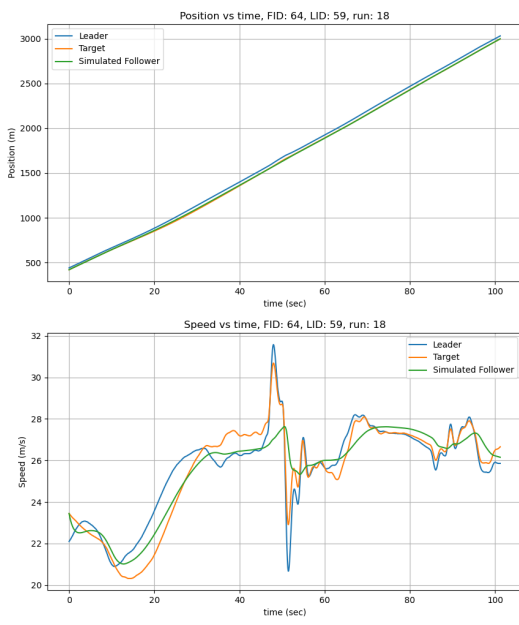
(b) Position and speed for IDM for vehicle 56 in run 18 I294L1 dataset.

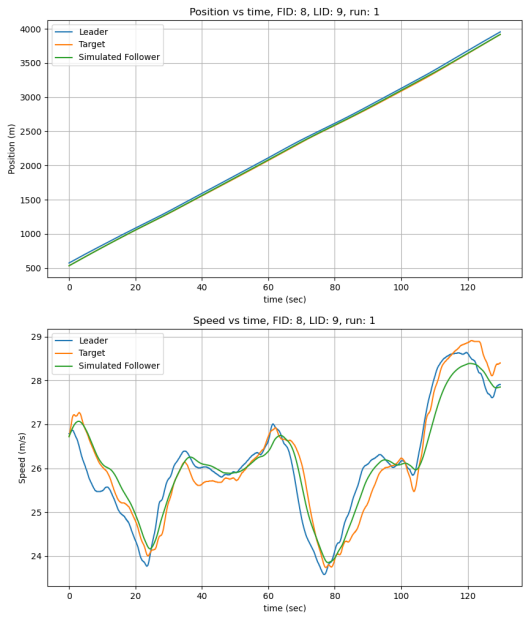


(a) Position and speed for IDM for vehicle 59 in run 18 I294L1 dataset.

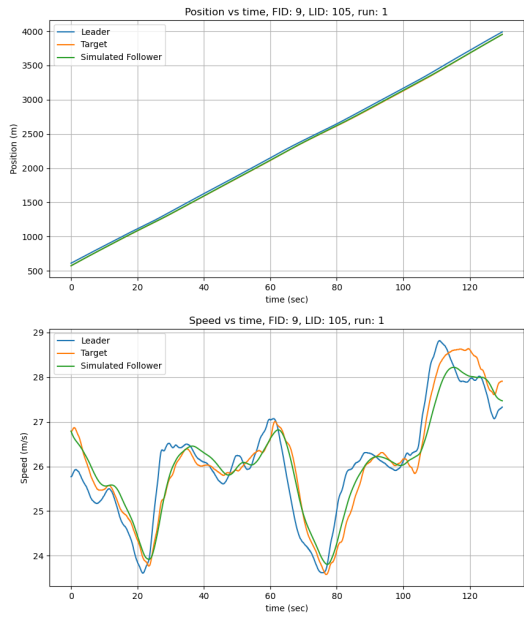


(b) Position and speed for IDM for vehicle 62 in run 8 I294L1 dataset.





(a) Position and speed for IDM for vehicle 8 in run 1
I294L1 dataset.



(b) Position and speed for IDM for vehicle 9 in run 1
I294L1 dataset.

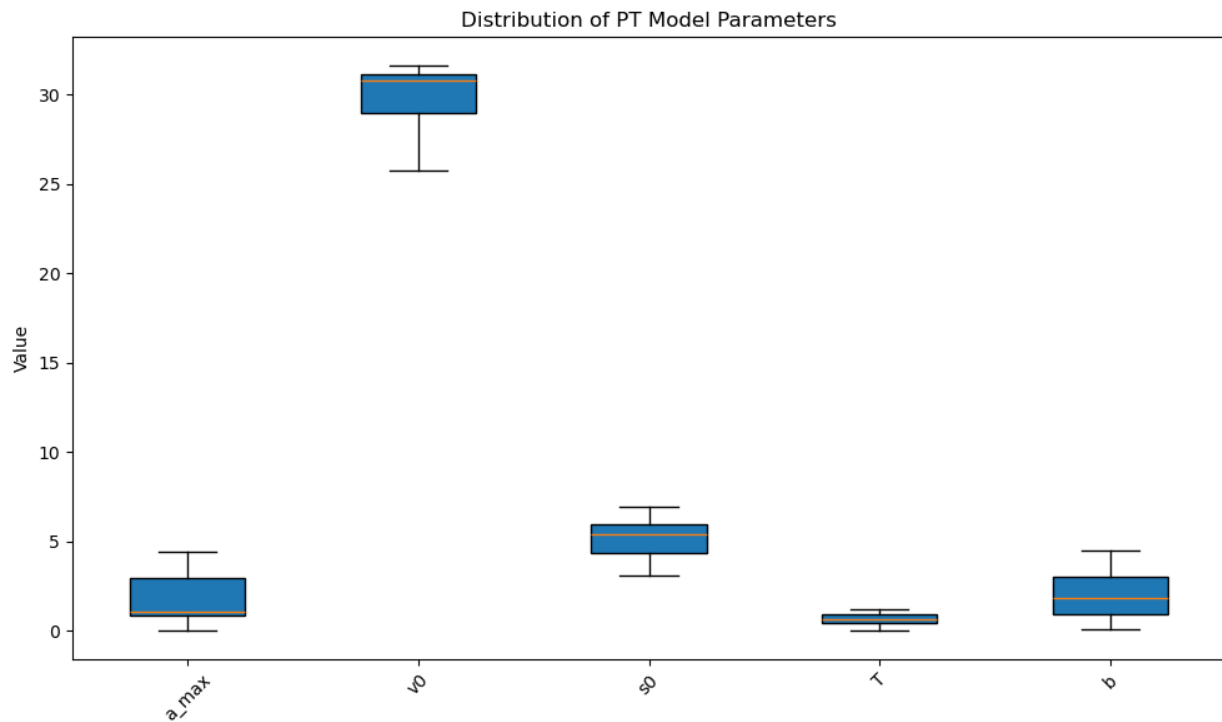


Fig. 106. Parameter ranges for 04IDM in I294L1 dataset.

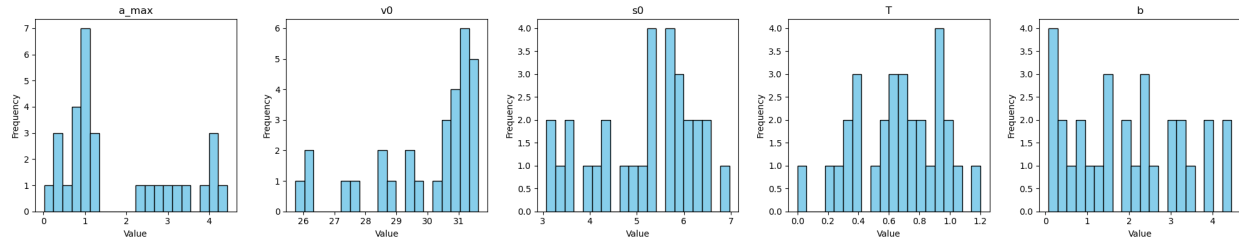
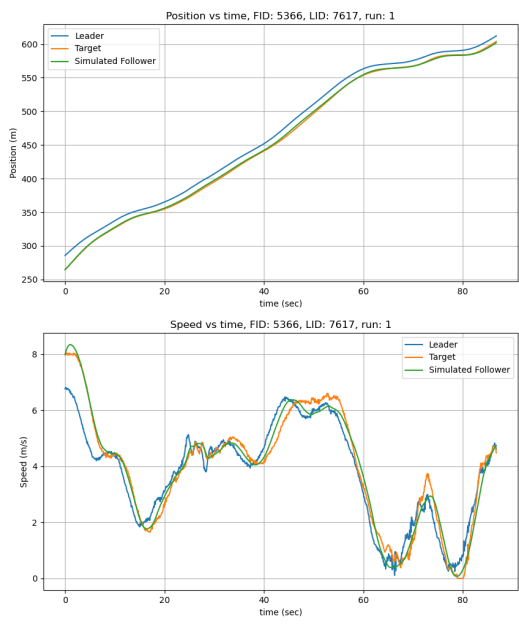
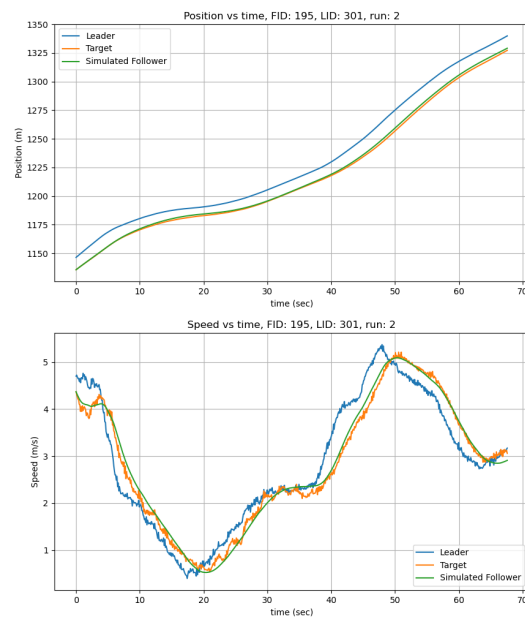


Fig. 107. Parameter histogram for 04IDM in I294L1 dataset.



(a) Position and speed for IDM for vehicle 5366 in I90/94 dataset.



(b) Position and speed for IDM for vehicle 195 in I90/94 dataset.

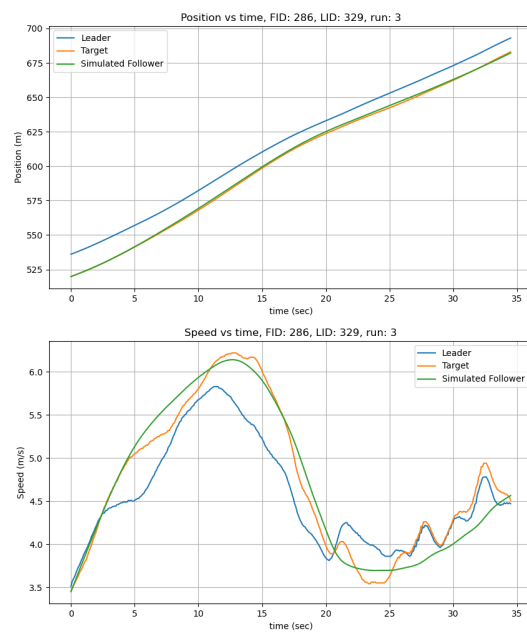


Fig. 109. Position and speed for IDM for vehicle 286 in I90/94 dataset.

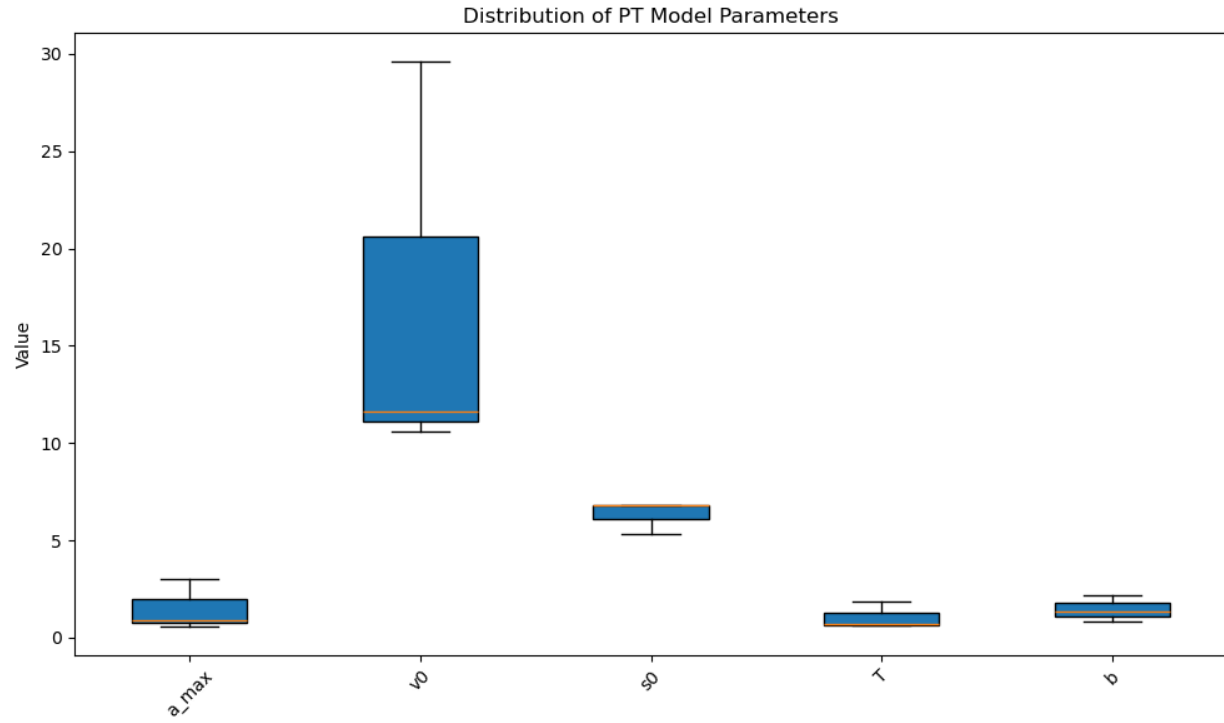


Fig. 110. Parameter ranges for IDM in I90/94.

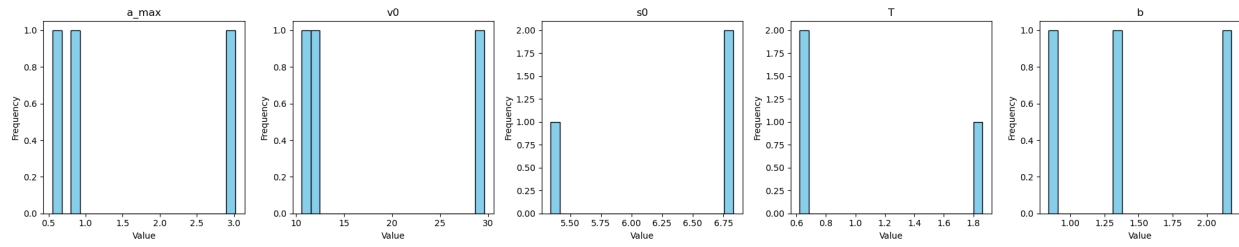
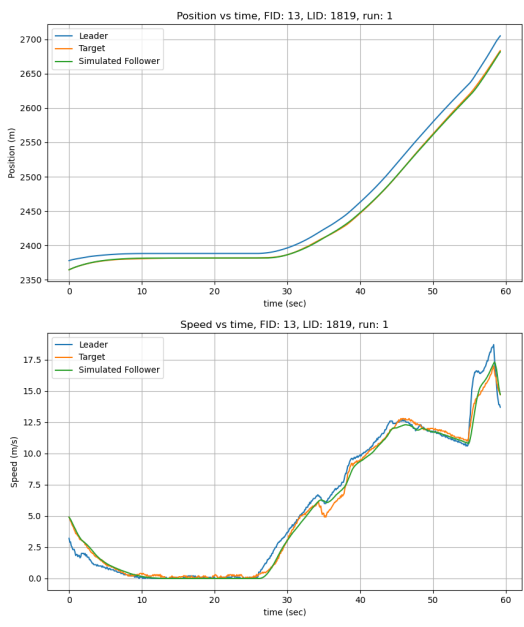
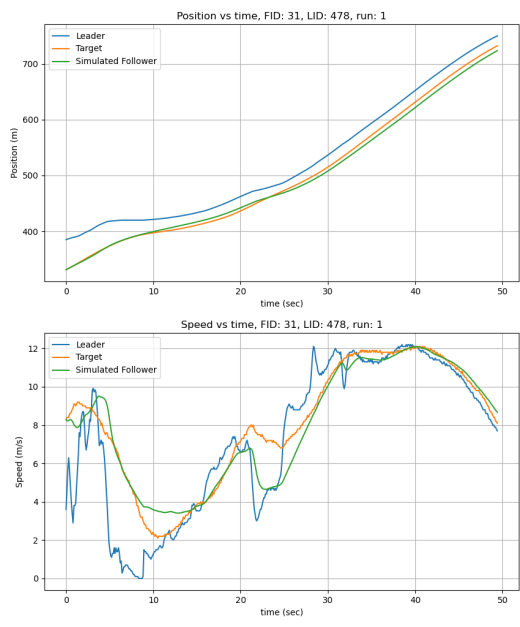


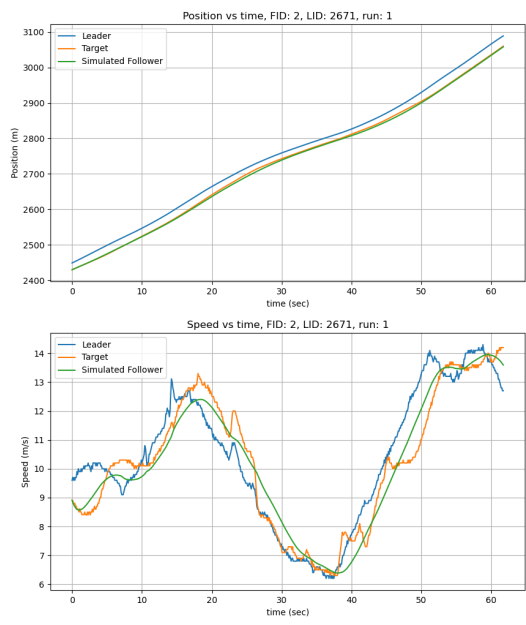
Fig. 111. Parameter histogram for IDM in I90/94.



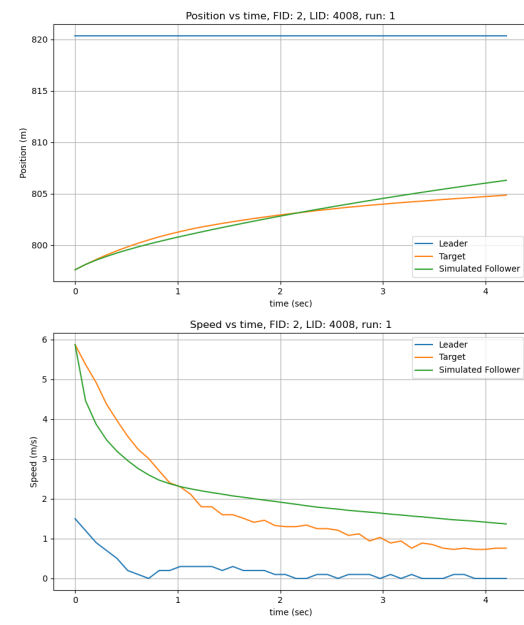
(a) Position and speed for IDM for vehicle 13 in Phoenix data H1A3 run 6.



(b) Position and speed for IDM for vehicle 31 in Phoenix data H1A3 run 1.



(a) Position and speed for IDM for vehicle 2 in Phoenix data H1A3 run 9 ES.



(b) Position and speed for IDM for vehicle 2 in Phoenix data H1A3 run 9 NS.

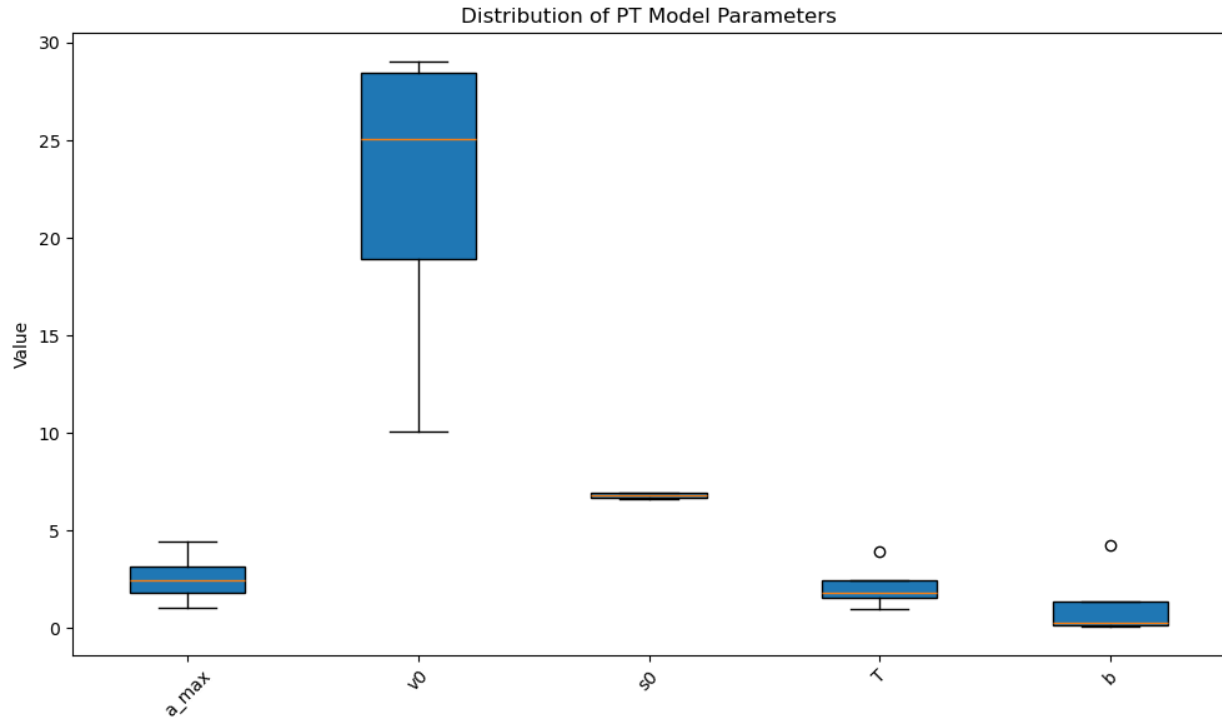


Fig. 114. Parameter ranges for IDM in Phoenix.

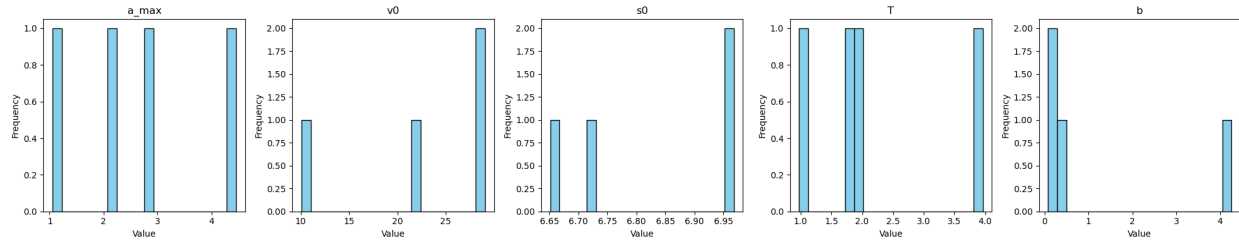


Fig. 115. Parameter histogram for IDM in Phoenix.